Real-time Power Management of Hybrid Power Systems in All Electric Ship Applications

by

Gayathri Seenumani

A dissertation submitted in partial fulfillment
of the requirements for the degree of
Doctor of Philosophy
(Mechanical Engineering)
in The University of Michigan
2010

Doctoral Committee:

Professor Jing Sun, Co-Chair
Professor Huei Peng, Co-Chair
Professor Jessy Grizzle
Professor Galip Ulsoy

To my beloved sister Sudha Mani, who through her grace, love and compassion transformed my life from a mere existence into an experience.

Acknowledgements

Even though my name appears on the cover of this dissertation, the production of this thesis work has been possible due to the contributions of many people. Hence I am sincerely thankful to all those people who have encouraged and helped me to finally finish this dissertation.

I first owe a great debt of gratitude to my advisors, Professor Jing Sun and Professor Huei Peng, at the University of Michigan. Their constant encouragement, trust and support helped me overcome many challenges and finish this dissertation. They have been remarkable mentors and have contributed a great deal in my growth as a researcher. They have exemplified the *lead by example* concept and have taught me many tangible and intangible aspects of being a good researcher, be it the control theory or work ethics. I only wish that I can understand how they can be so patient, yet so confident, that one day I will ultimately succeed in completing my research goals.

I wish to thank Professor Jessy Grizzle for his outstanding teaching, both linear system theory and functional analysis, which has provided me the theoretical knowledge in those fields. It has been a great honor to have been part of his class and such a pleasure to learn from someone who has so much passion and dedication to help the students understand the fundamental concepts. I am sincerely thankful to Professor Galip Ulsoy for all his constructive comments and suggestions which has significantly contributed to this research work.

I am truly thankful to Dr.Hosam Fathy for his valuable research insights, his willingness to help me at any time and am deeply touched by his belief in my abilities as a controls researcher. I still don't understand why he choose to have so much trust in me!! I wish to profusely thank Professor Romesh Saigal for helping me with aspects of optimization methodology development which was extremely useful to me. I wish to acknowledge the U.S. Office of Naval Research for the financial support under Grants No. N00014-08-1-0611 and N00014-05-1-0533.

I would like to thank all my friends and colleagues (Amey, Chris, Handa, Jacob,

Soryeok, Reza, Vasilios, Zhen and Zhao) in the RACE Lab at the University of Michigan for valuable discussions and enjoyable friendship. I would like to specifically thank Chris, Jacob, Reza and Yanhui for all the great lunches (even though I hated La Shish) and the great laughs together. Our common passion for you-tube"ing", South-Park"ing" and constantly repeating Woody Allen jokes made the days quite memorable.

I want to thank my friends who have helped me a great deal during the past years. I wish to thank my *quals* study partner Dr.Buz McCain for being such a good friend and for putting up with me for many years. We have sat through many courses together and I must say that it was a lot of fun and I miss it quite a bit. I wish to convey my heart-felt thanks and a great deal of gratitude to Devesh Kumar for his true friendship, kindness and above all, simply being there for me. I wish to profusely thank Rajeev Verma, Shilpa Gupta and Rhea Gupta for their support and their constant encouragement. It is quite amazing that they all truly feel happy for me all the time and I cannot express how lucky I feel.

I would like to thank my greatest friend, philosopher and guide and someone whom I admire the most, Kumar Velayudham, my husband. His sharp intellect and impeccable work ethics have been the greatest source of inspiration to me. I am sincerely grateful for all his help and encouragement during the past years and for his belief in my abilities. Finally, and most importantly, I would like to thank my mother Indra Ramakrishnan, my father Seenumani Kalyanaraman and my little sister Sudha Mani for their love, the most truthful feeling I have ever experienced. While no words can adequately express my gratitude for them, I would like to mention that I owe every aspect of myself to them. Without their himalayan suffering and sacrifice, nothing of who I am today could have been possible. I am much beholden to my family for having faith in me and giving me the support and strength to overcome the difficulties.

Contents

List of Figures

Figure

List of Tables

Table

LIST OF APPENDICES

Appendix

List of Abbreviations

AES	All Electric Ship
ABT	Auto Bus Transfer
CHP	Combined Heat and Power
DHPS	DC Hybrid Power System
EPM	Electric Propulsion Module
ESD	Energy Storage Device
FC	Fuel Cell
FPS	Fuel Processing System
FR	Fuel Reformer
FRODS	Failure, Reconfiguration, Operation and Drive Scenarios
GT	Gas Turbine
HDS	Hydro Desulphurizer
HEX	Heat Exchanger
HPS	Hybrid Power System
IPS	Integrated Power System
LP	Linear Programming
MOFD	Method Of Feasible Directions
MIXER	Mixer
MPC	Model Predictive Control

PM	Power Management
PEM	Polymer Electrolyte Membrane
PCM	Power Conversion Module
PEM	Polymer Electrolyte Membrane
PGM	Power Generation Module
PMSM	Permanent Magnet Synchronous Motor
QP	Quadratic Programming
RG	Reference Governor
RHC	Receding Horizon Control
RMSD	Root mean square deviation
SQP	Sequential Quadratic Programming
SF	Sensitivity Function
SFM	Sensitivity Function Method
SPS	Shipboard Power-system Simulator
TSS	Time Scale Separation
WGS	Water Gas Shift reactor

Abstract

Real-time Power Management of Hybrid Power Systems in All Electric Ship Applications

by

Gayathri Seenumani

Co-Chairs: Jing Sun and Huei Peng

Motivated by the need for achieving flexible shipboard arrangement and meeting future on-board power demand, the concept of all-electric ships (AES) has been pursued. The integrated power systems (IPS) enable this initiative by providing a common electrical platform for the propulsion and ship-service loads. Given the multiple power sources and the energy storage devices involved, shipboard power systems are a classic example of hybrid power systems (HPS). In order to leverage the complementary dynamic characteristics of the diverse sources, effective power management is essential to coordinate the HPS heterogenous sources and energy storage in order to achieve efficient power generation and fast load following. Although extensive research has been done on the power management of hybrid land vehicles for commercial applications, this problem for shipboard military applications remains largely unaddressed, leading to its exclusive focus in this dissertation.

While HPS brings in many opportunities for power management, there are many associated challenges for systems used in military applications since both performance

as well as survivability criteria have to be satisfied. While the on-demand goal for the power management problem makes real-time control a key requirement, leveraging the look-ahead opportunities for the shipboard missions makes it difficult to attain this goal. Furthermore, the nonlinearity and the complexity of hybrid power systems, make the optimal control of HPS challenging. In this dissertation, we address real-time power management for the AES and general hybrid power systems targeting military applications. The central theme of this work is the development of power management schemes with real-time computational efficiency by exploring HPS dynamic properties, for improved performance (namely fuel economy and fast load following) during normal mode conditions as well as increased survivability during component failure. This research has focused both on tools and methodology development for real-time power management.

A reduced order dynamic HPS model is developed as a numerical tool for controller design. In addition, a scaled test-bed to emulate the HPS is developed which serves as a rapid prototyping platform for controller validation. A novel trajectory optimization methodology, for systems with a multi-time scale property, is developed in order to address the real-time control requirements for the purposes of optimal power split planning. In addition, the power management (PM) schemes for both normal as well as failure mode conditions are proposed and implemented on a real-time simulator which demonstrated the real-time performance of the proposed method. While the normal mode PM leverages the complementary dynamic characteristics of the HPS for real-time performance, the failure mode PM uses a reference governor approach for real-time constraint enforcement. The results of a case study verifies that the proposed power management strategy could achieve fast and efficient load following during normal operation as well as improved survivability in the event of component failure, both of which are ensured by the real-time computational efficiency of the proposed controller.

Chapter 1

Introduction

The all-electric ship initiative [1] has been driven by the need for a flexible shipboard arrangement to improve cost effectiveness and also for effective use of on-board power in order to meet the future requirements for high power demands. This initiative has been pursued for both commercial and military applications. Integrated power systems (IPS) [2], [3] enable the AES initiative by providing it with a common electrical platform for propulsion and ship-service loads. The main IPS components comprises of power generation modules, power conversion modules, energy storage modules, electric propulsion modules as well as vital and non-vital ship-service loads. The power generation modules for the AES utilizes heterogenous power sources, which include heat engines as well as renewable energy sources. These sources along with energy storage devices support the load demands and is a representative example of an isolated hybrid power system.

The hybrid power systems (HPS) have not only been pursued for the AES, but have also found widespread applications in land vehicles due to their advantages in achieving clean and efficient power generation compared to conventional internal combustion engines. The design and control of hybrid power systems for mobile applications have hence received significant attention in both industry and academia. While

the control of HPS for commercial applications focuses on superior performance, fuel economy improvement and emission reduction, those used for military applications have an additional, but critical, requirement of ensuring survivability. Here survivability is measured in terms of the ability of HPS to provide continuous vital load support while recovering from component failure and damage. Consequently, there is a lot of ongoing research that focuses on HPS power management.

With the multiple power sources involved, while the HPS brings in many opportunities (e.g. fast load-following, system efficiency improvement) for power management through hybridization, there are many associated challenges, specially for those targeting military applications. For example, the HPS employed in military land hybrids and AES are not only put through a wide range of operating scenarios, but also have to deal with the possibility of component failures. This requirement, coupled with those of fast load following, maximizing overall efficiency and assuring system safety make the real-time control of HPS challenging. Motivated by the importance of the AES initiative and the associated challenges in the control of the HPS employed in military applications, this dissertation focuses on the *real-time power management of shipboard hybrid power systems* for fast load following as well as improving the system efficiency and survivability.

1.1 Background

1.1.1 Integrated Power Systems in All-Electric Ships

The IPS used in all-electric ships powers both propulsion and ship service loads through a common electrical platform. The electric drive offers significant advantages as compared to the mechanical drive in terms of meeting the increasing on-board power demand, improving cost effectiveness and survivability. This is because an

electric drive makes it possible to release large amounts of power, otherwise locked in mechanical propulsion, for other purposes such as supporting pulse weaponry or carrying the increased payloads required during battle scenarios. The improved cost-effectiveness stems from the following design: the use of a single set of engines for powering both propulsion and non-propulsion systems greatly improves the cost. Typically the diesel engines or gas turbine/generator sets can be used as primary power sources while the fuel cells can be used as auxiliary units.

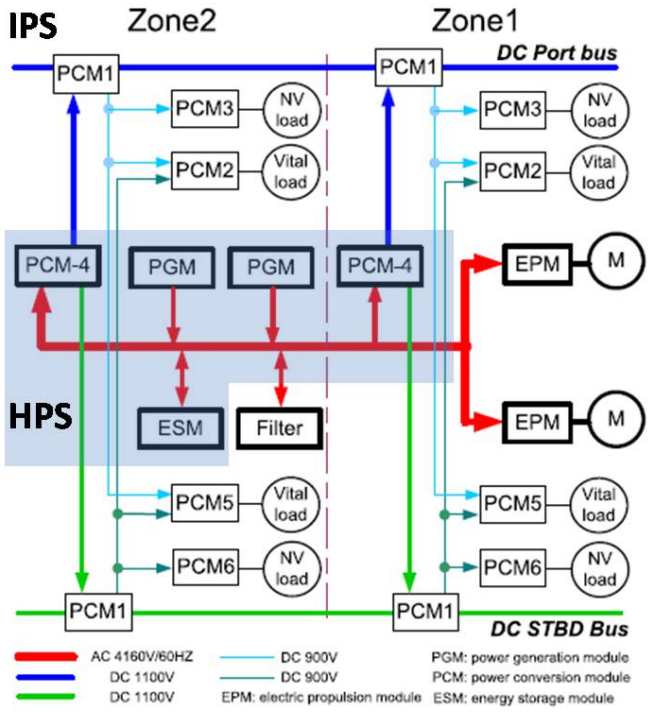

Figure 1.1: One-line diagram for integrated power system of an all-electric ship [4].

The all-electric ship for military applications considers the zonal electric distribution system (ZEDS) [4] as an architecture for power distribution (Fig. 1.1). Unlike the traditionally used radial distribution system, the ZEDS employs the dual port/starboard bus configuration. Such an arrangement enhances survivability by providing redundant flow paths for vital loads and by preventing the damage or faults occurring in one zone from propagating to the others.

Fig.1.1 illustrates a one-line diagram of the two-zone IPS with the zonal architecture. The two main buses of the ZEDS are simultaneously powered by both the primary power generation unit (marked as PGM1 in Fig.1.1) and the auxiliary power generation unit (marked as PGM2 in Fig.1.1), where the latter provides power for the ZEDS through a DC/DC converter. The main power generation system also provides power for the ZEDS through cascaded power conversion systems, which consist of a rectifier (AC/DC) and a DC/DC converter. In addition, an energy storage device is essential in order to improve the transient performance of the hybrid power system when large amount of power needs to be released quickly. Therefore, a bidirectional DC/DC converter is placed between the energy storage device and the DC bus. The PCM-4, which consists of the three isolated DC/DC converters, serves as the power conditioning system for the main power generation, auxiliary power generation and energy storage systems. The output terminals of the three converters for the PGM's and the ESD, that are connected together to feed DC buses of the ZEDS, forms a DC Hybrid Power System (DHPS) (shaded area in Fig 1.1) for an AES [5, 6].

1.2 Hybrid Power System

While the IPS is a classic example of the HPS in marine applications, many other stationary and mobile power generation stations also employ HPS. Other applications that utilize HPS are wind-diesel systems [7], [8], micro grids [9], hybrid trucks [10] and plug-in hybrid vehicles [11]. There are many characteristics that are shared among the HPS regardless of the type of application. First is their large scale and interconnected nature due to the multiple components involved. Second is the utilization of heterogenous power sources for hybridization. Third is the nonlinear dynamics of the HPS components.

These features, if leveraged appropriately, can be quite beneficial to achieve fuel

economy, reduce emissions and improve reliability. The wind energy, if combined with micro-hydro or diesel power generation, can provide low cost and high reliability power solutions for island and remote area communities. The integration of fuel cells into shipboard power systems [12, 13] and automotive power-trains [14–16] results in low emissions and high system efficiency.

However, in order to fully utilize the complementary characteristics of HPS components, coordination between them is essential. While the interconnected nature of HPS offers higher reliability, it also presents challenges in terms of managing individual components and their interactions. These challenges are more pronounced for the HPS used in military applications, as they have to operate in adverse conditions and deal with possible battle field damage. On the one hand, during normal operating conditions, the HPS has to meet the time varying power demands for a wide range of scenarios such as weapon launch, hard acceleration, crash stop, etc. On the other hand, the HPS has to satisfy resilience and survivability requirements to recover from damage quickly. While the requirements of high performance necessitates fast and efficient load following, those of survivability dictate stringent safety enforcement for device protection. These two mandates make most heuristic methods ineffective for the control of the HPS and motivates the need for systematic and rigorous study and development of power management schemes.

1.3 Power Management

The power management strategizes to effectively coordinate multiple power sources and loads, actively manage thermal and mechanical couplings, and strictly enforce constraints in order to achieve desired performance goals and assure safe system operation. For the HPS targeting military applications, the PM design has to consider two distinctive modes of operation, namely the normal and failure modes, each with

different objectives and challenges.

Normal mode: The goal in this mode is to support missions such as pulse weaponry or aircraft launches. The objective is to achieve mission effectiveness, as defined as the ability of the HPS to quickly meet the load demand while maximizing fuel economy throughout the mission. In this mode, achieving superior performance, measured by mission effectiveness, is a key consideration.

Failure mode: The goal in this mode is to protect the HPS from potential failures without causing further damage. The objective is to improve survivability, as defined as the ability of the power management system to sustain critical shipboard operations and restore normal functions without causing safety violations of the HPS components. In this mode, ensuring system safety is a key consideration.

The shipboard mission requests are represented as power demand profiles, where the demand information associated with the entire mission is known at the time of the request, thereby providing look-ahead opportunities for power management. In addition, some of the critical missions have to support pulse power demand requests. Hence optimal control is a natural formalism for solving the HPS power management problem. This involves determining an optimal control input sequence (e.g. input to the power plants, power electronic devices and others) as the solution to minimize a cost function (e.g. the penalty on power tracking error, fuel consumption and other performance variables) subject to constraints (e.g. control saturation, surge protection, critical demand sustainability). For the AES applications, the control design has to deal with the following problem characteristics regardless of the modes of operation:

- The *On-demand* goal driven by the lack of a priori knowledge of power demand profiles associated with mission requests during normal mode and unpredictable

timing and the nature of component failure.

- Long time horizons associated with the mission requests in the normal mode as well as a backup component's warmup period during the failure mode.
- Active use of energy storage to support pulse power demands during normal mode and critical load demands during failure mode.
- Difficulties in obtaining analytical models for HPS components.
- Presence of disturbances in the HPS, such as load fluctuations.

In order to achieve the on-demand goal, the optimal control solutions have to be computed online, thereby making the real-time execution of the power management algorithm without computational delay a key requirement. In order to achieve fast load following in the presence of disturbances, the control algorithm must be robust. In addition, during the failures, the controller must be able to enforce component safety throughout the extended horizon while the back-up strategies are being activated. These two mandates, along with the need for real-time execution, make the control problem challenging, given the non-linear and high dimensional HPS dynamics.

1.4 Literature Survey

Addressing the HPS power management within an optimization framework requires a dynamic HPS model and a real-time feasible optimization algorithm. Hence a survey of the most important work on the PM as well as HPS modeling relevant to this dissertation is presented. The power management problem of integrated systems involving multiple power sources has been studied in many applications including land hybrid vehicles [10], [17–23], shipboard power systems [24–31]and portable electronic

devices [32–36]. Each of the applications have different perspectives and treat the problem using a specific set of control methodologies.

1.4.1 PM in Land Hybrid Vehicles

The existing work on power management in commercial land hybrid vehicles has been primarily driven by a need to improve fuel economy and reduce tailpipe emissions. In light of these goals, the power management problem has been treated as a trajectory optimization problem [37], where many optimization based methods have been used.

Trajectory Optimization

An excellent summary of the optimization methods used for solving trajectory optimization problems is available [38]. These methods include dynamic programming (DP) [39], stochastic dynamic programming (SDP) ([18–21] and references therein) and equivalent consumption minimization strategy based approaches (ECMS) ([22, 23]).

The DP based approach has been used to address power management for a hybrid electric truck [10] and a hybrid vehicle using fuel cell and battery [17]. This approach has the drawback of computational burden (namely, the *curse of dimensionality*) that makes it unsuitable for real-time control. Hence researchers have proposed many mechanisms at the implementation level to mitigate the computational burden. For example, iterative dynamic programming (IDP) has found wide-spread applications, especially in the chemical process industry ([40–44]). While this method could alleviate the computational complexity for some applications, it still retains the exponential computational effort with respect to the optimization variables.

The stochastic DP based approaches [18] have been considered in the literature for the power management problem for hybrid land vehicles, in order to address the real-

time control requirements. Here, the power demand was modeled as a Markov chain and the transition probabilities were determined using automotive drive database. Previously, the shortest path-stochastic dynamic programming (SP-SDP) has been proposed for solving the power management problem in order to reduce the tailpipe emissions in an electric hybrid vehicle [19]. Furthermore, linear programming techniques were used to simplify the SP-SDP approach. For the same application, more recently, research has shown performance improvement as compared to legacy controllers in terms of fuel economy by incorporating drivability metrics and using an SDP based approach [20, 21].

In addition to the above methods, an equivalent consumption minimization strategy has also been proposed to determine an implementable controller for the power management [22]. A similar approach for the power management of an experimental fuel cell/supercapacitor-powered hybrid vehicle has been proposed to achieve real-time control [23]. While a great deal of work has been done in PM, most of it focuses on hybrid power systems that are used in commercial applications and hence improving survivability has not been a key consideration.

Receding horizon control

Even though the existing work for the land hybrids have been treated as a trajectory optimization problem, model predictive control (MPC) [45, 46] is another approach that is applicable for the problem under consideration. This approach has been widely used to solve constrained optimization problems given its suitability for real-time implementation as compared to trajectory optimization. Here a relatively short horizon can be considered for solving the optimal control problem and the receding horizon approach is adopted to deal with the longer horizon. The sequential quadratic programming (SQP) [47] based optimization algorithm has been widely employed to solve the MPC problems. There has been a lot of research in improving

the computational efficiency of this algorithm. An integrated perturbation approach has been proposed to achieve real-time computational efficiency [48]. Collocation-based methods have also been proposed to improve the computational effort of the SQP algorithm [49]. It must be noted that most of these algorithms require either computation or a good approximation of the second order derivatives of the cost function.

1.4.2 PM in shipboard power systems

As compared to the land hybrid vehicles, the power management for shipboard power systems is a relatively new topic of research. While some of the approaches for hybrid commercial land vehicles may be applicable for shipboard power systems, a new set of shipboard specific characteristics (e.g. multiple sources and loads etc.) adds new challenges and demands new effective design and analysis approach to deal with power management. The existing literature for PM in shipboard power systems have primarily focused on recovery from power system failure through network reconfiguration [24–26], where the goal is to determine alternate power flow paths for load restoration based on the load priority after damage.

Many different techniques such as multi-agent, expert system and optimization based methods have been proposed to address this problem. An optimal load shedding strategy has been proposed by solving a static optimization problem with line current constraints using linear programming algorithm [27]. A restoration strategy based on an expert system has been proposed [28]. This is a centralized scheme, where a rule-based approach is used to restore de-energized loads and the maximum line current and generation capacity are treated as constraints. A decentralized version of this approach using multi-agent techniques have also been proposed [29–31]. In all these works, the performance in terms of fast load following or system efficiency improvement have not been considered.

1.4.3 PM in portable electronic devices

In portable electronics, the power consumption is managed through reconfiguration between active and sleep modes to extend the battery life. Extensive literature can be found regarding power management in portable electronics that is solved using predictive as well as stochastic techniques [32–36]. Even though the portable devices present an interesting application for the PM problem, most of the optimization techniques deal with lower dimension systems.

1.4.4 Modeling of HPS

A great deal of work has been done in developing high fidelity models for the HPS components such as those for the gas turbine [50–52], fuel cells [53–55], and power converters [56]. A detailed compressor model for gas turbines has been proposed [51] and a gas turbine model for heavy duty applications such as stationary power generation has been developed using the real world experimental data [52]. The existing work on the fuel cell modeling includes both solid oxide (SOFC) and polymer electrolyte membrane (PEM) fuel cells. A six state model using minimum Gibbs free energy method was proposed for developing models for the SOFC [55], while a ten state model for the PEM fuel cell has been proposed in [54].

The existing work for the shipboard application has only considered the SOFC-GT modeling which focuses on the combined heat and power generation (CHP) system [57–59]. However, the GT models used in the CHP applications are for smaller sized units, since they are used as auxiliary devices to recover heat from the fuel cell exhaust and, therefore are unsuitable for power generating units in shipboard HPS.

1.4.5 Dissertation Scope

A discussion on the gap between what is available in the literature and what is required for the control of HPS targeting military AES is essential to set the scope of this dissertation. The control of HPS requires both effective power management schemes as well as power converter control. The power management determines the optimal power split among multiple sources and energy storage while the power converter control tracks these optimal power demands as quickly as possible.

While the problem of the power converter control for shipboard applications in order to achieve fast demand tracking has been effectively addressed [60, 61], the design of a power management strategy for shipboard application remains largely unaddressed. One may argue that an easy way to approach this problem is to leverage the methodologies used in land hybrids. Even though the state-of-art HPS power management in commercial land hybrid vehicles is mature, the unique characteristics along with the requirements for the military shipboard power systems, raises several unsolved issues that call for new methodologies for design, analysis and implementation of power management for hybrid power systems in AES for military applications:

- *HPS models targeting AES applications*: While many high-fidelity models are available in the literature for the individual HPS components, an integrated model suitable for the AES application is required. Note that the existing models for CHP systems targeting marine applications cannot be used to model the shipboard HPS. This is because the gas turbines used in these systems are treated as auxiliary units and have lower power outputs and cannot meet the ship service power requirements. For that reason, an HPS model which is appropriately rated to meet the ship-service power requirements needs to be developed, given the challenges due to the lack of availability of experimental data for the power sources in the public domain. Such a model should be simple

enough for control design and also capture all the relevant component dynamics.

- *Real-time control for on-demand mission planning:* While the HPS power management shares common goals (e.g. fuel economy) between commercial land vehicles and military AES, the key differences lie in the problem characteristics between the two applications namely:

    1. The large dimensional nature of the AES power management due to the multiple power sources as well as the extended horizons. Here, the control has to manage power flows between multiple power sources and energy storage as compared to a single engine and electric motor in land vehicles.
    2. The larger constraint set due to the many components involved, namely the hard constraints associated with the physical component limits such as gas turbine surge/stall, fuel cell starvation, battery state of the charge maintenance, critical demand satisfaction, etc.
    3. The pulse power demand requirement to support critical missions such as weapon or aircraft launches, during which both transient performance and constraint enforcement are critical.

    These features, compounded with the on-demand goals and lack of a transition probability function for the AES application, necessitates the development of real-time feasible control methodology for the shipboard HPS power management.

- *Improving Survivability during failure*: This issue is typically not a consideration for the land hybrid vehicles used for commercial applications. For shipboard systems, existing work partially addresses the survivability issue, where network reconfiguration and load-shedding have been used to deal with component failures. However in order to improve the survivability for HPS used in military

applications, alternative strategies need to be explored so that loads can be sustained as much as possible even during failures. Since the on-board energy storage capacity is limited, the big challenge is to determine the means of managing the power flows from working sources and energy storage devices given that each of these components has physical operating limits.

This dissertation focuses on the development of tools and the control methodologies to address the real-time power management for the HPS, which deals with the problem characteristics similar to those of the AES targeting military applications. We consider a hybrid power system (HPS), whose configuration is shown in Fig. 1.2. The HPS used in this dissertation is an abstracted and a scaled representation of the IPS (Fig. 1.1), where the heterogenous power generation units are represented using Power Sources 1 and 2. The two uni-directional and one bi-directional power converters used in Fig. 1.2 represents the PCM4 in the ZEDS (Fig. 1.1), while the energy storage captures the functionality of the ESD in the IPS. We use this abstraction for two reasons:

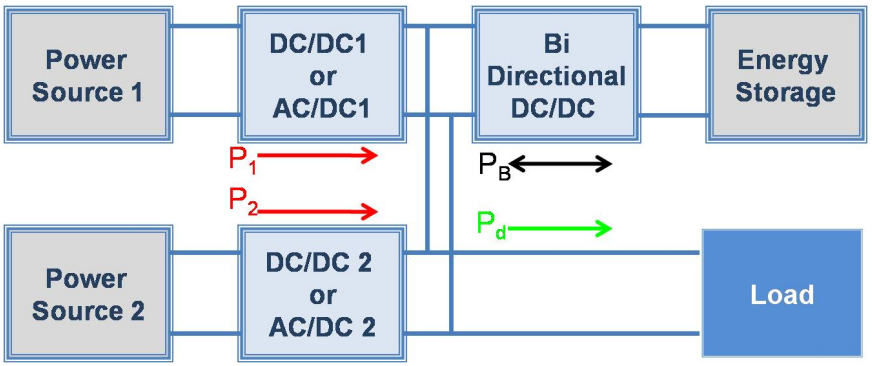

Figure 1.2: Schematic of a Hybrid Power System.

1. The control methodologies developed for the HPS considered in this dissertation can be directly applied to the power management of the IPS. In addition, the controller validation using this HPS is much simpler as well as cost-effective to build the HPS test-bed as compared to the IPS given the university setting.

Hence this HPS configuration can be used for pursuing all research related activities for the AES applications.

2. While the considered HPS configuration in Fig. 1.2 captures the features of shipboard power systems, it is also quite generic and hence can be used to pursue other research activities for the HPS used in Auxiliary Power Unit (APU) such as those in automotive applications.

The research effort is focused on both model and control development as well as real-time implementation.

1.5 Key Contributions

The contributions of this dissertation on real-time power management of the HPS for AES applications are highlighted in Fig. 1.3 and are summarized as follows:

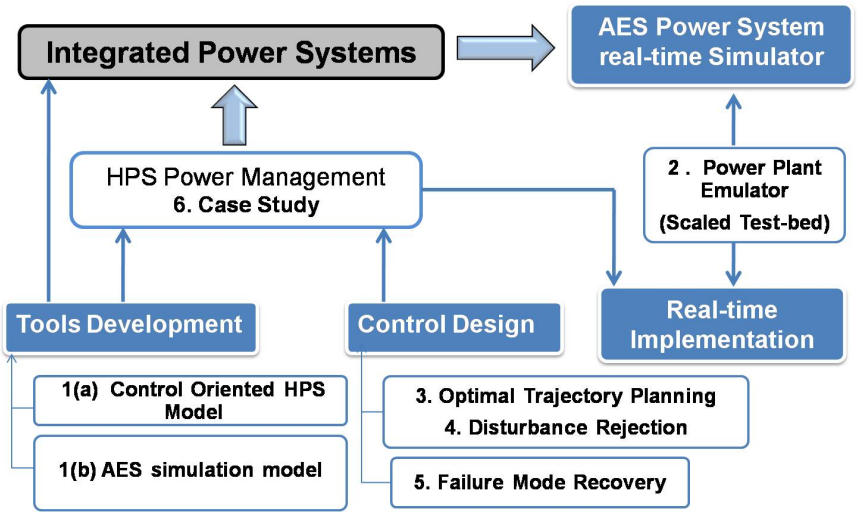

Figure 1.3: Key Contributions and Research Road-map

1. *Model Development*

   (a) An optimization-oriented dynamic model of the HPS that consists of a gas turbine, fuel cell and energy storage device targeting shipboard applica-

tions was developed as a numerical tool for power management strategy development.

(b) This model has also been integrated with ship-board power distribution and service load network models to serve as a numerical test-bed for the failure emulation and monitoring of shipboard power systems, thereby providing an effective tool for AES system level research.

2. *Hardware Test-bed Development:* This was a collaborative effort between the members of the Real-Time Advanced Controls Engineering (RACE) lab. As part of this work, the power plant emulators to represent the electric characteristics of gas turbine/generator sets and fuel cells was developed. The emulators will provide the scaled test bed for control strategy validation for the multi-load, multi-source power management systems.

3. *Optimization Methodology Development:* A novel two time-scale optimization methodology for HPS real-time trajectory planning using a sensitivity function (SF) based gradient method has been developed and implemented on the Opal®RT real-time simulator. The novelty of the proposed methodology lies in the following aspects.

(a) Identified a specific structure in the computation of the SF, namely the band diagonal structure, and effectively utilized this to reduce the effort required to compute the SF which directly reduces the overall computational effort of the optimization method.

(b) Instead of developing methodology for solving a generic trajectory optimization problem, the design focused on exploring HPS system dynamics to achieve real-time control. One such property, namely the multi-time-scale property, was utilized not only to leverage the band diagonal structure

but also approximate the optimal control solutions using two-time-scale optimization, where the approximations at each level can be made available sooner than the true optimal solutions.

The key merits of the proposed design are, (1) real-time computational efficiency and (2) real-time performance improvement.

4. *Normal Mode PM Strategy Development:* A real-time hierarchical controller for normal mode HPS power management was proposed and implemented. The focus is on achieving optimal power split between power sources and energy storage in terms of fuel economy and fast demand following to support critical missions. The novelty lies in the hierarchical controller development which (1) utilizes the energy storage to quickly support pulse power demands (2) leverages time scale separation to achieve optimal power split in real-time between power sources and (3) achieves zero steady state error by formulating an offset-free linear quadratic tracking problem around the optimally planned trajectories. The key merit of the proposed hierarchical approach, as compared to a holistic one, is that both the long term optimal power demand planning and short term disturbance rejection can be solved in real-time within a sampling interval.

5. *Failure Mode PM Strategy Development:* A real-time reference governor based controller for the failure mode HPS power management was proposed and implemented. The focus is on improving survivability, namely ensuring system safety while energizing as many loads as possible until a backup source is activated. The main idea is in exploring the primary considerations of the failure mode PM, namely safety enforcement and leveraging this to treat the performance (in terms of load following) as secondary to the constraint enforcement. This allows the reference governor based method to be utilized for constraint satisfaction given the benefits of computational simplicity. A two level controller is

proposed, where a sub-optimal power split that is required to meet the total HPS demand is determined, after which the reference governor enforces safety constraints. The key merit of this approach is that the long term constraint enforcement could be achieved in real-time within a sampling interval.

6. Two separate case studies for the shipboard power management during normal and failure modes were developed. A hypothetical weapon launch scenario was considered for the normal mode and a power source failure was considered for the failure mode. The proposed controllers were experimentally validated on the scaled test-bed and real-time computational efficiencies were achieved for both normal and failure modes. Comparison of the proposed method as compared to the receding horizon controller was performed in terms of computational effort and performance. The proposed controller yielded better performance in terms of power tracking and fuel economy along with constraint satisfaction.

To the best knowledge of the author, this work is one of the earlier reported studies on the real-time power management strategy to achieve fast and efficient demand following as well as survivability for the HPS used in AES military applications.

1.6 Dissertation Overview

The dissertation is organized as follows: In Chapter 2 the component models of the shipboard power systems are introduced and a control oriented dynamic HPS model is developed. A shipboard power system simulator and a scaled HPS test-bed is developed in Chapter 3, which will provide the rapid prototyping platform for the controller validation. A two-time-scale methodology for the real-time trajectory optimization for a system with multi-time-scale behavior is developed in Chapter 4, in order to address the optimal power split planning associated with power management

of hybrid power systems in AES applications. The closed loop power management of shipboard hybrid power systems during the normal and failure mode operations are proposed along with the respective case study in Chapters 5 and 6. Finally, Chapter 7 presents conclusions and discusses the future research plans.

Chapter 2

Modeling and Simulation of a Hybrid Power System for an All Electric Ship

A dynamic model for shipboard power systems is essential in order to solve the power management problem using model based design. The model should be detailed enough to capture the key characteristics of the AES power systems, but also has as few states as possible to facilitate model based design, analysis and real-time implementation. While this research is motivated by the AES for military applications, most of the work on power management, presented in this dissertation considers the HPS (Fig. 1.2) as a scaled but representative of the IPS (Fig. 1.1) used in AES. Hence, we develop two versions of the hybrid system model, each with specific scope:

Control-oriented HPS Model This model is developed to be used for control and optimization of HPS targeting shipboard IPS as well as auxiliary power units and is based on the configuration shown in Fig. 1.2.

Simulation-oriented IPS Model : This model is developed to be used for real-time simulation and analysis of IPS to facilitate AES research related activities and is based on the configuration shown in Fig. 1.1

For the system shown in Fig. 1.2, the power source dynamics, with time constants of the responses in the order of *milli s* to *seconds*, are slower as compared to the power converters with μs response times. Hence the control oriented HPS model considers only the dynamics of the power sources and with energy storage. A simulation oriented IPS model is then obtained by integrating [1] the HPS model with the zonal electric distribution model (ZEDS), which is comprised of power conversion modules, distribution, propulsion load networks. The road-map for the model developed in this chapter, along with the components considered is shown in Fig. 2.1.

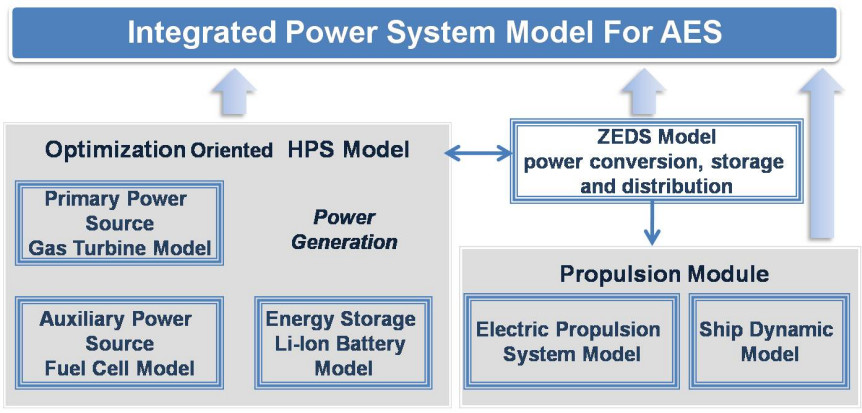

Figure 2.1: Model Development Road-map

Even though the components for the next generation AES have not been clearly defined, this dissertation considers representative units for the key components involved and are summarized as follows:

Power Sources This includes a single shaft gas turbine/generator set (GT) and a reformer/fuel cell (FC) system. They were chosen due to their complementary time response and efficiency characteristics, where the GT has faster response and the FC is slower but more efficient.

Energy Storage Device A Lithium-Ion battery pack, targeting military land hybrids, is considered, given its high power and energy density.

[1] The integration with ZEDS modules is a collaborative effort with the RACE lab members.

Power Converters This includes AC/DC and DC/DC converters to model the PCM 4 and PCM 1 shown in Fig. 1.1 as well as DC/DC converter and DC/AC invertor and DC/DC converter for the vital and non-vital loads.

Propulsion System The electric propulsion system consists of a AC/DC/AC variable speed drive system.

The component model development for the HPS and the IPS consists of a combination of both physical as well as empirical relationships. Even though the fundamental dynamics of some of the components are well established (e.g. [54], [50]), the lack of experimental data in the public domain for the individual components used in shipboard applications makes the model development challenging. For example, the difficulty in obtaining the gas turbine compressor and turbine performance maps. Our efforts focuses on 1) Scaling existing performance maps and validating the design point of this scaled gas turbine against a commercial one, 2) Validating the model output against typical characteristics such as speed protection for single shaft GT and hydrogen starvation for fuel cell.

In this chapter, all the components for the power generation modules, energy storage devices, power and propulsion subsystem are introduced. The optimization oriented HPS model is obtained by integrating the power source and energy storage subsystems, while the detailed IPS model for the AES is the HPS model integrated with the distribution and load networks. It must be noted that in the rest of the dissertation, the HPS model will be used for the controller development, while the IPS model will be used for shipboard power system real-time simulator (SPS) development. We present the dynamics analysis as well as the simulation results of the HPS model in this chapter and develop the SPS using the IPS model in the next chapter.

2.1 Component Models

2.1.1 Battery Model

Even though many battery models have been proposed [62] (and references therein), we consider the widely used resistance model. The battery voltage V_B is given as

$$V_B = V_{oc}(Q_B) - I_B R_B, \tag{2.1}$$

where V_{oc} is the open circuit cell voltage, Q_B is the charge and R_B is the internal resistance of the battery. For this work, we consider 23 modules of $VL34P$ Li-Ion battery with 70 cells per module. Using the data sheet, the open circuit voltage can be curve-fitted (Fig. 2.2) by a sixth order polynomial of the battery capacity (Q_B in Amp-Hr) and is given by,

$$\begin{aligned} V_{oc} = -2.372 \times 10^{-6} Q_B^6 + 0.0001555 Q_B^5 - 0.002856 Q_B^4 - \\ 0.009836 * Q_B^3 + 0.8005 * Q_B^2 - 8.669 * Q_B + 243.8. \end{aligned} \tag{2.2}$$

The internal resistance of the Li-Ion battery is assumed to be constant and is $R_{Batt} = 65\ milli\Omega$ per module.

2.1.2 Gas Turbine

The gas turbine model captures the dynamic characteristics of compressor, turbine, combustor and the coupling between turbine and compressor. Figure 2.3 illustrates the key components and the associated state and input variables. The combustor mass and temperature dynamics along with turbocharger rotational dynamics are considered, while the compressor and turbine air mass flows and efficiencies are modeled by empirical relations. The input to the gas turbine is assumed to be $JP5$

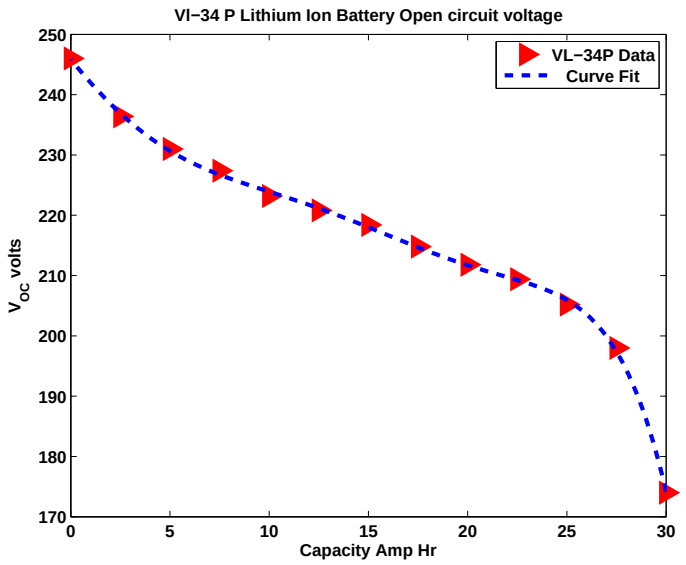

Figure 2.2: Open Circuit Voltage of VL34P Li-Ion Battery Module

fuel flow injected into combustor, and the torque input on the turbocharger shaft, reflecting the power demand, is the disturbance. The variables and parameters used in the GT model are defined in Table 2.1. The following standard assumptions have been made for the gas turbine model [50].

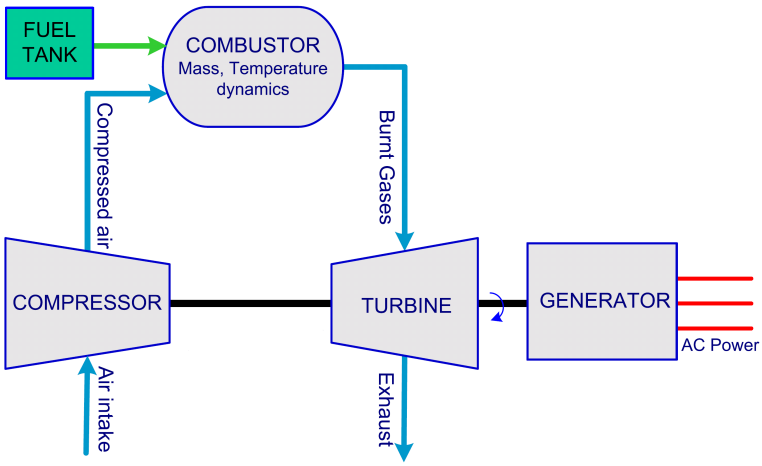

Figure 2.3: Schematic of a Gas Turbine/Generator set

- The heat loss in the compressor is negligible.
- Compression and expansion processes are adiabatic.

Table 2.1: GT Modeling Nomenclature

Variable	Description (Unit)
$c_{p,air}$, $c_{p,f}$, $c_{p,gas}$	Specific heat at constant pressure of air, fuel and burnt gas (kJ/kg K).
$c_{v,b}$	Constant volume specific heat for burner material (kJ/kg K).
J_I	Shaft inertia (Kgm^2)
m_b	Mass inside burner (Kg),
$M_{b,in}$	Molecular mass of air-fuel mixture inside burner (Kg/mole)
p_{amb}, p_b	Ambient and combustor pressure (Pa)
P_c, P_t	Compressor and Turbine Power (KW)
Q_{LHV}	JP_5 lower heating value (kJ/kg)
R	Universal Gas constant (kJ/K mol),
T_{amb}, T_{ref}, $T_{c,out}$, $T_{t,out}$, T_b	Ambient,reference, compressor outlet, turbine outlet, Combustor Temperature (K)
V_b	Burner Volume (m^3)
W_f, W_t, W_c	Fuel flow, Compressor, Turbine air flow (kg/s)
τ_{dem}, ω_{tc}	Load Torque (N-m), Shaft rotational speed (rad/s)
γ	Specific heat ratio
η_{gen} η_m	Generator electrical and Turbine mechanical efficiency (%)
$\eta_{is,c}$, $\eta_{is,t}$	Compressor and turbine isentropic efficiency (%)

- Fuel injector dynamics are much faster than the burner temperature and mass dynamics and are neglected.
- Perfect combustion occurs inside the burner.
- The generator is modeled as an efficiency transfer function from mechanical power input to electrical power output.

Under these assumptions, the equations representing the dynamics can be derived using first principles, such as energy, mass and power balance and curve fitting as follows:

Compressor, Turbine

The compressor and turbine mass flow and the isentropic efficiency (*Appendix A*) are obtained by curve fitting the performance maps scaled from an automotive application [63] using the techniques suggested in previous work [64, 65]. They are functions of pressure ratio ($\frac{p_b}{p_{amb}}$), combustor temperature (T_b) and the shaft speed (ω_{tc}).

The compressor power is determined using first law of thermodynamics and is given by

$$P_c = W_c c_p (T_{c,out} - T_{amb}), \tag{2.3}$$

where the compressor exit temperature $T_{c,out}$ is given as

$$T_{c,out} = T_{amb} \left[1 + \frac{1}{\eta_{is,c}} \left(\left(\frac{p_b}{p_{amb}} \right)^{\frac{\gamma-1}{\gamma}} - 1 \right) \right]. \tag{2.4}$$

Similarly the turbine power is given by

$$P_t = W_t c_p (T_b - T_{t,out}), \tag{2.5}$$

where

$$T_{t,out} = T_b \left[1 - \eta_{is,t} \left(1 - \left(\frac{p_{amb}}{p_b} \right)^{\frac{\gamma-1}{\gamma}} \right) \right]. \tag{2.6}$$

Combustor

The burner mass is determined using the mass balance and is given by

$$\dot{m}_b = W_f + W_c - W_t \tag{2.7}$$

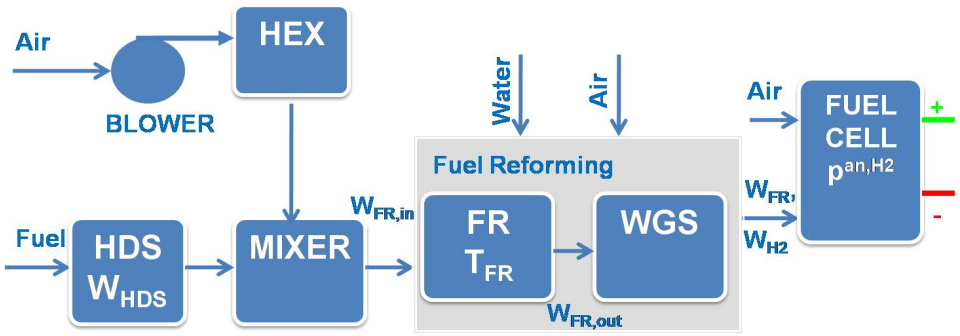

Figure 2.4: Schematic of fuel processing system

and the temperature is determined using energy balance as

$$\dot{T}_b = \frac{1}{m_b c_{v,b}} \left((W_c c_{p,air} + W_f c_{p,f})(T_{c,out} - T_{ref}) + W_f Q_{LHV} \right.$$
$$\left. - W_t c_{p,gas}(T_b - T_{ref})) - c_{v,b}(T_b - T_{ref})\dot{m}_b \right).$$

The burner pressure p_b is derived using ideal gas law:

$$p_b = \frac{m_b}{M_{b,in} V_b}(RT_b). \tag{2.8}$$

Rotational Dynamics

The shaft speed is determined using the power balance on the shaft given by

$$\dot{\omega}_{tc} = \frac{1}{J_I}\left(\frac{\eta_m P_t - P_c}{\omega_{tc}} - \tau_{dem} \right). \tag{2.9}$$

Since the torque input is directly applied to the single shaft gas turbine, the electrical power output is then given by $P_{elec} = \eta_{gen}\tau_{dem}\omega_{tc}$.

2.1.3 Fuel Cell and Reforming Unit

We consider a Polymer Electrolyte Membrane (PEM) fuel cell along with a fuel processing system (FPS). The FPS+FC (Figure 2.4) system consists of a hydro desul-

phurizer (HDS), heat exchanger (HEX), mixer (MIXER), fuel reformer (FR), water gas shift reactor (WGS), fuel cell anode dynamics and other components (blower, humidifier, etc.) which are not included. A detailed 10 state model of the FPS+FC system has been developed previously [54]. The effort here was to develop a reduced order model that still captures the system dynamics as well as operating constraints such as fuel starvation. Based on the linear analysis of the 10 state model around different operating points, we found that the dominant modes corresponded to the FR temperature, HDS and the anode hydrogen partial pressure. Therefore our reduced order model has three states. The inputs to the FPS+FC are fuel and air flow, while the stack current is considered as a disturbance. The variables and parameters used in FC model are defined in Table 2.2. The following assumptions were made for the simplified FC+FPS model.

- Due to the relatively large volume of the reformer, we assume that the dynamics associated with the fuel path are slower than those with the air path. Consequently, the cathode dynamics are neglected.
- WGS reactions are fast and perfectly controlled and hence the dynamics are neglected.
- The temperature inside the fuel cell is assumed to be controlled to remain constant.

Since the stack current (I_{st}) is measured, the fuel and air flow are determined by a static feedforward map to control the steady state fuel utilization (U_{H_2}) to 0.8 .

Hydro Desulphurizer

The HDS is represented as a large volume and is simplified as a first order lag with a slow time constant ($\tau_{HDS} = 5sec$) that reflects the slow dynamics of the linearized model [54]. The other two states representing slow dynamics in [54] are the FR

Table 2.2: FC Modeling Nomenclature

Variable	Description (Unit)
$c_{p,FR}$	Constant ratio specific heat of FR material (kJ/kg K)
E	Open circuit Fuel cell voltage (Volt)
h_{in}, h_{out}	Specific enthalpy (J/kg) of inlet and outlet FR flows
m_{FR},	mass inside the reformer unit (kg)
M_{an}, M_{H_2}	Molecular mass of anode material and hydrogen(kg/mol)
n_c	Number of fuel cells in the stack
N_{in}, N_{out}	Molar flow rates in and out of the FR (mol/s)
p_{an},$p_{H_2,an}$	Anode total and partial pressure (Pa)
R	Universal gas constant (J/K mol)
T_{FR}, T_{an}	FR and anode temperature (K)
v_{ohm}, v_{act}, v_{conc}	Ohmic, activation and concentration loss respectively (volt)
V_{an}	Anode volume (m^3)
$W_{FR,in}$ W_{FR,H_2}, $W_{FR,out}$	Total flow into the FR (kg/s) Hydrogen and total flow out of FR (kg/s)
$W_{H_2,react}$	Reacted Hydrogen inside anode (kg/s)
$W_{H_2,an}$, W_{an}	Hydrogen and total anode exit flow (kg/s)

temperature and the anode hydrogen partial pressure.

Fuel Reformer

The FR model is developed in the work done by *Jay et.al* [54] and is summarized here. The temperature dynamics using energy balance is given by

$$\frac{dT_{FR}}{dt} = \frac{1}{m_{FR}c_{p,FR}}\left[N_{in}h_{in} - N_{out}h_{out}\right] \tag{2.10}$$

where N_{in} and N_{out} are the inlet and the outlet flows to the fuel reformer respectively.

Anode

The anode partial pressure dynamic using mass balance is given by

$$\frac{dp_{H_2,an}}{dt} = \frac{RT_{an}}{M_{H_2}V_{an}}(W_{FR,H_2} - \chi^{an}_{H_2}W_{an} - W_{H_2,react}),$$
$$\chi^{an}_{H_2} = \left(\frac{M_{H_2}}{M_{an}}\right)\left(\frac{p_{H_2,an}}{p_{an}}\right), \tag{2.11}$$

where W_{FR,H_2} is the hydrogen flow from the reformer, W_{an}, $W_{H_2,react}$ are the anode outlet flow and reacted hydrogen as given in *Appendix B*. The air supply is assumed to be instantaneous and the cathode pressure follows the anode pressure.

Stack Voltage Model

The stack voltage is a function of the fuel cell temperature and pressure and is given by $v_{st} = n_c(E - v_{act} - v_{ohm} - v_{conc})$ and further details of this model can be obtained from the earlier work [54].

The component models for ZEDS and the propulsion module that will be used in the IPS model are presented in the remainder of this chapter.

2.1.4 ZEDS Module

We consider a DC ZEDS with a starboard-port bus arrangement for the two-zone IPS model (Fig. 2.5, repeated from Chapter 1 for easier reference), given the many advantages of DC zonal architecture as compared to AC [66] for shipboard applications. The key components of DC ZEDS are vital/non-vital loads and power conversion modules, where we consider 4 kinds of conversion modules [4].

PCM4 This is an AC/DC converter for converting the 3-phase 4100V-60Hz on the main bus to 1100V DC and 2 of these are used for the ZEDS model.

PCM1 This is a step-down DC/DC converter for converting the 1100V DC to 900V

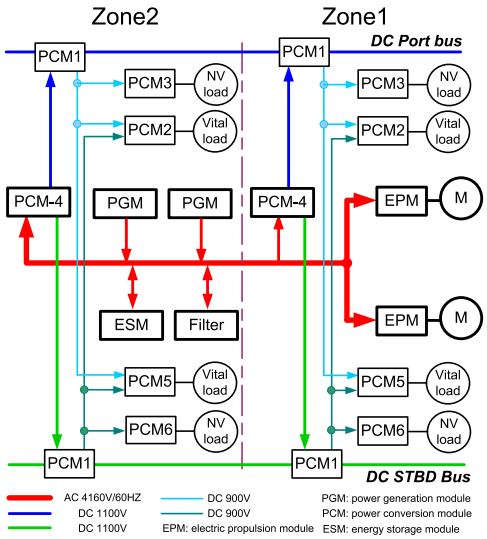

Figure 2.5: Schematic of two zone IPS

DC and 4 such PCM1's are used in the 2 zone ZEDS model

PCM 2/5 This is a DC/AC inverter used for the vital load on the port and the starboard side and two of them are required for each zone.

PCM 3/6 This is a DC/DC converter used for the non-vital loads on the port and the starboard side and two of them are required for each zone.

The models for individual components are discussed briefly in the sequel.

Power Conversion Module1 (PCM1)

Fig.2.6 shows the model of PCM1. PCM1 is a step down DC/DC converter with three reconfigurable switches S1, S2 and S3. The step down DC/DC converter is modeled with the 1-leg Time-Stamped Bridge of the ARTEMIS® toolbox while other PCM1 components are modeled with SimPowerSystems® toolbox. Manipulating the three switches can reconfigure the power flow path of each electric zone and facilitates the DC bus failure and recovery emulation. The output voltage of PCM1 is 900VDC which is 200V less than the main bus. The loads of PCM1 are one non-vital load and one vital load under normal situations. One vital load will be added if the opposite

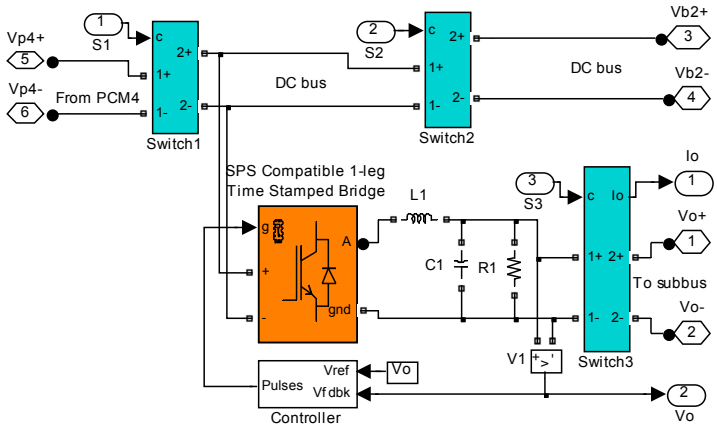

Figure 2.6: SimPowerSystems/ARTEMIS model of PCM1 in ZEDS.

main bus, which can be the starboard or the port side bus, or PCM4/PCM1 is down because of either equipment failure or battle damage.

PCM2/5 (DC/AC inverter for vital load)

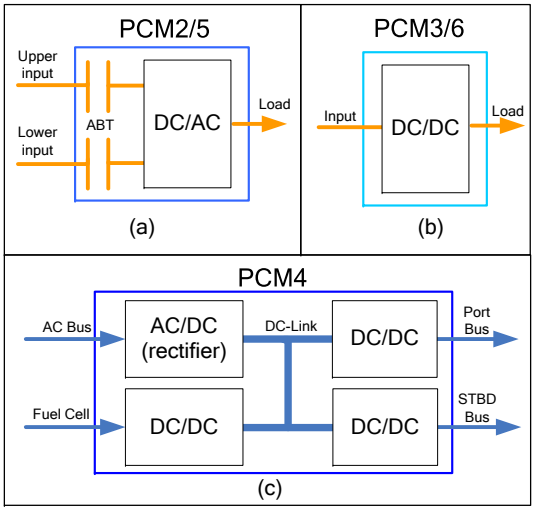

Figure 2.7: Diagram of PCMs in ZEDS.

Fig.2.7a shows the diagram of PCM2/5. PCM2/5 is a DC/AC inverter which is modeled with SimPowerSystems® Compatible 3-leg Time-Stamped Bridge of the ARTEMIS® toolbox. Since they energize the vital load which should be supported in any circumstance, there is an Auto Bus Transfer (ABT) circuit which can automati-

cally select power input port between the upper input and lower input. Usually the upper input has higher priority than the lower one and the switch from the upper to lower input happens only when the voltage of the upper port decreases to 100V lower than the lower input. However, to balance load for the two DC buses, the upper input will take over again if its voltage is recovered to 50V lower than the lower input.

PCM3/6 (DC/DC converter for non-vital load)

Fig.2.7b shows the diagram of PCM3/6 which is a DC/DC converter. In comparison with PCM1, PCM3/6 doesn't have the switches for load redirection. PCM3/6 is modeled with the 1-leg Time-Stamped Bridge of the ARTEMIS® toolbox too. There is no ABT in PCM3/6 given the nonvital nature of the loads connected to it. The nonvital load will lose its power if the main bus or sub-bus on its side is down.

PCM4

Fig.2.7c is the diagram of PCM4 which conventionally is an AC/DC converter converting three-phase AC power to DC power by controlling the rectifier firing angle. Since the power generation modules includes both gas turbine and fuel cell, PCM4 consists of both AC/DC as well as DC/DC conversion modules, where the output of AC/DC was connected with output of the DC/DC converter of fuel cell model through DC-Link. The proportion of power drawn from AC bus and fuel cell respectively can be dynamically managed by splitting the desired current to the two input converters. To get well regulated DC voltage on the port bus and starboard bus, there are DC/DC converters drawing power from DC-Link and regulating the voltage on the two DC buses to 1100VDC. The modeling of the two output DC/DC converters is similar to the DC/DC converter in PCM1, the buck converter topology is adopted and modeled with SimPowerSystems® compatible 1-leg Time-Stamped Bridge of the ARTEMIS® toolbox. Both of the output converters are regulated by their dedicated PI controller.

Loads

Vital/nonvital loads were modeled as constant power loads. All of the loads can draw a certain amount of power from the DC bus according to commands from the energy management module. More detailed load models such as those for DC motor or AC motor also could be modeled and integrated in the future.

2.1.5 Propulsion Module

Electric Propulsion System Model

The electric propulsion system modeled in this work consists of a three-phase AC/DC/AC variable speed drive system and a low speed, high torque Permanent Magnet Synchronous Motor (PMSM) driving the propeller. The AC/DC rectifier is modeled with SimPowerSystems® toolbox Universal Bridge. There is also a braking chopper on the DC-Link to absorb the regenerated energy by the motor at the crash stop situation. The AC/DC rectifier together with the DC/AC inverter works as the frequency converter and drives the propulsion PMSM, where the inverter is modeled with Time-Stamped Bridge of the ARTEMIS toolbox. The DC/AC inverter is controlled based on the PMSM speed error signal, where the output speed of the PMSM is measured. Other than the AC/DC/AC propulsion system (three-phase input), other AC propulsion technologies such as cyclo-convertor [67], matrix converter [68] and high temperature superconductor (HTS) motor [69] also can be modeled and integrated into the propulsion module in the future.

Ship Dynamic Model

The load torque to the electric propulsion motor is determined by the ship dynamic model, which calculates the ship speed and propeller speed according to hydrodynamic loads. The ship model given in [70] is adapted. It includes the added

mass and hydrodynamic forces and moments acting on the ship. Given a desired ship speed, the desired motor speed and torque are calculated in this module and fed to the propulsion motor control unit.

The component models have been implemented, tested and integrated using Simulink®. While the HPS model used for the controller development consists only of the power sources and battery pack, the simulation oriented IPS model integrates all of the components described above. Note that while the former is a lower order model suitable for design and optimization, the latter is a large-scale model that can only be considered for simulation and analysis purposes. In the rest of this chapter, we present the simulation results of the lower order HPS model that will be used in power management strategy developed in Chapters 4-6.

2.2 Optimization Oriented HPS Model: Dynamic Analysis and Simulation Results

The control inputs to the HPS model are the fuel flow to the gas turbine and fuel cell along with the battery current. The total power produced by the HPS is the sum of the power that can be generated by the sources and that drawn from the battery. The HPS model is analyzed using two metrics, namely efficiency and transient response speed, to verify that the developed model captures the benefits of hybridization. In order to establish that the power sources are complementary to each other, we consider that the transient power output response of the gas turbine should be much faster (about 5-10 times order) than the fuel cell. In order to validate the model behavior against typical open loop characteristics for GT and FC, the simulation results of the two sources are presented, where the step changes in load torque and stack current are applied to the generator and fuel cell respectively,

HPS Efficiency and Multi Time Scale characteristics: The GT and FC

models described above were simulated over the entire range of fuel inputs and the associated power output and efficiencies are summarized in Table 2.3. The lower and upper fuel input limits for the gas turbine are imposed by the surge and the stall phenomena. The GT has an output in the range 1531-4122KW, while a single fuel cell stack module outputs power in the range between 55-230KW. We consider an arrangement of eight fuel cell modules connected in series such that there is an overlap in the maximum power that can be drawn from the fuel cell (1840KW) and the minimum power produced by GT that is determined by its turn-off ratio. From Table 2.3, it can be seen that FC is much more efficient than the GT.

Table 2.3: FC, GT Key Characteristics

Variable	Fuel Cell	Gas Turbine
Power	$440 - 1840KW$	$1531 - 4122KW$
Fuel min-max limits	$0.022 - 0.124$kg/s	$0.137 - 0.345$ kg/s
Efficiency	$35 - 51\%$	$23.5 - 28.1\%$

To understand the complementary time response characteristics between GT and FC, we consider the speed of response from fuel input to power output as the metric given that the HPS model is nonlinear. More specifically, we consider the settling time of the response as the measure and look at the normalized step response from fuel to power for both the gas turbine and fuel cell systems for different fuel inputs inside the operating range. One such step response is shown in Figure 2.8. It can be seen that the settling time of gas turbine power output ($\approx 1s$) is about 7 times faster than that of the fuel cell ($\approx 7s$). Hence it can be said that the fuel cell and gas turbine exhibits complementary characteristics in terms of system efficiency and transient response.

To verify the transient response of a single shaft gas turbine, a step increase in the load torque (1780N-m to 2570N-m) was applied along with an increase in the fuel input, from $0.21kg/s$ to $0.3kg/s$, to support the increase in power demand in the

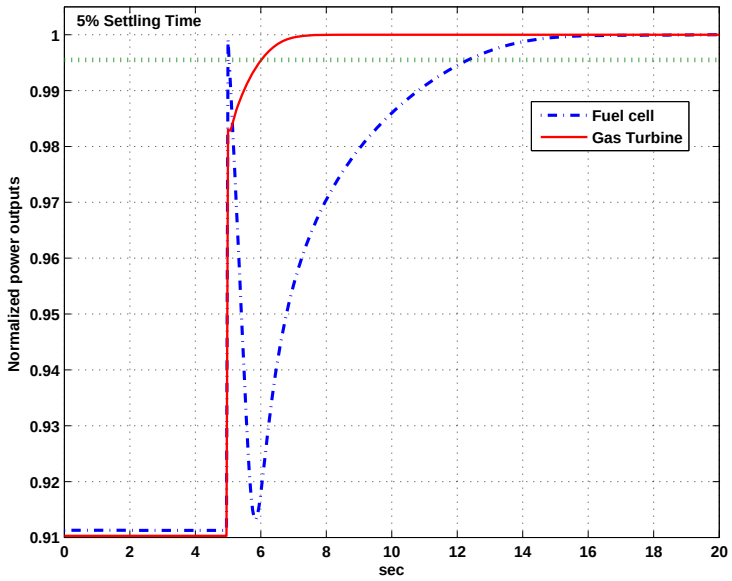

Figure 2.8: Normalized Step Response of a Gas Turbine and Fuel Cell

most efficient way (as suggested by the open loop optimization) and the simulation results are presented in Figure 2.9. Since we consider a single shaft GT, where the compressor, generator and turbine are all rotating with a common shaft, any increase in generator load (i.e., in power demand) will result in a drop in shaft speed, the extent of which depends on the shaft inertia. Consequently, the air flow decreases, which coupled with an increase in fuel flow, causes the mixture in the burner to be rich and lead to a transient overshoot in the burner temperature. After a short transient, the increased energy of the burnt gases drives the shaft to a higher speed, thereby increasing the flow through the system and providing the desired power demand.

Figure 2.10 shows the simulation results of the FC+FPS model (single unit), when the load current is increased from $240A$ to $280A$. Note that the feed-forward computes the desired air and fuel flows to reject for the step-change in stack current. While the air flow increase is almost instantaneous, the presence of the HDS slows down the fuel flow into reformer, thereby increasing the oxygen-to-carbon ratio and the reformer temperature. The delayed fuel flow also leads to a reduced hydrogen production,

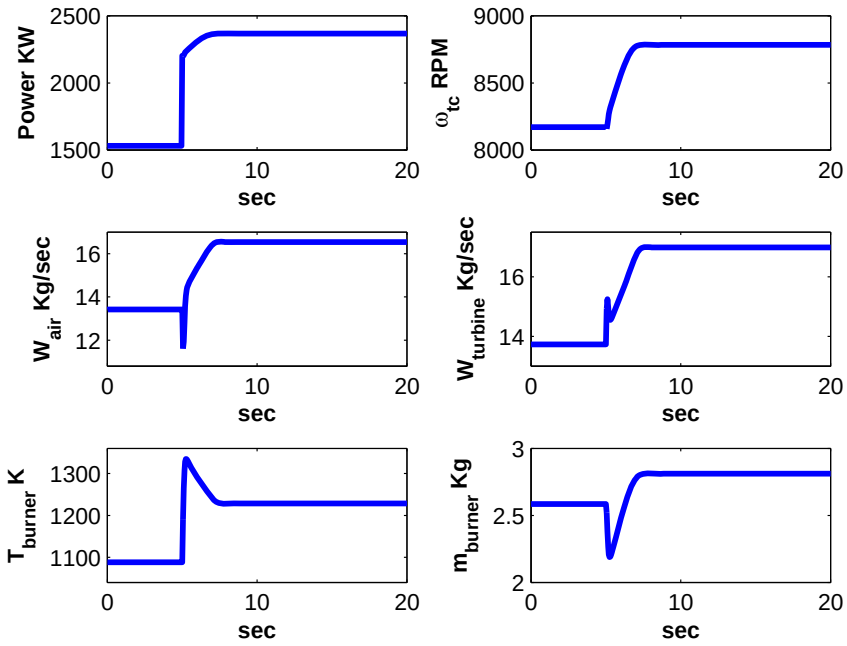

Figure 2.9: Step response of gas turbine

causing drops in both the partial pressure of hydrogen in the anode ($p_{H_2,an}$) and hydrogen mole fraction.

The instantaneous increase in power seen in Figure 2.10 at the initial phase of the transient can be attributed to the fact that there is a certain amount of H_2 in the anode at the time of the current step to support the reaction. However, this stored hydrogen is quickly depleted while the supply of H_2 is delayed due to the slow reformer dynamics. As a result, drawing the current at a higher rate cannot be sustained, thereby resulting in a non-monotonic power response. The concentration losses increase with the stack current and causes a transient undershoot in the stack voltage, the extent of the undershoot depends on the step increase in stack current.

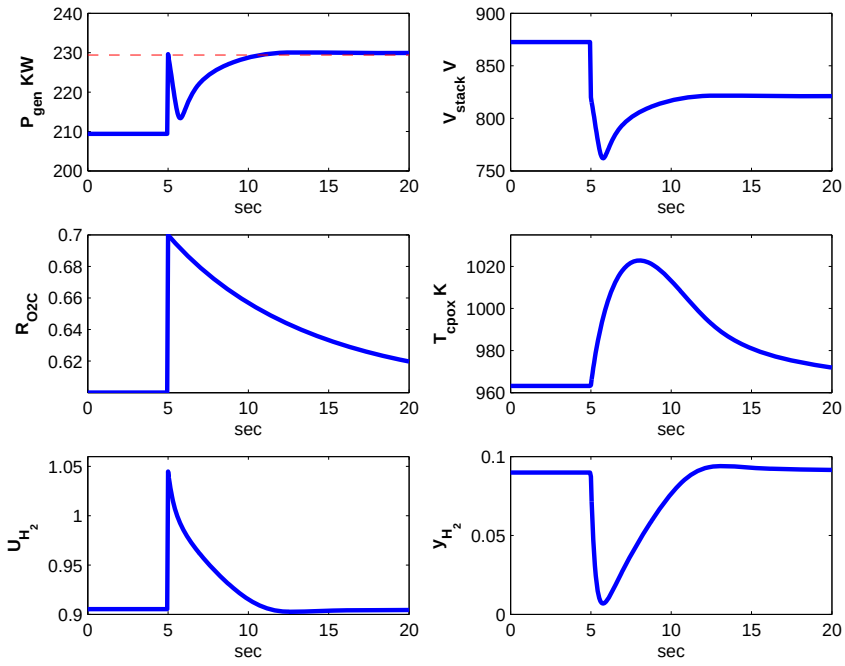

Figure 2.10: Step Response of a single fuel cell

2.3 Summary

In this chapter, we addressed one aspect in the tool designs and developed the component models required for both the optimization oriented HPS model and the detailed IPS model. We made the distinction that the HPS model, being a scaled and representative of the IPS model, will be used for methodology development in this dissertation, while the IPS model will serve as the real-time shipboard power system simulator for future AES research activities. The simulation results show that the optimization oriented dynamic HPS model is rated appropriately to meet ship-service power requirements. It also captures the nonlinearities such as compressor surge and fuel cell hydrogen starvation and indicates the expected response in the operating range.

Chapter 3

DC Hybrid Power System Testbed Development

While the previous chapter discussed the component modeling for both the scaled HPS model and detailed AES/IPS model, this chapter presents the hardware and tools required for establishing a rapid prototyping platform, in order to facilitate AES system level analysis and optimization. This platform is developed to serve two purposes, namely,

Shipboard Power System Simulator (SPS) This real-time simulator facilitates fundamental and advanced research activities for shipboard integrated power systems such as shipboard automation, failure mode analysis, etc.

Hybrid Power System Test-Bed This test-bed provides the real-time computation platform for controller implementation and validation for hybrid power system research related activities. While in this dissertation, the test-bed was used to demonstrate the real-time computational efficiency and performance of the proposed power management strategies, the scope of the test-bed is not restricted to this work alone. For example, the same test bed has been used for validating the power converter control schemes proposed in the previous work [61].

In order to accommodate both these requirements, the rapid prototyping platform should have the following features: (1) It has the real-time and digital simulation capability to support the modeling of complex and large scale systems such as the shipboard power system, (2) A complete hardware setup that can fully emulate all the functions of the hybrid power system components (e.g., power sources, energy storage device, power converters, etc.) (3) It is cost effective given that the research is undertaken in a university setting.

Even though this research is motivated by the AES application, the power management controller developed in this dissertation considers a HPS system. For the same reason, while a real-time simulator is developed for the detailed IPS model (Fig.1.1) for analysis, the hardware, i.e., the test-bed, is developed for the HPS model (Fig.1.2), where the latter is a scaled representation of the shipboard power systems. The entire hardware development is a collaborative effort among the members of Real Time and Advanced Control Engineering lab at The University of Michigan. At the core of both the SPS as well as the scaled HPS test-bed lies a PC cluster based OpalRT® real-time simulator. We first introduce the real-time cluster arrangement and then present the details of the SPS along with the real-time simulation results and the HPS test-bed.

3.1 OpalRT® PC Cluster

A PC cluster based simulation system has been considered for the real-time digital simulator given the low hardware cost, high simulation performance as well as the flexibility provided by the modular system architecture. RT-LAB® is a PC-cluster based expandable real-time simulator which is compatible with Matlab/Simulink®, thereby allowing effective leverage of commercially available MATLAB/Simulink® toolsets, such as control system design and analysis toolboxes, code generation toolboxes,

and Physical Modeling toolboxes. Specialized tools such as ARTEMIS® and RT-Events® support multi-rate fixed-time-step real-time simulation of power systems with dramatically improved computation speed and accuracy [71].

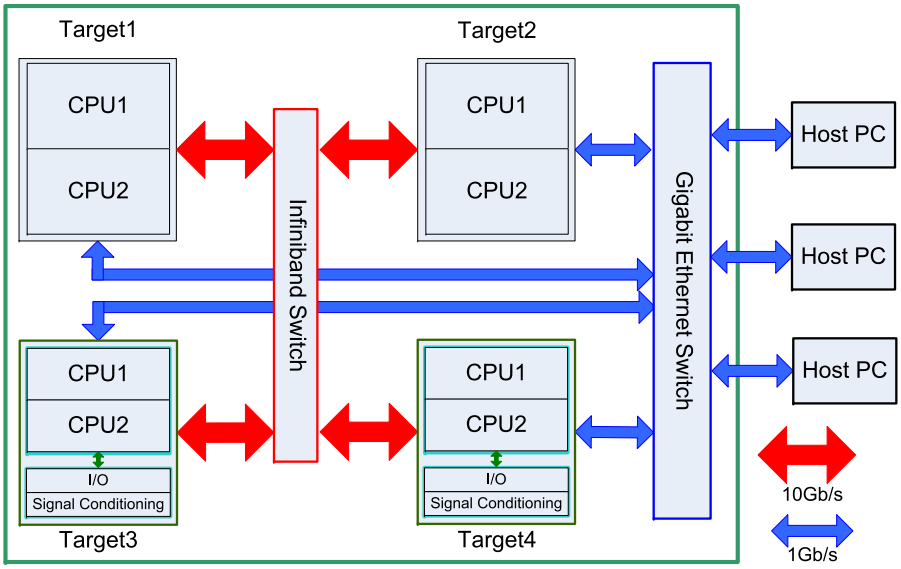

Figure 3.1: RT-Lab real-time simulation system configuration.

Fig.3.1 shows the configuration of the real-time simulation platform while its hardware is shown in. This system has 8 CPUs allocated in 4 physically separated targets. The CPUs in the same target exchange information through the shared memory while the different targets communicate through infiniband switch with 10Gb/s speed. There are three host PCs which can talk with each target via a 1Gb/s Ethernet switch. The targets can interact with the external hardware through 32bits PCI Bus I/O interfaces. Combining the FPGA event detection with specialized real-time interpolation algorithms toolbox RT-Events®, the effective I/O timing could be better than 1μs.

The I/O interface provides a platform for data acquisition and signal conditioning modules that enable the implementation of high frequency analog/digital I/O, event capture, and event generation. All of the targets and CPUs are synchronized either by software or by hardware. Thus all of the CPUs can synchronously interact with

the analog and digital I/O. This feature makes it possible for the system to implement physical components for hardware-in-the-loop simulation or to perform control prototyping experiments. The synchronized targets can run real-time simulations at different time steps, making it very flexible to distribute the complex model to different targets or CPUs within the simulation platform. In addition, the real-time simulator also can interact with other stand alone RT-Lab targets through Ethernet.

In this dissertation, the Opal-RT PC cluster will be the hardware that will be leveraged for SPS as well HPS test-bed delineated in the following sections.

3.2 SPS simulator

The SPS simulator is developed primarily to achieve real-time simulation of the AES integrated power systems represented using the detailed IPS model, whose components were developed in Chapter 2. Note that this detailed model can be obtained by integrating the optimization oriented HPS model with the ZEDS and propulsion modules. To develop the integrated model, all of the PCMs and loads are interconnected to form the two zones of the ZEDS. Then the ship dynamics and the propulsion model are added. The desired propeller torque and speed signals which are calculated by ship dynamic model are sent to the motor in the propulsion model. Then ZEDS and propulsion modules are connected with the power generation module.

It should be noted that the detailed IPS model is large scale in terms of the number of components involved and the associated state variables, and has multi-rate dynamic characteristics. For example, the dynamics of power sources are relatively slow, and sampling at 1ms time step is sufficient. On the other hand, PCMs have high frequency power switches, the subsystem time step is 50μs in our case which is much shorter than PGMs'. In order to get real-time simulation performance, the model has to be properly distributed among all the 8 CPUs of the SPS simulator (Fig. 3.1). Here

the factors that need to be considered during CPU assignment are: (1)Guarantee simulation performance by eliminating the overruns; (2) Assure data integrity by reducing the inter-target communication. Therefore, we consider the arrangement shown in Fig. 3.2, for the SPS simulator, where we assign one CPU for subsystems PGM (Gas Turbine), PGM (Fuel Cell) and EPM while splitting the ZEDS into two subsystems with two associated CPUs.

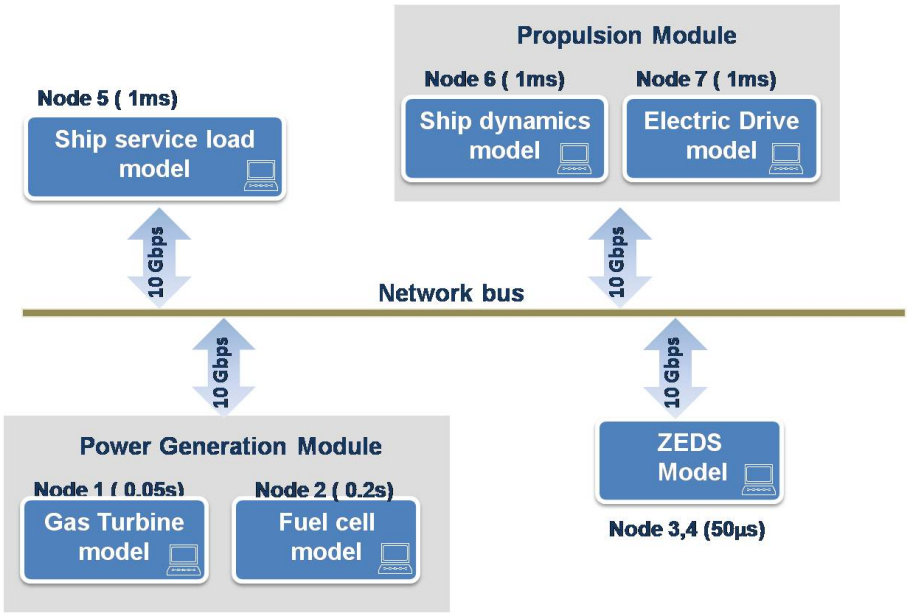

Figure 3.2: Schematic of the SPS Simulator.

Real-time IPS Model Simulation Results

The transient response, failure emulation and power flow path reconfiguration capability of the IPS model were validated by running the SPS simulator developed above. We consider the ship propulsion power requirement as 1.3MW and a ship-service load of 330 KW.

Fig.3.3 shows power consumed by loads during a failure and reconfiguration process where four scenarios are represented. Scenario 1: the port bus and local PCM1/PCM4 is down, the non vital load loses its power while the vital load draws power from the

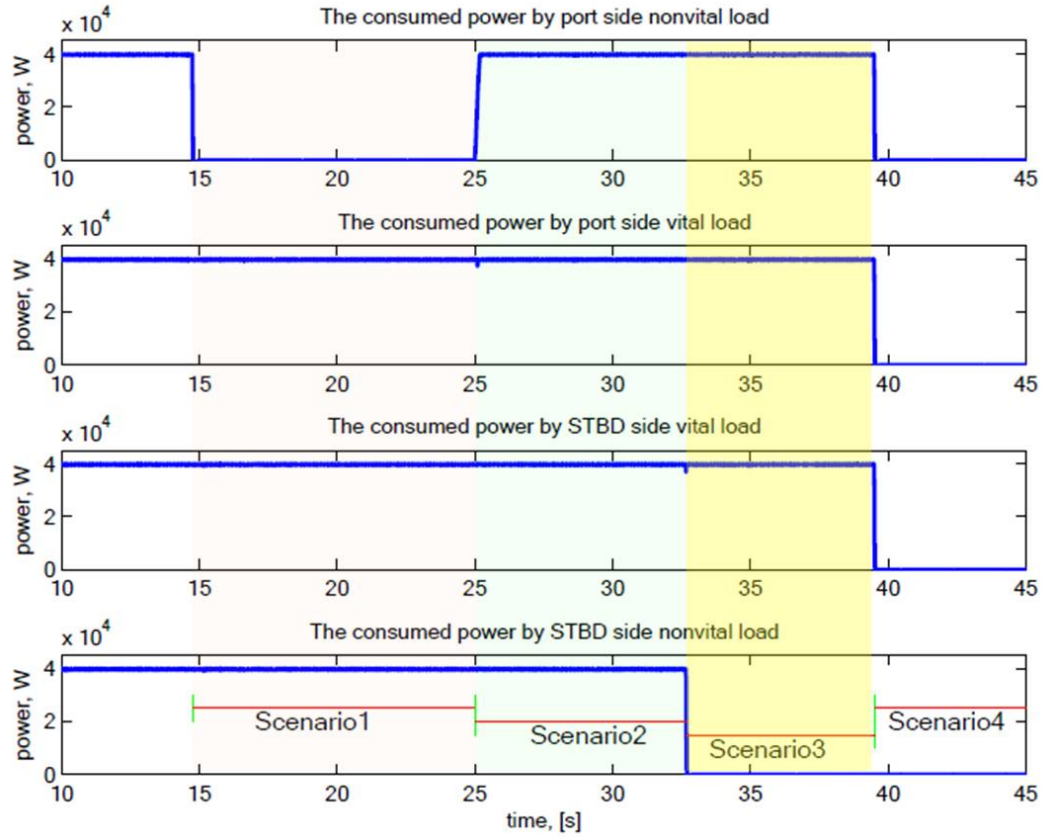

Figure 3.3: Power consumed by loads at failure and reconfiguration scenarios.

STBD bus. Scenario 2: the port bus is reconfigured or the PCM1/PCM4 is recovered, all loads draw equally 40KW power from both buses. Scenario 3: the STBD bus is down which leads to the STBD side nonvital load losing its power. The vital load works fine since it is switched to draw power from the port bus. Scenario 4: both buses are down, consequently all of the loads lose their power. This testing verified the failure emulation and reconfiguration capability of the ZEDS model, which is critical to enable the algorithm development of intelligent reconfiguration of ZEDS in the future.

Fig.3.4 shows the transient response of the propulsion motor when the ship speed is accelerated from 0 knot to 8 knots. It can be seen that, during the launching, the actual torque is larger than the desired value which can be attributed to modeling

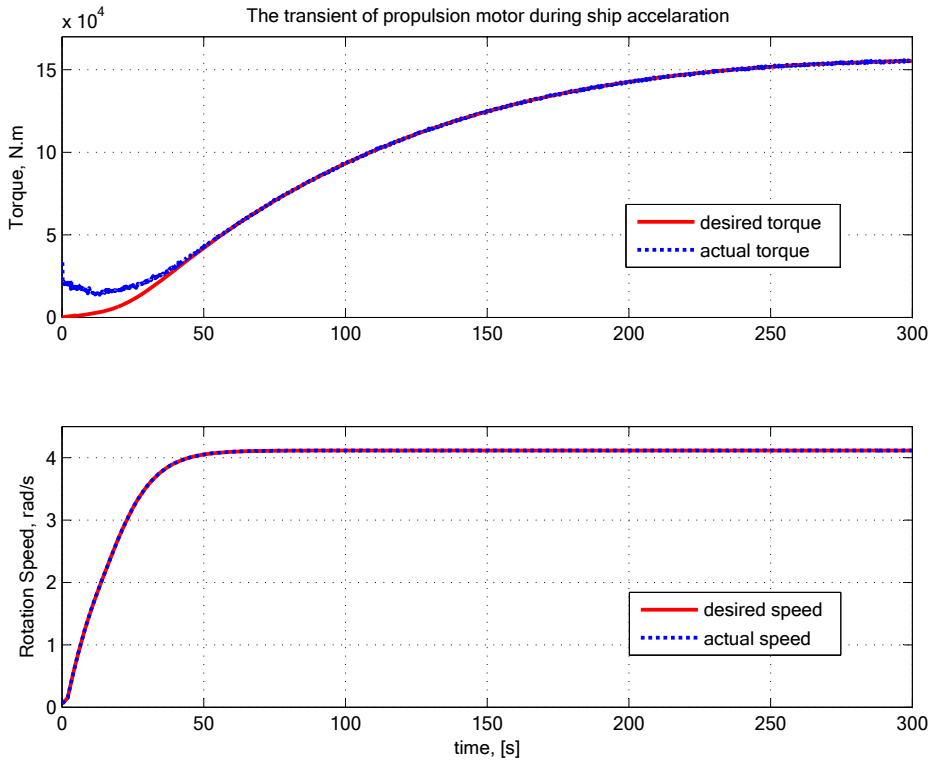

Figure 3.4: Propulsion motor transient.

error. However, both the actual torque and speed curves match with the desired curves very well after that, which confirms that the propulsion model captures the ship dynamic model as required.

3.2.1 Graphical User Interface (GUI) Development

A graphical user interface needs to be developed as a front-end to the SPS simulator in order to have user-friendly simulations of the failure and drive scenarios and also monitor the signals during the simulation remotely.

The GUI was developed using LabView® and it uses the TestDrive® V2.1.3 software in order to communicate in real-time with the SPS simulator for data acquisition. The design is such that the top level GUI (Fig.3.5) is similar to the structure shown in Fig.1.1, where the displayed signals can be used to indicate the health and status

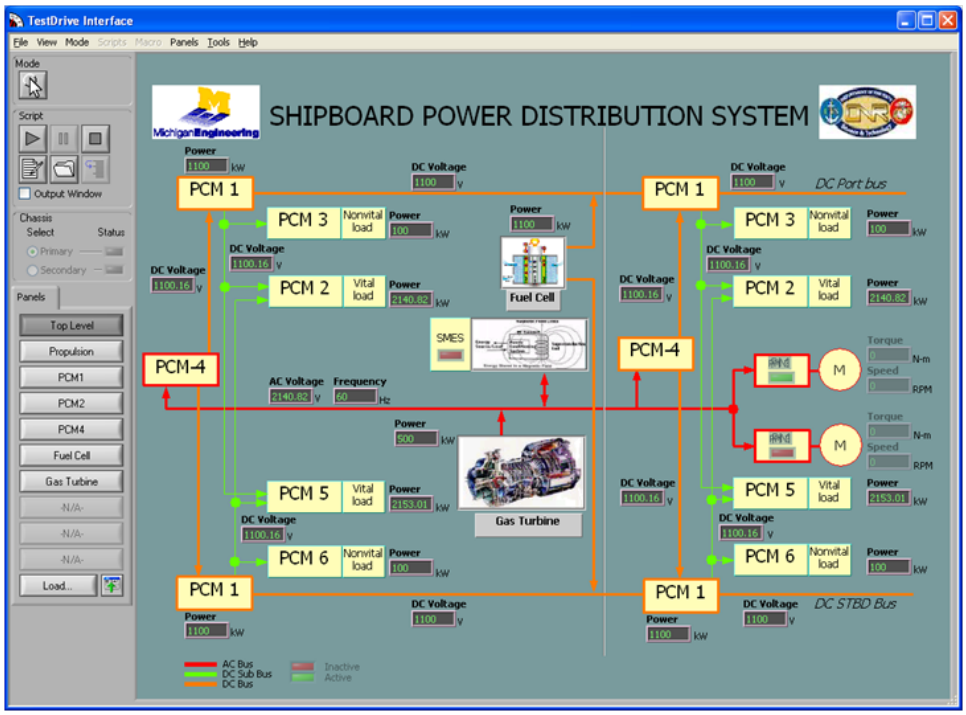

Figure 3.5: The top level GUI of the IPS.

of the system. All the control and monitoring signals for each of the subsystem are displayed in the sub-level GUI's.

As an example, the Failure, Reconfiguration, Operation and Drive Scenarios (FRODS), a sub-level GUI for power management, is given in Fig.3.6. The FRODS GUI is the one which can set the ship speed, emulate PCM or DC bus failure and reconfigure the power flow path. The buttons on the GUI, corresponding to Switch1, Switch2 and Switch3 of PCM1 in Fig.2.6, can be pushed on or off to emulate bus crashing or to redirect the power flow. Numeric boxes next to the PCMs allow manual inputs to change the loads associated with corresponding PCMs. The ship velocity command knob controls ship speed. The two waveform charts (at the upper right corner) display the desired and actual speed and torque for the propeller.

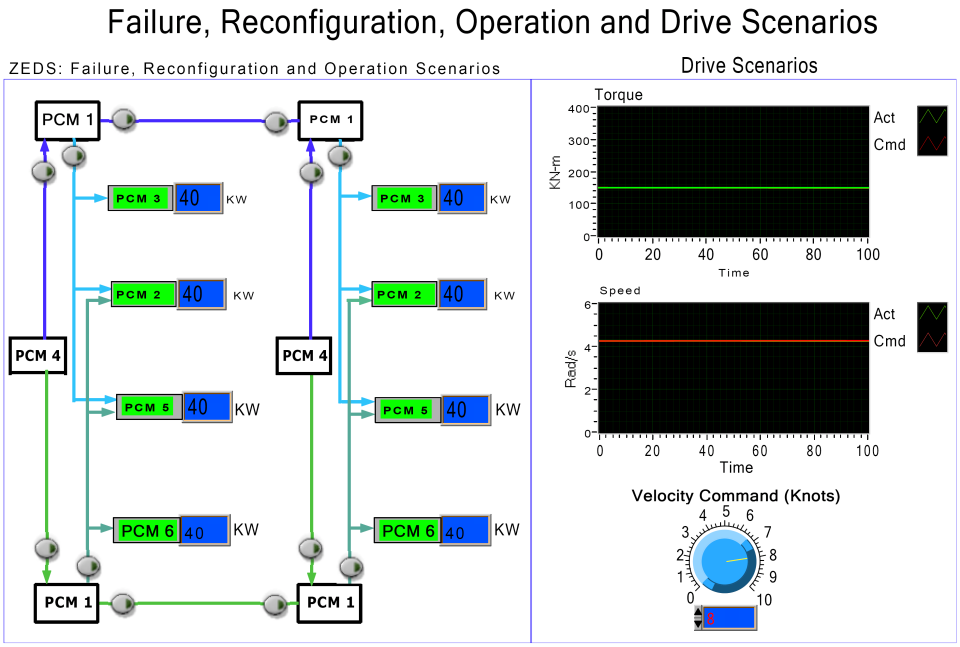

Figure 3.6: Failure, reconfiguration, operation and drive scenarios GUI.

3.3 DHPS Testbed Development

The DHPS test-bed is developed as a real-time validation platform for the normal and failure mode power management algorithms developed in this dissertation. Since we consider the scaled HPS model for the controller developed in this work, the test-bed is based on the configuration shown in Fig. 1.2. It should be noted that it is infeasible to have the exact shipboard hardware setting given the university infrastructure constraints, we considered alternate cost effective solutions for the test bed, namely power plant emulators with programmable power supplies and loads. The hardware in-the loop arrangement supported by physical models running in real-time are used to represent the function of power generation and load modules and ultra-capacitor instead of the $VL-34P$ batteries for the energy storage device.

Fig.3.7 shows the hardware setup of the DHPS, while Fig. 3.8 shows the system diagram of this set-up to illustrate the use of the test-bed in this work as a rapid prototyping platform for the controller validation. The entire system is comprised

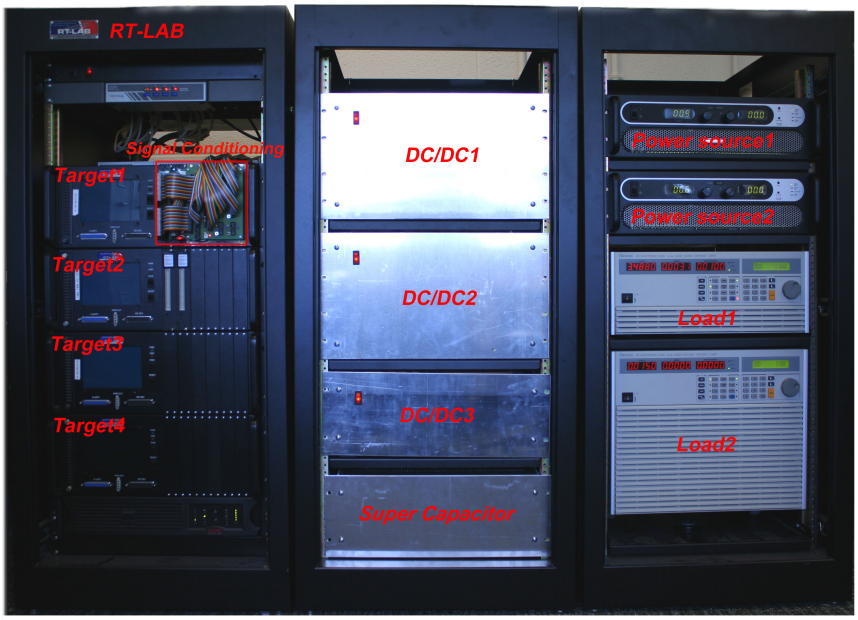

Figure 3.7: DC hybrid power system testbed setup.

of the RT-LAB® real-time simulation system, two isolated unidirectional DC/DC converters (DC/DC 1,2 in Fig. 3.7), a bidirectional DC/DC converter (DC/DC 3 in Fig. 3.7), two programmable power sources, two programmable electronic loads and a super-capacitor based energy storage bank. For the DHPS testbed, the RT-LAB® system serves the following three functions: (1) as a real-time simulator to simulate power source models and to control programmable power supplies to emulate the characteristics of a specified power source; (2) as an embedded controller for which the C code generated in a host PC can be downloaded and executed in target CPUs to control power converters; (3) as a data acquisition device to sample and store experimental data for feedback control and detailed offline analysis. The two programmable power supplies (Power Source 1,2 in Fig. 3.7) are the Sorensen® SGA 100A/100V 10KW AC/DC power supply. The output voltage of the programmable power supplies can be controlled through an analog signal. Therefore, one can use RT-LAB® target to simulate a power source model and then to control the power supplies through the RT-LAB® target analog interface so that the power supplies

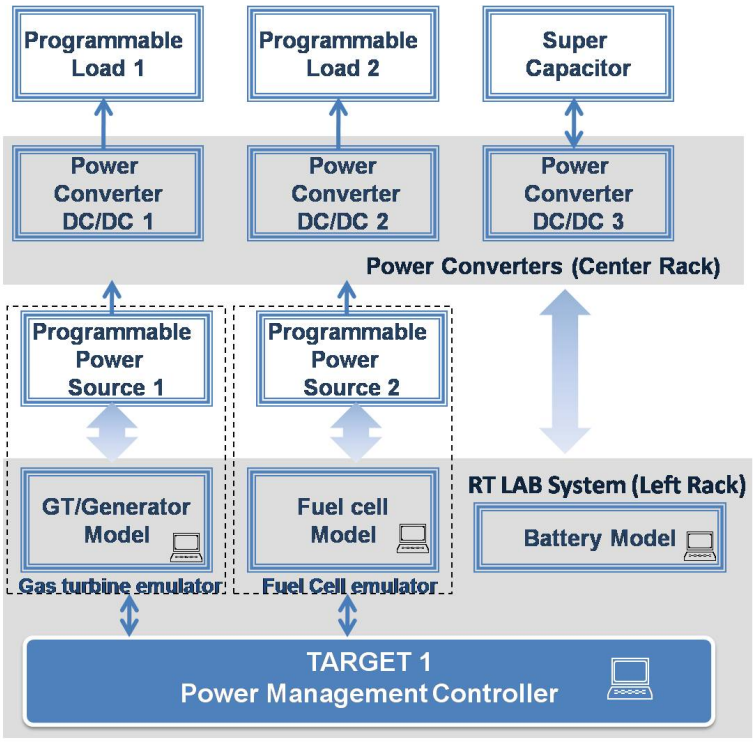

Figure 3.8: System Diagram of DHPS test-bed.

emulate the characteristics of DC power sources. The two programmable electronics loads are Chroma® 63202 5A/50A 125V/500V 2.6KW DC load and Chroma® 63204 10A/100A 125V/500V 5.2KW DC load, respectively. Similarly, the two DC electronic loads can also be controlled by RT-LAB® targets to emulate different types of ship-service loads.

The two unidirectional DC/DC converters are the Full Bridge Converter while the bidirectional DC/DC converter is the Dual Active Bridge Converter (DABC). The convertors used in the test-bed require 10kHZ modulation signals and have a bandwidth of 1kHz and are much faster than the power sources considered in this work which have a bandwidth of about 10 Hz. The details on the hardware development for the DC-DC converters can be found in [72]. The energy storage bank is composed of two branches of super-capacitors. One branch includes five BOOSTCAP® BPAK0020-15V modules which are connected in series and offer total $4F$ capaci-

tance. The other branch has five BOOSTCAP® BPAK0052-15V modules, therefore it provides $10.2F$ capacitance. Both the two branches have a $75V$ working voltage. Moreover, they can be connected in parallel to provide $14.2F$ capacitance. Therefore, the energy storage bank can be reconfigured for different applications.

3.4 Summary

This chapter developed the SPS simulator and the DHPS scaled test bed, both provide the tools required for real-time simulation and the controller rapid prototyping platform. While the simulator facilitates the analysis and monitoring of the detailed IPS model, the test-bed along with the optimization oriented HPS model developed in Chapter 2 provide the complete set of tools required for the control methodology development which is described in the subsequence chapters.

Chapter 4

Real-time Trajectory Optimization for Multi Time-Scale Systems

The power management design of the hybrid power systems for AES targeting military applications requires an algorithm for the optimal power split planning among multiple power sources. Such a planning is essential, in order to take advantage of the look-ahead opportunities, during the critical missions such as weapon or aircraft launches, in order to meet the load demand associated with these missions in a fast and efficient manner. The *On-demand* goals associated with the optimal planning necessitates real-time control, which is defined as the ability of the algorithm to compute the control solutions for the optimal power split planning problem within a sampling interval. Without the real-time control, either the missions have to be delayed or the solutions based on heuristic strategies have to be delivered till the optimal solutions are available, thereby resulting in a tradeoff between *optimality* or *on-demand planning*.

Motivated by the significance of the real-time control for the optimal power split planning for military applications, in this chapter, a methodology for solving trajectory optimization problem in real-time is developed. The goals of the methodology design are to exploit the system dynamic characteristics to facilitate real-time opti-

mization. One such property that has been explored is the multi-time scale behavior, due to the complementary time response characteristics of the HPS components. Note that while the specific application considered in this research targets shipboard HPS (Fig. 1.2), the scope of the proposed methodology extends to other HPS with multi-time scale property such as wind-diesel systems, etc. The objectives of this chapter are to,

- Develop analytical tools that can be directly applied to the constrained optimal power split planning of the shipboard HPS given the non-analytical nature of the dynamic model.

- Establish real-time computational effectiveness of the proposed method as compared to the generic optimization methods through analytical estimates as well as real-time implementation.

The trajectory optimization problem associated with the power management for the HPS considered in Fig. 1.2 is formulated along with a review of the existing methods that have traditionally been used to solve this problem. In order to address the real-time control requirements, a two level controller which is applicable only to system with multi-time scale property is proposed. A case study is presented where the proposed methodology was applied to the optimization oriented HPS model developed in Chapter 2 along with real-time validation results.

4.1 Optimization Problem Formulation and Review of Existing Methods

We consider a generic optimization for the problem formulation in order to capture the different considerations in the PM such as fast load-following, maximizing fuel economy and voltage regulation. For the problem formulation, we consider the power

source dynamics of the HPS (Fig. 1.2), which exhibit multi time-scale behavior. For example, the faster subsystem (e.g. gas turbine) is less efficient than the slower one (e.g. fuel cell) and are treated as physically separated entities. We first describe the power plants dynamics and constraints before formulating the PM optimization problem.Let $x_{1,2}$, $u_{1,2}$, denote the states and control inputs of the fast (subscript 1) and slow (subscript 2) sources.

Let $f_1(x_1, u_1)$, $f_2(x_2, u_2)$ denote the fast and slow power source dynamics. Then, the nonlinear IPS is described by

$$x_{k+1} = f(x_k, u_k) \tag{4.1}$$

where $x_k = \begin{bmatrix} x_{1,k} \\ x_{2,k} \end{bmatrix}$, $(x \in \Re^n)$, $u_k = \begin{bmatrix} u_{1,k} \\ u_{2,k} \end{bmatrix}$ $(u \in \Re^m)$ and $f = \begin{bmatrix} f_1(x_{1,k}, u_{1,k}) \\ f_2(x_{2,k}, u_{2,k}) \end{bmatrix}$
We consider two types of constraints that the control algorithm has to enforce:

1. Component constraints denoted by $\Phi_1(x_{1,k}, u_{1,k})$ and $\Phi_2(x_{2,k}, u_{2,k})$ for the fast and slow subsystems. This includes the physical limits and the input saturation limits of the power sources.

2. Power generation constraints $(\Phi_G(x_k, u_k))$ to ensure that the critical load demand is satisfied.

The power management objectives (e.g. fast load-following, maximum fuel economy, etc.) are captured using a generic cost function (J) which is given by,

$$J(x_0, u_{[0,N-1]}) = h(x_N) + \sum_{k=0}^{N-1} g(x_k, u_k) \tag{4.2}$$

where $h(x_N) \geq 0$ is the terminal cost function, $g(x_k, u_k) \geq 0$ is the instantaneous cost function, N is the time window over which the cost will be evaluated, x_k, u_k are the

instantaneous values of the states and controls at time k respectively. We also use the notation $u_{[0,N-1]} = [u_0, u_1, ..., u_{N-1}]$ to denote the control sequence over the window.

The optimization problem $\mathcal{P}_N$ is formulated as to find $u^*_{[0,N-1]}$, where

$$\mathcal{P}_N : u^*_{[0,N-1]} = arg \left\{ \min_{u_{[0,N-1]}} J(x_0, u_{[0,N-1]}) \right\} \tag{4.3}$$

subject to constraints (4.1) and

$$\Phi(x_k, u_k) \leq 0, \tag{4.4}$$

where $\Phi(x_k, u_k) = \begin{bmatrix} \Phi_1(x_{1,k}, u_{1,k}) \\ \Phi_2(x_{2,k}, u_{2,k}) \\ \Phi_G(x_k, u_k) \end{bmatrix}$ Since the method used for solving the trajectory optimization problem in $\mathcal{P}_N$ has to be directly applicable for power management of shipboard HPS targeting military applications, the methodology design should consider the following factors: (C1) Lack of a transition probability function for shipboard applications, (C2) Non-analytical representations for the HPS dynamics. A detailed survey of numerical methods to solve trajectory optimization problem is available in [38], where the applicability of each of these methods is elaborated. The computational efficiency of these methods is mostly defined by the dimensions of the optimization problem, namely, the number of states, inputs and the optimization horizon. As mentioned in Section 1.4.1, grid based methods including DP ([17, 18, 39]), IDP ([40–44]), SDP ([19–21]) have been proposed to solve the optimization problem. The *Curse of dimensionality* of DP and IDP along with the lack of a transition probability function (C1) makes SDP and its variants inapplicable.

The SQP is so far the most well known gradient based method and has found wide applications in model predictive control [45]. There has been a lot of work in applying this method to solve large scale trajectory optimization problems, by improving the

efficiency of the SQP ([49]) algorithm using collocation methods. The main issue in using SQP for our application is due to the non-analytical nature of the HPS mode (C2), where obtaining second order derivatives for the HPS model is very difficult. Moreover our numerical experiments in using the SQP based on collocation methods revealed that there exists a tradeoff between reducing the computational effort and obtaining the optimal cost for the problem in Eq. (4.3).

In this work, we consider the sensitivity function (SF) based iterative method for solving the trajectory optimization problem $\mathcal{P}_N$. This method is chosen for two reasons: (1) Its ability to deal with the shipboard problem specific characteristics (C1 and C2) and, (2) It can be utilized to leverage the multi-time scale property in order to facilitate real-time optimization. To do so, a two level optimization on slow and fast time scales is proposed, where approximation to the optimal solutions of (4.3) are computed much more quickly than the true optimal solutions and the accuracy of these approximates are improved at each level. In the remainder of the chapter, the SF based method along with the two time scale optimization is developed and is implemented using the optimization oriented HPS model developed in Chapter 2, to illustrate the computational efficiency.

4.2 Sensitivity function based method for optimization

Consider the performance index in (4.2), whose first order approximation can be expressed as:

$$J(u^0_{[0,N-1]} + \Delta u_{[0,N-1]}) \;=\; J(u^0_{[0,N-1]}) + \sum_{i=0}^{N-1} \frac{\partial J}{\partial u_i}|_{u^0_{[0,N-1]}} \Delta u_i$$

where $u^0_{[0,N-1]}$ is any given control trajectory.

Let $J_{u_i} = \left[\frac{\partial J}{\partial u^1} ... \frac{\partial J}{\partial u^m}\right]\Big|_{(x_i,u_i)}$, $g_{u_i} = \left[\frac{\partial g}{\partial u^1} ... \frac{\partial g}{\partial u^m}\right]\Big|_{(x_i,u_i)}$ and $g_{x_i} = \left[\frac{\partial g}{\partial x^1} ... \frac{\partial g}{\partial x^n}\right]\Big|_{(x_i,u_i)}$, where $J_{u_i}, g_{u_i} \in \Re^{1\times m}$ and $g_{x_i} \in \Re^{1\times n}$. Then the sensitivity function defined as $\frac{\partial J}{\partial u_{[0,N-1]}} = \left[J_{u_0}\, J_{u_1} \,...J_{u_{N-1}}\right]^T$ can be expressed as

$$\frac{\partial J}{\partial u_{[0,N-1]}} = G_u + ZG_x. \tag{4.5}$$

where, $Z \in \Re^{mN\times n(N+1)}$, $G_x \in \Re^{n(N+1)}$ and $G_u \in \Re^{mN}$ and are defined as

$$\begin{aligned} G_x &= \begin{bmatrix} g_{x_0} & .. & g_{x_{N-1}} & g_{x_N} \end{bmatrix}^T, \\ G_u &= \begin{bmatrix} g_{u_0} & .. & g_{u_{N-1}} \end{bmatrix}^T, \end{aligned}$$

$$Z = \begin{bmatrix} \mathbf{0}_{n\times m} & B_0^T & (A_1B_0)^T & .. & (A_{N-1}\cdots A_1B_0)^T \\ \mathbf{0}_{n\times m} & \mathbf{0}_{n\times m} & B_1^T & .. & (A_{N-1}\cdots A_2B_1)^T \\ .. & .. & .. & .. & .. \\ \mathbf{0}_{n\times m} & \mathbf{0}_{n\times m} & \mathbf{0}_{n\times m} & .. & B_{N-1}^T \end{bmatrix} \tag{4.6}$$

with $A_i = \frac{\partial f}{\partial x_i}$ and $B_i = \frac{\partial f}{\partial u_i}$ evaluated at $u^0_{[0,N-1]}$, $x^0_{[0,N]}$, where, $x^0_{[0,N]} = [x^0_0, x^0_1, \ldots x^0_N]$ is the state trajectory sequence corresponding to the input $u^0_{[0,N-1]}$. The matrix Z will be referred to as the state sensitivity matrix in the sense that $z_{ij} = (\frac{\partial x_i}{\partial u_j})^T$.

Remark 4.2.1 *Since the IPS model is nonlinear, in order to compute the A_i and B_i matrices, the dynamics need to be linearized. This is performed numerically given the non-closed form representation of the IPS model. For example, Matlab® offers a function linmod to determine the linearized dynamics around a given operating point.*

The cost associated with the given trajectory $(u^0_{[0,N-1]})$ can be further reduced by updating the control sequence in the direction of descent. To ensure constraint satisfaction, the descent direction can either be in the steepest descent [79] or in the

feasible direction [80], where the latter is defined as the steepest descent direction that does not violate any constraints. Let $\mathbf{K}^a$ denote the active set defined as

$$\mathbf{K}^a \triangleq \{k|\Phi(x_k, u_k) = 0,\, k \in [0 : N-1]\}.$$

For any given control sequence, if the active set $\mathbf{K}^a$ is empty, the descent direction is $d = -\nabla J$. Otherwise, in the neighborhood of a given control sequence, the feasible descent direction will be the solution to a linear programming problem, defined as follows:

$$\min_{d_{[0:N-1]}, l} l \tag{4.7}$$

subject to constraints

$$\begin{aligned} \nabla J^T d - l &\leq 0, \\ \nabla \Phi_a^T d - l &\leq 0, \\ -1 \leq \|d\|_\infty &\leq 1. \end{aligned}$$

where minimizing l leads to reducing the cost as well as the constraint violation in the direction d. Here ∇J, $\nabla \Phi_a$ are the normalized gradient of the cost function and active constraint set respectively and are defined as follows:

$$\begin{aligned} \nabla J &\triangleq \frac{\partial J}{\partial u_{[0:N-1]}} / \max |\frac{\partial J}{\partial u_{[0:N-1]}}| \\ \nabla \Phi_a &\triangleq \frac{\partial \Phi(x_k, u_k)}{\partial u_{[0:N-1]}} / \max |\frac{\partial \Phi(x_k, u_k)}{\partial u_{[0:N-1]}}|,\ \forall k \in \mathbf{K^a}, \end{aligned}$$

where $\max |y|$ for any vector $y \in R^N$ is defined as $\max(|y_1|, |y_2|, ..., |y_N|)$.

The control updates are then computed by performing a 1-D search over the step

size δ as follows

$$\delta^* = arg(\min_{\delta} J(u_{[0:N-1]} + \delta d^*), s.t., 0 < \delta \leq \delta_0, \tag{4.8}$$

where δ_0 is chosen such that the updates are in the neighborhood of the control sequence ($||\delta_0 d_k - u_k|| << 1$) and constraints (4.1) and (4.4) are satisfied.

Remark 4.2.2 *The state sensitivity matrix Z contains information of the effects of changes in the control input sequence on the state. This matrix is upper triangular as a direct consequence of the causality, which dictates that the control input applied at time k can only affect future state trajectories $x_{k+1} : x_N$. In addition, for a stable system, the Z matrix will be sparse and has a band diagonal structure, where the number of band diagonal elements is defined as the index N_B such that $\forall i > N_B$, $\| \prod_{k=1}^{i} A_k \| \approx 0$. The faster the dynamics, the more sparse the Z matrix.*

Remark 4.2.3 *Even though the first order methods have been used, leveraging the band diagonal structure reduces the computations required to determine the sensitivity functions, hence the control updates. This will be especially useful in solving extended horizon optimization problems.*

We now propose an iterative procedure for trajectory optimization of systems whose models do not have an explicit analytical form:

Algorithm 4.1 (Sensitivity function method): Given a feasible initial control trajectory $u_{[0,N-1]}$, tolerance $\sigma > 0$,

1: *Simulate the dynamic model, determine the state trajectories and compute the performance index $J(u_{[0,N-1]})$.*

2: *Compute the sensitivity matrices Z, G_x, G_u and using (4.5), compute the sensitivity functions, $\left(\frac{\partial J}{\partial u_{[0,N-1]}}\right)$, with the band diagonal structure of size N_B. (See Remark 4.2.2).*

3: *Determine the active set* $\mathbf{K}^a$. *If active set is empty, set* $d^* = -\nabla J$, *otherwise compute* d^* *using equation (4.8).*

4: *Compute optimal step size* δ^* *using equation (4.9) and the optimal update vector* $\Delta u^*_{[0,N-1]} = \delta^* d^*$.

5: *If* $J(u_{[0,N-1]}) - J(u_{[0,N-1]} + \Delta u^*_{[0,N-1]}) < \sigma$, *stop. Otherwise update* $u_{[0,N-1]} = u_{[0,N-1]} + \Delta u^*_{[0,N-1]}$ *and go to step (1).*

Proposition 4.2.1 *For a given number of states (n) and control inputs (m), the computational effort (flop count) required per iteration of Algorithm* 4.1 *(C_{SF}) when $N_B = N$ and $N >> m, n$ is $\mathcal{O}(N^2)$.*

The key ideas used in deriving proposition 4.2.1 are given in *Appendix C.*

Corollary 4.2.1 *Let C_{BD} denote the computational effort (flop count) for sensitivity function generation when we leverage band diagonal structure, i.e., we assume a sparse structure for the Z matrix and set upper triangle elements as zero, then, the ratio $\frac{C_{BD}}{C_{SF}}$ is of $\mathcal{O}(\frac{N_B}{N})$.*

Proof: If we consider the band diagonal structure (*See Remark 4.2.2*), then the flop count for determining the Z matrix and the inner product of $\langle G_x^T, Z_i \rangle$ is given by $(N_B \frac{(N_B+1)}{2} + N_B(N - N_B))(p_5 + p_6)$. Then for $N_B >> 1$ the total effort for SFM algorithm can be given as

$$C_{BD} = N_B \left(N - \frac{N_B}{2} \right) (p_5 + p_6). \tag{4.9}$$

With a large length of horizon ($(N > N_B) >> 1$), we have $\frac{C_{BD}}{C_{SF}} \approx \frac{2N_B}{N} \left(1 - \frac{N_B}{2N}\right)$, which is $\mathcal{O}(N_B/N)$. □

Remark 4.2.4 *One possible way of choosing the initial control sequence $u_{[0,N-1]}$ is using the steady state optimal control input, which is determined by solving $\mathcal{P}_N$ as a*

static optimization problem. However such a choice need not satisfy the constraints (4.4). Therefore, in this work, the initial control sequence is chosen either as the unfiltered or the filtered steady state optimal control, where the latter is used when the constraints are violated.

Remark 4.2.5 *The tolerance parameter (σ) used in the stopping criteria for the Algorithm 4.1 is typically a small parameter [80] and influences the optimization accuracy as well as the computational effort. While the exact value depends on the order of the associated cost function J, in this work this value is chosen such that* $\sigma J(x_0, u^0_{[0:N-1]}) \leq 10^{-8}$.

4.2.1 Proposed Two Time Scale Optimization

Since the complexity of Algorithm 4.1 is $\mathcal{O}(N^2)$, we seek ways to simplify the dimensions of the optimization problem $\mathcal{P}_N$ as this would yield considerable savings in the computational effort. To do so, we exploit the multi-time scale property and consider a two-level optimization approach, where the optimal solutions at each level is the initial control sequence for subsequent optimization. The potential benefits of such an approach is that the control solutions at each level can be made available much earlier than the optimal control solutions ($u^*_{[0,N-1]}$) computed using Algorithm 4.1. On the top-level, we simplify the optimization problem $\mathcal{P}_N$ on the time scale of the slower power source dynamics. Then, to account for under-sampling the fast dynamics at the slow time scale, we seek transient corrections on the time scale of the faster power source.

Let τ_f, T_f and τ_s, T_s denote the time constant and the sampling time for the fast and slow subsystems respectively. If the total time interval is t_f and $\rho = \frac{T_s}{T_f}$ is an integer [1], we now consider the following two optimization problems:

[1] One can chose T_s, T_f such that ρ is an integer and the Nyquist rule, i.e., $T_f \leq \frac{\tau_f}{2}$, $T_s \leq \frac{\tau_s}{2}$ is satisfied.

Level 1 Optimization ($\mathcal{P}^s_{N_s}$)

In this level, we solve the problem $\mathcal{P}_N$ on the time scale driven by the slower power source. The problem is formulated to determine the optimal control sequence $u^{s,*}_{[0:N_s-1]}$ on the slow time scale given by,

$$\mathcal{P}^s_{N_s} : u^{s,*}_{[0:N_s-1]} = \arg\left\{ \min_{u^s_{[0,N_s-1]}} J(x_0, u^s_{[0:N_s-1]}) \right\} \tag{4.10}$$

subject to constraints

$$x_{k_s+1} = f(x_{k_s}, u_{k_s}), \tag{4.11}$$

$$\Phi(x_{k_s}, u_{k_s}) \leq 0, \tag{4.12}$$

where k_s is the discrete time index on the slower time scale and $N_s = \frac{t_f}{T_s}$ is the size of the time window on the slower time scale. Then, level 1 solution is the control sequence $u_{1,[0:N-1]}$, $u_{2,[0:N-1]}$ given by,

$$u_{1,k} = u^{s,*}_{1,k_s},\ \forall \rho k_s \leq k \leq \rho k_s + 1, \tag{4.13}$$

$$u_{2,k} = u^{s,*}_{2,k_s}. \tag{4.14}$$

Remark 4.2.6 *Under the assumption that the dynamics of the subsystem 1 are much faster than those of system 2, we have $N_s << N$ and make the following observations*

- *Since the SFM algorithm is $\mathcal{O}(N^2)$, the optimization problem $\mathcal{P}^s_{N_s}$ defined by (4.11-4.13), is simpler than (4.3-4.4). The effort can be reduced further if the band diagonal structure is used.*

- *The level 1 solution (u_k) can be treated as sub-optimal to the true optimal solutions u^*_k. Note that for piecewise constant power demands we have $u_k \approx u^*_k$ for all instants except around transients. It must be noted that the length of*

the time interval around the transients, during which the level 1 solutions differ from the true optimal solutions, depends on the ratio $\frac{N_s}{N}$. *If* $\varepsilon \triangleq \frac{N_s}{N}$ *and the length of the interval is denoted as* $\wp\varepsilon$ *then, for a step change in the reference trajectory (namely the power demand), the difference in the cost associated with optimal solutions* ($u^*_{[0:N-1]}$) *and the level 1 solutions* ($u_{[0:N-1]}$) *can be described by* $J(x_0, u^*_{[0:N-1]}) - J(x_0, u_{[0:N-1]}) = \mathcal{O}(\varepsilon)$ *(See Appendix C)*

Level 2 Optimization ($\mathcal{P}^f_N$)

This problem is formulated on the fast time scale ($N = \frac{t_f}{T_f}$) , to account for under-sampling the faster dynamics on the previous level and computes the corrections $u^{f,*}_{1,[0:N-1]} = arg(J_f)$, where J_f is computed as,

$$\mathcal{P}^f_N : J_f = \min_{u^f_{1,[0,N-1]}} J(x_0, u_{1,[0:N-1]} + u^f_{1,[0:N-1]}, u_{2,[0:N-1]}) \tag{4.15}$$

subject to constraints

$$x^f_{1,k+1} + x_{1,k+1} = f_1(x_{1,k} + x^f_{1,k}, u_{1,k} + u^f_{1,k}), \tag{4.16}$$

$$\Phi_1(x_{1,k} + x^f_{1,k}, u_{1,k} + u^f_{1,k}) \leq 0, \tag{4.17}$$

$$\Phi_G(x_{1,k} + x^f_{1,k}, u_{1,k} + u^f_{1,k}) \leq 0, \tag{4.18}$$

where, $x_{1,[0:N]}$ is the states associated with the level 1 control inputs to the fast subsystems ($u_{1,[0:N-1]}$) computed using (4.14), (4.15). Note that based on *Remark 4.2.6*, the initial control sequence for the level 2 optimization is chosen as $\mathbf{0}_{1\times N-1}$

Remark 4.2.7 *If SFM method is used to solve the optimization defined in* $\mathcal{P}^f_N$, *since only the fast dynamics are considered the sparsity of the Z matrix will be high thereby making* $\mathcal{P}^f_N$ *much simpler to solve than* $\mathcal{P}_N$ *(See Remark 4.2.2).*

Algorithm 4.2: Given a feasible initial control trajectory $u^0_{[0,N-1]}$ (See *Remark 4.2.4*), we propose the following algorithm to solve the optimization problem $\mathcal{P}_N$ defined by (4.3):

1. At k=0, determine $u^{s,*}_{[0,N-1]}$ by solving the optimization problem $\mathcal{P}^s_{N_s}$ using SFM and compute the sub-optimal control trajectories $u_{[0,N-1]}$ using (4.14), (4.15).

2. Given $u_{[0,N-1]}$ and using $\mathbf{0}_{1\times N-1}$ as the initial control sequence, compute $u^{f,*}_{[0:N-1]}$ by solving the optimization problem $\mathcal{P}^f_N$ using SFM.

3. *If $\mathcal{P}^f_N$ can be solved in real time, i.e, $k < 1$:* Compute $u_{1,[0,N-1]} + u^{f,*}_{[0,N-1]}$ and $u_{2,[0,N-1]}$ as the sub-optimal control inputs to the power plants.

4. *Else:* Compute $u_{1,[0,N-1]}$ and $u_{2,[0,N-1]}$ as the sub-optimal as the sub-optimal control inputs to the power plants.

Computational Efficiency Vs Optimization Accuracy: It must be noted that there are three possible solutions to the optimization problem defined in $\mathcal{P}_N$, namely,

FS Full Scale (FS) control sequence obtained by solving the optimization problem defined in $\mathcal{P}_N$ (*Algorithm 4.1*).

L1 Level 1 control sequence obtained by solving the optimization problem defined in $\mathcal{P}^s_{N_s}$, i.e, step 1 of *Algorithm 4.2*.

L2 Level 2 control sequence obtained by solving the optimization problem defined in $\mathcal{P}^f_N$, i.e, steps 1 and 2 *Algorithm 4.2*.

In addition to the above solutions, which are determined by solving the dynamic optimization problem, another option is to compute solutions for steady state optimal performance which is denoted as steady state (SS) solutions. While the FS solutions

have the best optimization accuracy, followed by the $L2$, $L1$ and the steady state solutions, this order is reversed with respect to the computational effort required to solve these problems. However, in real-time the ability to solve the optimization problem with minimum computational delay is a key factor in deciding the performance (i.e. optimization accuracy) associated with these approaches. Therefore the most suitable algorithm is the one that can achieve a good trade-off between the real-time computational efficiency and optimization accuracy. In light of this, we only quantify the reduction in computational effort associated with computing the solutions using L1 and L2 as compared to the full scale (FS) approach. We rely on the assumption that given that sufficient difference in the dynamics of fast and slow subsystems exist, the optimization accuracy of the $L1$ or $L2$ can be comparable to the FS solutions, where the benefits of the improved computational efficiency can achieve better real-time performance. We now provide estimates of the computational effort reduction in the following proposition.

Proposition 4.2.2 *Let C_{SF}, C_{slow}, C_{TS} denote the flop count per iteration using FS, $L1$ and $L2$ optimization respectively and $\varepsilon \triangleq \frac{N_s}{N}$ capture the multi time scale property. Under the assumption $\varepsilon << 1$, we have (a): $\frac{C_{slow}}{C_{SF}} = \mathcal{O}(\varepsilon^2)$ and (b): $\frac{C_{TS}}{C_{SF}} = \mathcal{O}(\varepsilon)$.*

Proof (a): This follows from *Proposition 4.2.1.* Since $N_s = \varepsilon N$, we have $C_{slow} = \mathcal{O}(N_s^2) = \varepsilon^2 \mathcal{O}(N^2)$. $\square$

Proof (b): The flop count with the $L2$ optimization that incudes level 1 slow time scale optimization as well as the fast time scale corrections is given by,

$$C_{TS} = C_{slow} + \beta \left(N - \frac{\beta}{2} \right) \left(p_5^f + p_6^f \right) \tag{4.19}$$

where, (p_5^f, p_6^f) corresponds to the flop counts (p_5, p_6) to compute $\frac{\partial x_{k+1}}{\partial u_i}$ and $\langle G_x^T, Z_i \rangle$ for the fast subsystems and $\beta \propto \frac{\tau_f}{T_f}$ is the number of band diagonal element of fast dynamics on the fast time scale. If α_s denotes the number of band diagonal elements of

the slow dynamics on the slow time scale and γ denotes the number of band diagonal elements of the overall system dynamics on the fast time scale, by definition, we have $\beta = \varepsilon\gamma$ and $\alpha_s = \varepsilon\gamma$. Then,

$$\frac{C_{TS}}{C_{SF}} = \frac{C_{slow}}{C_{SF}} + \varepsilon\frac{N - \varepsilon\gamma/2}{N - \gamma/2}$$

where $\frac{C_{slow}}{C_{SF}} = \mathcal{O}(\varepsilon^2)$ from *Proposition 4.2.2*. Under the assumption $\varepsilon << 1$, we have $\frac{C_{TS}}{C_{SF}}$ is $\mathcal{O}(\varepsilon)$ which proves the corollary. $\square$

The effectiveness of the proposed algorithm and the validity of the estimates in effort reduction will be demonstrated through the case study.

4.3 Case Study

A case is developed in order to solve the PM associated with the shipboard hybrid power systems for AES. We apply the proposed methodology, which leverages the multi-time scale property. We consider the gas turbine and the fuel cell models developed in Chapter 2 for the power source dynamics, where the power delivered is the sum of their respective power outputs. The objectives of the power management in this case study is to determine the optimal fueling trajectories to gas turbine and fuel cell in order to support the load demands as quickly and as efficiently as possible. Here, the loads are represented as time varying power demands. For this case study, we consider a hypothetical pulse power profile (Fig. 4.2 black solid line) associated with an aircraft or a weapon launch scenario, where the optimal power split planning is done over a 40s time window. The terminal and the instantaneous cost function (Table 6.2) captures the PM objectives, where the latter is the weighted sum of power tracking error and total fuel consumption. The constraints along with the other optimization parameters are given in Table 6.2. Here $u_{1,k}$, $u_{2,k}$ are the fueling

rates to the gas turbine and fuel cell and $P_{1,k}$, $P_{2,k}$ are the associated power outputs.

Table 4.1: IPS state and optimization parameters used in the case study.

Name	Value
Gas turbine states ($x_{1,k}$)	$[m_{b,k},\, T_{b,k},\, \omega_{tc,k}]^T$
Fuel cell states ($x_{2,k}$)	$[W_{FR,in,,k},\, T_{FR,k},\, p_{H_2,an,k}]^T$
Final Time	40s
Sample Times	$T_f = 0.05s,\, T_s = 0.2s$
Horizon Length	$N_s = 200,\, N = 800$
Tolerance Value	$\sigma = 10^{-9}$
Terminal Cost function	$h(x_{1,N}, x_{2,N}) = 20\left(\frac{P_{d,N}-P_{1,N}-P_{2,N}}{P_{d,N}}\right)^2$
Instantaneous Cost function	$g(x_{1,k}, x_{2,k}, u_{1,k}, u_{2,k}) = u_{1,k}^2 + u_{2,k}^2 + 20\left(\frac{P_{d,k}-P_{1,k}-P_{2,k}}{P_{d,k}}\right)^2$
Gas Turbine Surge, saturation Constraints $\Phi_1(x_{1,k}, u_{1,k})$	$[0.00385 m_{b,k} T_{b,k} - 0.98(\omega_{tc,k} - 19.483),$ $0.137 - u_{1,k},$ $0.345 - u_{1,k}]^T \leq \mathbf{0}_{3\times 1}$
Fuel Cell Starvation, saturation Constraints $\Phi_2(x_{2,k}, u_{2,k})$	$[0.04 - \frac{p_{H_2,an,k}}{p_{an,k}},$ $0.022 - u_{2,k},$ $0.124 - u_{2,k}]^T \leq \mathbf{0}_{3\times 1}$

The main purpose of the case study is to illustrate the benefits of the multi-time scale approach by comparing the FS and $L1$ solutions in terms of the following aspects.

- Comparable optimization accuracy of the $L1$ with respect to the FS approach, when the optimization problems were solved off-line, which is due to the complementary dynamic response characteristics of the power sources.
- Real-time computational efficiency of the $L1$ optimization as compared to the FS one, a direct consequence of which is an improved real-time power tracking performance of the $L1$ optimization.

Table 4.2: Real-time computational effort reduction using TSS

Method	Real-time Computation Effort (s)	Real-time Cost	Offline Cost
FS	≈ 1.6	30.2	4.49
$L1$	≈ 0.045	4.6	4.6

The implementation of the controller was done both off-line and in real-time where we used a Pentium® processor for the off-line optimization. The OpalRT® real-time PC cluster and the DHPS test-bed developed in Chapter 2 were used for online optimization and the corresponding results are presented in Table 5.3. The first point to be noted is that the optimization accuracy of the full-scale solutions is only about 3% higher than the $L1$ solutions, when both the optimization problems were solved off-line. However it can be seen (Column 3) that the real-time cost of the $L1$ optimization (4.6) is much better than the FS one (30.2) which seems counter-intuitive, but can be explained as follows. While it takes $0.045s$ ($< T_f$) to get the control solutions of the $L1$ optimization, the corresponding FS problem takes $1.6s$ ($>> T_f$) to be solved. During this interval, since the optimization solutions are not available, the steady state optimal control input needs to be applied to the power sources. This computational delay leads to a performance deterioration in terms of power tracking using the FS solutions. The actual computational reduction is 32 which is $\mathcal{O}(\varepsilon^2)$ ($\varepsilon^2 = 16$) and is according to the *Proposition. 4.2.2.*

The steady state control solutions along with the L1 and FS optimization solutions are shown in Fig. 4.1. It should be noted that the initial control sequence for the gas turbine and fuel cell is the filtered and unfiltered steady state fuel trajectories respectively. As expected, except around the transients, the optimization solutions for the case L1 and FS is the same as the steady state solution.

Fig. 4.2 shows the power demand along with the power output associated with the steady state and optimal fuel trajectories using $L1$ (blue dashed line denoted

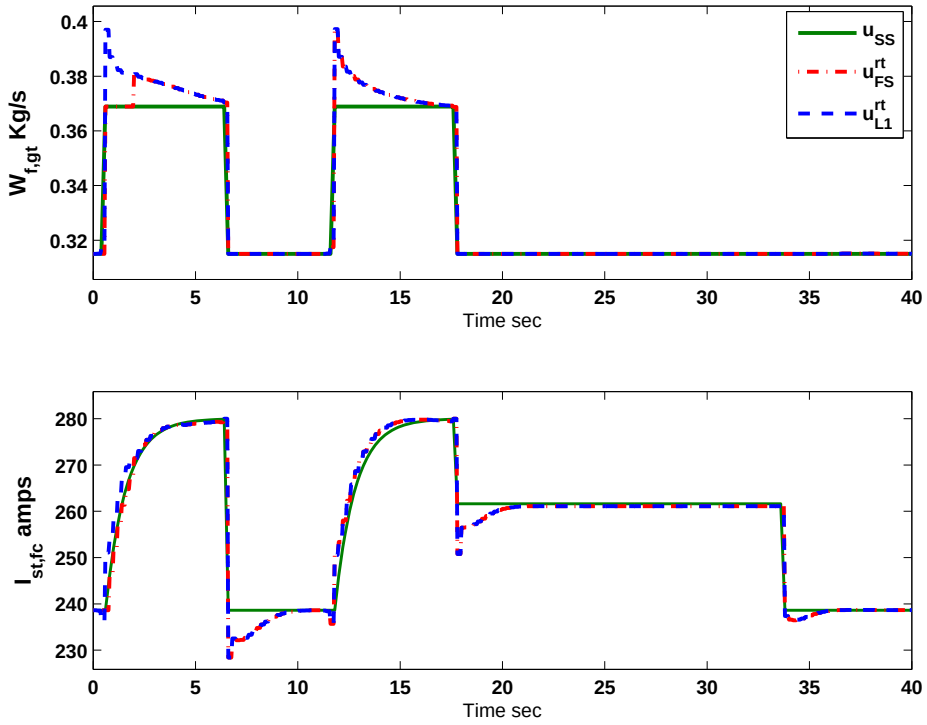

Figure 4.1: Control Input Trajectories: Static optimal control (u_{SS}); L1 (u^{rt}_{L1}) and full scale (u^{rt}_{FS}) optimization solutions.

by P^{rt}_{L1}) and FS (red dash-dotted line) optimization. The green dashed line is the power associated with the static feed-forward control optimized for steady state power tracking, where the presence of slow dynamics causes the mismatch between the response of the static optimal control and the actual demand. From Fig. 4.3, it must be noted that the control solutions of the $L1$ optimization satisfies both hydrogen mole fraction and surge constraints, with the corresponding maximum values being 0 (active) and -0.45 respectively.

4.4 Summary

In this chapter, a sensitivity function based trajectory optimization methodology, for systems with multi time scale behavior, was proposed. The real-time computa-

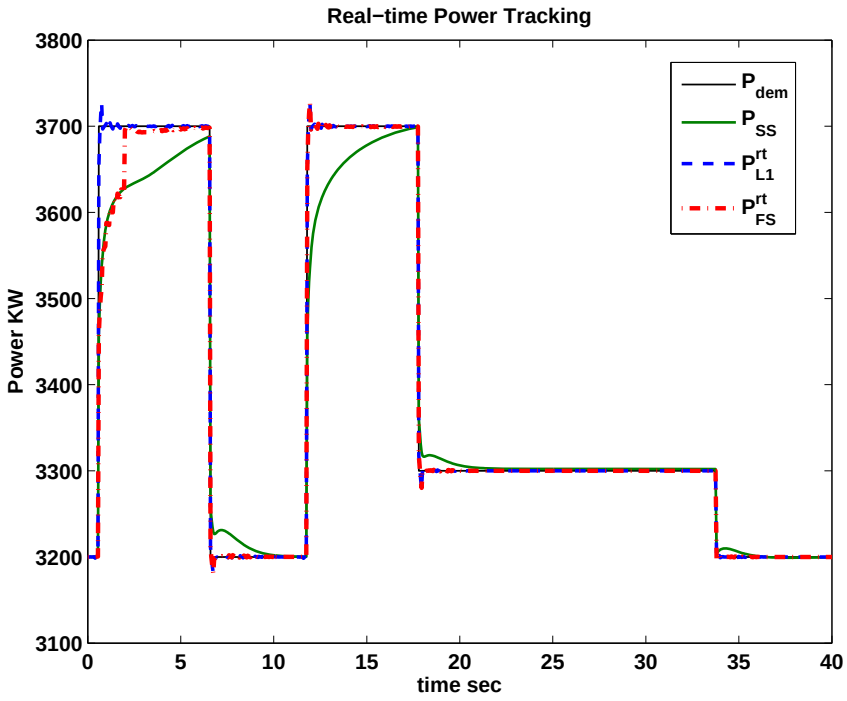

Figure 4.2: Power Trajectories: Demanded Power (P_{dem}), Real-time Power Tracking with static feed-forward optimal control (P_{SS}), Level 1 optimal control (P_{L1}^{rt}) and True optimal control using full-scale optimization (P_{FS}^{rt})

tional efficiency of the proposed method as well as its applicability to the optimal power split planning for the shipboard HPS has been illustrated through the case study on the real-time simulator. The methodology development is of central importance as it provides the framework towards the power management design for the HPS in military AES that is developed in the subsequent chapters.

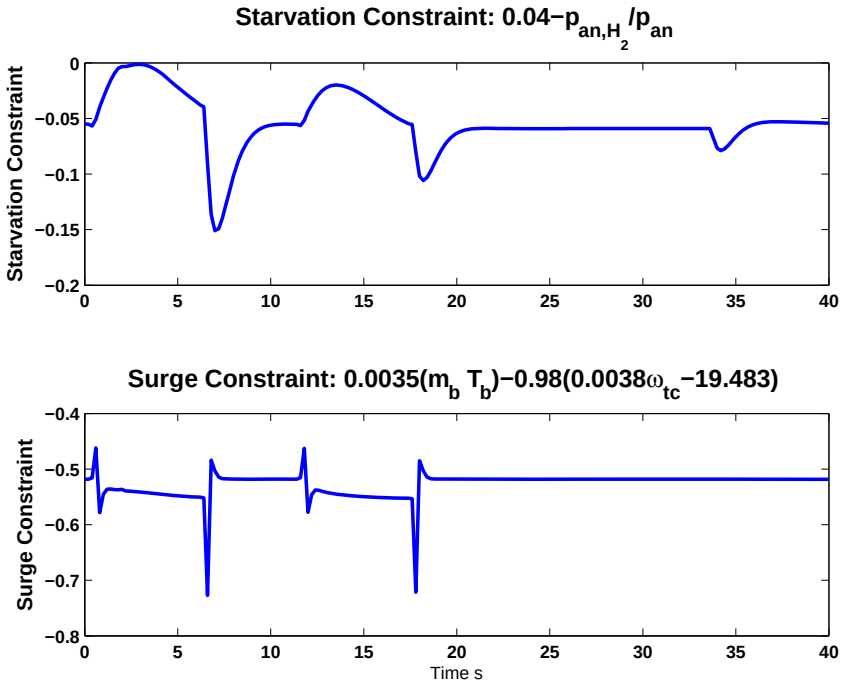

Figure 4.3: L1 Optimization: Surge and Starvation Constraints.

Chapter 5

Normal Mode Power Management of HPS in All-Electric Ship Applications

The hybrid power systems in AES targeting military applications have to support the critical missions such as hard acceleration, crash stop, weapon or aircraft launches during the normal mode operations. The power management is essential in order to coordinate among the power sources and energy storage devices to meet the demand associated with the normal mode missions. While the trajectory optimization methodology developed in Chapter 4 provides an algorithm for real-time optimal power split planning, the considerations of disturbance rejection as well as energy storage utilization needs to be addressed in order to provide a complete solution for the AES power management problem. Therefore in this chapter, the normal mode HPS power management is developed, which considers feedback control and actively utilizes the energy storage device.

For the HPS (Fig. 1.2) considered in this work, the control objective is to achieve an optimal power split between gas turbine, fuel cell and battery for energy efficiency and power tracking while ensuring system safety and mission effectiveness. In this work, mission effectiveness is defined as the ability of HPS to quickly meet the load demand while maximizing fuel economy all through the mission. The optimal control

of the shipboard HPS has to deal with following problem characteristics,

C1 *On-demand* nature of the problem, namely the power demand profile for the mission is not given apriori and optimal solutions have to be computed online.

C2 Long horizons associated with a mission planning request due to the look-ahead requirements.

C3 Difficulties in obtaining analytical models for HPS components.

C4 Active use of battery during pulse power demand.

C5 Presence of disturbances in the HPS such as load fluctuations.

These characteristics make the control algorithm development quite challenging due to two reasons: (1) The real-time requirement, where the optimal control algorithm needs to be executed within minimum computational delay, (2) The algorithm should take advantage of the look-ahead opportunities as well as achieve disturbance rejection. Both of them should be simultaneously satisfied in order to achieve mission effectiveness. While the trajectory optimization methodology, developed in the previous chapter, utilizes the look-ahead opportunity for the purposes of optimal power split planning, the presence of load disturbances makes this open loop control alone unsuitable to achieve mission effectiveness. Even though the model predictive control offers all the benefits of feedback design, there is a tradeoff between the length of the prediction horizon and the computational efficiency. This means that in order to achieve real-time control, there is a potential risk of making short sighted decision, wherein the long horizon power demand information is not fully utilized.

To address the afore-mentioned challenges imposed by the nature of the AES application, we propose a hierarchical optimal control strategy which solves both long term trajectory planning and short term disturbance rejection to achieve mission effectiveness. The key contributions are the real-time computational efficiency

(namely, the control algorithm can be implemented at the required sampling rate) of the proposed controller and the experimental validation results. To achieve real-time computational efficiency, we explore the specific structure of the HPS and use a three level control, in which the optimal trajectory planning is solved in the first two levels and the third level deals with trajectory following. At the first level, we ignore the power source dynamics and determine the approximation of the optimal power split between the battery and power sources. At the second level, we include the power source dynamics and leverage the multi time scale so that the optimal power split between gas turbine and fuel cell can be computed in real-time. The optimal trajectory tracking is then formulated as a quadratic programming (QP) based offset-free MPC problem [84] to achieve disturbance rejection and can be easily solved in real-time.

In the remainder of this chapter, the normal mode power management is formulated, the hierarchical controller is proposed and validated on the real-time simulator developed in Chapter 3.

5.1 Problem Formulation and Proposed Control Architecture

For the problem formulation we consider the optimization oriented model of the HPS developed in Chapter 2 where we ignore the dynamics of the power converters. We first describe the power plants and the physical constraints before formulating the PM problem. The nomenclature adopted in the power management controller development is given in Table 5.1. Let $f_1(x_1, u_1)$, $f_2(x_2, u_2)$ denote the gas turbine and fuel cell dynamics and $\Pi_1(x_1, u_1)$, $\Pi_2(x_2, u_2)$ denote the gas turbine and fuel cell output functions.

Table 5.1: Nomenclature used in PM controller design

Variable	***Description***
x_1, u_1, P_1	Gas turbine states, control inputs and power output
x_2, u_2, P_2	Fuel cell states, control inputs and power output
SOC, Q_B	Battery state of charge and capacity (Amp-Hr)
I_B	Current drawn from the battery (Amps)
V_B, P_B	Battery voltage and power output
Script	***Description***
cr	Vital/critical load
d	Demand/ reference variable
SS, $*$	Steady state and optimal variables

Then, the nonlinear HPS is described by

$$\bar{x}_{k+1} = \bar{f}(\bar{x}_k, \bar{u}_k) \tag{5.1}$$

$$SOC_{k+1} = f_B(SOC_k, I_{B,k}) \tag{5.2}$$

$$\bar{P}_k = \bar{\Pi}(\bar{x}_k, \bar{u}_k)$$

$$P_{B,k} = \Pi_B(SOC_k, I_{B,k})$$

where $\bar{x}_k = \begin{bmatrix} x_{1,k} \\ x_{2,k} \end{bmatrix}$, $\bar{u}_k = \begin{bmatrix} u_{1,k} \\ u_{2,k} \end{bmatrix}$, $\bar{P}_k = \begin{bmatrix} P_{1,k} \\ P_{2,k} \end{bmatrix}$, $\bar{f} = \begin{bmatrix} f_1(x_{1,k}, u_{1,k}) \\ f_2(x_{2,k}, u_{2,k}) \end{bmatrix}$ and $\bar{\Pi} = \begin{bmatrix} \Pi_1(x_{1,k}, u_{1,k}) \\ \Pi_2(x_{2,k}, u_{2,k}) \end{bmatrix}$.

We consider three constraints that the control algorithm has to enforce:

1. Component Physical Constraints:

   - To prevent gas turbine compressor surge (Φ_1), fuel cell hydrogen starvation (Φ_2) and ensure that the battery power and capacity are less than their corresponding maximum limits (P_B^{Max}, Q_B^{Max}). These constraints are given

by,

$$\bar{\Phi}(\bar{x}_k, \bar{u}_k) \leq 0, \tag{5.3}$$

$$\Phi_B(SOC_k, I_{B,k}) \leq 0, \tag{5.4}$$

where $\bar{\Phi}_k = \begin{bmatrix} \Phi_1(x_{1,k}, u_{1,k}) \\ \Phi_2(x_{2,k}, u_{2,k}) \end{bmatrix}$ and $\Phi_B = \begin{bmatrix} P_{B,k} - P_B^{Max} \\ Q_{B,k} - Q_B^{Max} \end{bmatrix}$

- To ensure that the control inputs are within the saturation limits given by,

$$\bar{u}_k \in [\bar{u}^{Min},\ \bar{u}^{Max}] \tag{5.5}$$

2. Critical demand constraint given by,

$$-P_{1,k} - P_{2,k} - P_{B,k} \leq -P_{cr,k}. \tag{5.6}$$

3. Terminal SOC constraint: To ensure that at the end of the mission, batteries need to be recharged to the initial SOC. If N denotes the planning horizon, namely the length of the power demand profile associated with the mission, the terminal SOC constraint is given by,

$$SOC_N = SOC_0. \tag{5.7}$$

It must be noted that the control inputs to the power sources are the fueling rates. Hence, to capture the mission effectiveness, the cost function J is defined in terms of power tracking error and fuel consumption over the planning horizon (N), and it is

given as,

$$J(\bar{x}_k, SOC_k, \bar{u}_k, I_{B,k}) = \lambda(P_{d,N} - P_{1,N} - P_{2,N} - P_{B,N})^2$$
$$+ \sum_{k=0}^{N-1} u_{1,k} + u_{2,k} + \lambda(P_{d,k} - P_{1,k} - P_{2,k} - P_{B,k})^2 \tag{5.8}$$

where $\lambda >> 1$ is a penalty factor to achieve proper trade-off between fast power tracking and low fuel consumption. Then, the problem formulation is given as

$$[\bar{u}^*_{[0:N-1]}, I^*_{B,[0:N-1]}] = \arg \min_{\bar{u}_k, I_{B,k}} J(\bar{x}_k, SOC_k, \bar{u}_k, I_{B,k}) \tag{5.9}$$

subject to constraints (5.1)-(5.7).

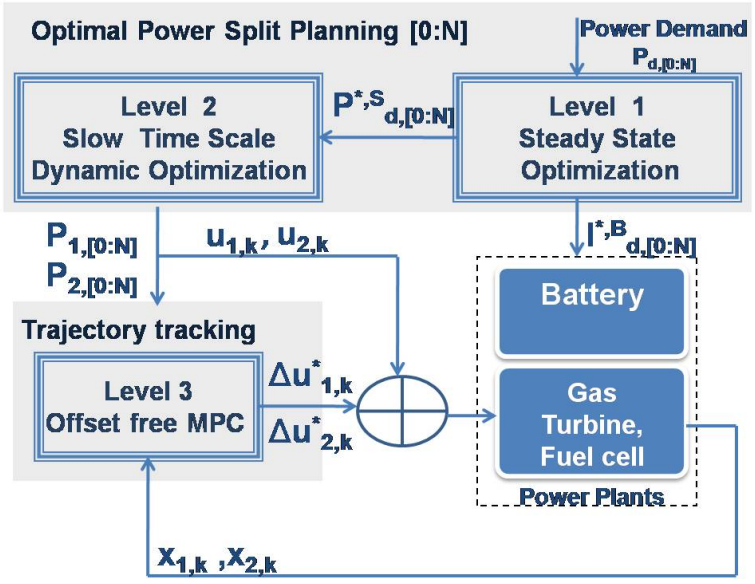

Figure 5.1: Structure of proposed hierarchical controller.

5.1.1 Hierarchical Controller

Given the extended time horizon and the large scale nature of the problem, our approach is to simplify the problem in (5.9) by leveraging the HPS dynamic characteristics. The following assumptions that are relevant to HPS for AES application

have been made for controller development.

A1 For the battery used in military applications, we can discharge and charge instantaneously subject to the power limits. Furthermore, battery charge-discharge losses are neglected.

A2 The HPS power sources exhibit sufficient time scale separation, namely the time response characteristic of gas turbine is much faster than the fuel cell.

A3 For the HPS considered in this work, the combined fuel consumption for the power sources at steady state (W_f) is a quadratic function of the delivered power (P), with $W_f = \Lambda(P)$.

A4 The power demand profile associated with a mission request is piecewise constant with κ step changes in load, where the constant value and the time associated with each step is denoted by P_d^j and K^j for $j \in [1, \kappa]$.

A5 The disturbances in HPS are the variations in the actual power consumption by the load, and they are treated as output disturbances on the power sources.

Under these assumptions, we propose the three-level hierarchical controller (Fig. 5.1). At the top level, the power source dynamics are ignored and an approximate power split between the source and the battery is computed by solving a static optimization problem for optimal steady state performance. While the charge/discharge dynamics are ignored the dynamics associated with the storage are treated using constraints. We consider the top level power split as approximate solutions because the power sources are neglected. Hence in the next level, we include these dynamics and solve a dynamic optimization problem to determine the optimal power trajectories that the sources should be following. Under assumption A2, we approximate the solutions of the second level optimization problem on the slow time scale (See Level 1 optimization in Chapter 4).

Remark 5.1.1 *It must be noted that the fuel-power mapping function of the gas turbine or fuel cell need not be a quadratic function of the power delivered. However in this work, we make assumption A2 based on curve-fitting the total fuel consumption and power output using the steady state fuel-power map of fuel cell and gas turbine. Then we have* $W_f = 0.036P^2 - 0.12P + 0.45$*, where* W_f *is the total fuel flow in* kg/s *and* P *is the output power in* W*.*

Remark 5.1.2 *Leveraging the multi-time scale property facilitates real-time computation efficiency, without which an approach similar to the top-level optimization needs to be adopted to determine the power split between the gas turbine and fuel cell. Since the dynamics are ignored, we need to rely on feedback during transients to improve the power tracking performance and ensure constraint satisfaction. However, the feedback, being a short horizon control can yield a sub-optimal performance since it does not utilize the long term power demand information. Another issue with ignoring the power source dynamics at the planning level is the possible violation of component constraints by the feedback control during transients. These issues can be mitigated when the slow time scale optimization is solved at the second level.*

In the remainder of this section, we delineate the three level controller, where the first two levels deal with the optimal trajectory planning and the third level deals with offset free trajectory tracking.

5.1.2 Level 1: Quadratic Programming for Battery and Source Power Split Planning

In this level, the optimal power split between the battery and power sources over the planning horizon $[0 : N]$ is determined by solving a steady state optimization problem given the computational simplicity. Let α_B^j, α_S^j denote the battery, source power split parameter associated with each piecewise constant (See assumption A4)

power level P_d^j and $P_{d,k}^S$, $P_{d,k}^B$ denote the power demand on the battery and source given by,

$$P_{d,k}^S = \alpha_S^j P_d^j,\ k \in (K_j,\ K_{j+1}) \tag{5.10}$$

$$P_{d,k}^B = \alpha_B^j P_d^j. \tag{5.11}$$

The key idea is to formulate the cost function and the constraints in terms of the power split parameters because at this level our goal is to solve a steady state optimization problem. The cost function to achieve fast and efficient power tracking is defined as

$$J_1 = \sum_{k=0}^{N} \lambda((P_{d,k} - P_{d,k}^S - P_{d,k}^B)^2 + W_{f,k},$$

where $W_{f,k} = \Lambda(P_{d,k}^S)$ is the fuel consumption.

For the power sources, since we ignore the dynamics, the input saturation constraints in (5.5) are specified in terms of the steady state minimum ($P_1^{Min},\ P_2^{Min}$) and maximum ($P_1^{Max},\ P_2^{Max}$) power from the sources associated with the fuel limits. The constraints are given by,

$$P_1^{Min} + P_2^{Min} \leq P_{d,k}^S \leq P_1^{Max} + P_2^{Max}. \tag{5.12}$$

The battery constraints namely, the power and capacity limits along with the terminal SOC constraint , are given by

$$-P_B^{Max} \leq \quad P_{d,k}^B \quad \leq P_B^{Max},\ \forall k \in [0:N], \tag{5.13}$$

$$0 \leq \tfrac{1}{V_{dis}} \textstyle\sum_{i=0}^{k} P_{d,i}^B \leq Q_B^{Max}. \tag{5.14}$$

Under assumption A1, the terminal SOC constraints is given by.

$$\frac{1}{V_{dis}} \sum_{k=0}^{N} P_{d,k}^{B} = 0, \tag{5.15}$$

where V_{dis} denote the battery voltage discharge limit. The critical demand constraint in (5.6) is enforced using

$$-P_{d,k}^{S} - P_{d,k}^{B} \leq -P_{cr,k}. \tag{5.16}$$

If $\alpha_S = [\alpha_S^1, ..., \alpha_S^\kappa]$ and $\alpha_B = [\alpha_B^1, ..., \alpha_B^\kappa]$, the top level steady state optimization problem is then given by

$$[\alpha_S^*, \alpha_B^*] = \arg \min_{\alpha_S, \alpha_B} J_1 \tag{5.17}$$

subject to constraints (5.12) - (5.16). The top level battery, source power split is denoted as $P_d^{*,B}$, $P_d^{*,S}$ and is computed using (5.10), (5.11).

Remark 5.1.3 *Under assumption A3, the optimization problem in (5.17) is a quadratic programming (QP) problem. The computational effort does not depend on the length of the planning horizon (N) or the number of states (n) and control inputs (m) and hence suitable for real-time implementation.*

5.1.3 Level 2: Sensitivity Function Method (SFM) for gas-turbine, fuel cell power split planning

Under assumption A1, we can draw the battery power $P_d^{*,B}$ instantaneously. Hence to achieve fast and efficient demand tracking, the level 2 controller determines the optimal power split between gas turbine and fuel cell to track the demand to the

power sources ($P_d^{*,S}$). The cost function is then defined as,

$$J_2 = \lambda(P_{d,N}^{*,S} - P_{1,N} - P_{2,N})^2 + \sum_{k=0}^{N-1} u_{1,k} + u_{2,k} + \lambda(P_{d,k}^{*,S} - P_{1,k} - P_{2,k})^2 \quad (5.18)$$

The dynamic optimization problem $\mathcal{P}_N$ to determine the optimal gas turbine-fuel cell power split planning is given as,

$$\mathcal{P}_N : \bar{u}_{[0:N-1]}^* = arg \min_{\bar{u}_k} J_2 \quad (5.19)$$

subject to constraints (5.1), (5.3), (5.4), (5.6), (5.7) and

$$-P_{1,k} - P_{2,k} \leq -P_{cr,k} + P_{d,k}^{*,B}.$$

Using A2, since the HPS exhibits time scale separation, we can apply the trajectory optimization methodology developed in Chapter 4 in order to solve the problem given by (5.19) in real-time. The slow time scale optimization problem is formulated to determine the near-optimal approximations to $\mathcal{P}_N$.

Near-optimal Trajectory Planning: As defined in Chapter 4, (τ_f, T_f) and (τ_s, T_s) denote the sampling time and time constant for gas turbine and fuel cell respectively, t_f denotes the total time interval and $\rho = \frac{T_s}{T_f}$. Then, the cost function on the slow time scale is given as

$$J_{slow} = \lambda(P_{d,N_s}^{*,S} - P_{1,N_s} - P_{2,N_s})^2 + \sum_{k_s=0}^{N_s-1} u_{1,k_s} + u_{2,k_s} + \lambda(P_{d,k_s}^{*,S} - P_{1,k_s} - P_{2,k_s})^2$$

where k_s is the discrete time index on the slower time scale and $N_s = \frac{t_f}{T_s}$ is the size of the time window on the slower time scale.

The slow time scale optimization problem $\mathcal{P}_{N_s}$ is given by

$$\mathcal{P}_{N_s} : [\bar{u}^*_{[0:N_s-1]}] = arg\min_{\bar{u}_{k_s}} J_{slow} \tag{5.20}$$

subject to system dynamics (5.1) and the power source physical constraints (5.3) discretized on the slower time scale along with the input saturation constraints (5.5).

Let $\bar{u}_k$ denote the approximations to the true optimal solutions defined in (5.19) and are given by,

$$\bar{u}_k = \bar{u}^*_{k_s},\ \forall \rho k_s \leq k \leq \rho k_s + 1,\ \forall k \in [0 : N-1]. \tag{5.21}$$

Then the near-optimal gas turbine, fuel cell power trajectories denoted by $P_{1,[0:N]}$, $P_{2,[0:N]}$ are the power outputs associated with $u_{1,[0:N]}$, $u_{2,[0:N]}$ determined using (5.25) and the corresponding physical constraint trajectories are denoted as $\Phi_{1,[0:N]}$, $\Phi_{2,[0:N]}$.

Remark 5.1.4 *With assumption A2, we have $N_s << N$. Since the SFM is $\mathcal{O}(N^2)$, solving the optimization problem in (5.22) has reduced computational effort and hence can achieve real-time computational efficiency.*

5.1.4 Level 3: Offset free MPC for trajectory tracking

We consider the linearized system around the level 2 trajectories given by

$$\begin{aligned} \Delta\bar{x}_{k+1} &= A_k \Delta x_{1,k} + B_k \Delta\bar{u}_k \\ \Delta\bar{P}_k &= C_k \Delta\bar{x}_k + D_k \Delta\bar{u}_k + \Delta\bar{d}_k \end{aligned} \tag{5.22}$$

where $\bar{d}_k$ is the output power source disturbance vector (See Assumption A5), $A_k = \frac{\partial \bar{f}}{\partial \bar{x}}|_(\bar{x}_k, \bar{u}_k)$, $B_k = \frac{\partial \bar{f}}{\partial \bar{u}}|_(\bar{x}_k, \bar{u}_k)$, $C_k = \frac{\partial \bar{P}}{\partial \bar{x}}|_(\bar{x}_k, \bar{u}_k)$ and $D_k = \frac{\partial \bar{P}}{\partial \bar{x}}|_(\bar{x}_k, \bar{u}_k)$ are the linearized system matrices of the gas turbine and the fuel cell systems.

The linearized constraints are given by

$$E_k \Delta \bar{x}_k + F_k \Delta \bar{u}_k \leq -\bar{\Phi}_k \tag{5.23}$$

$$\bar{u}^{Min} - \bar{u}_k \leq \Delta \bar{u}_k \leq \bar{u}^{Max} - \bar{u}_k \tag{5.24}$$

where $E_k = \frac{\partial \bar{\Phi}}{\partial \bar{x}}|_(\bar{x}_k, \bar{u}_k)$, $F_k = \frac{\partial \bar{\Phi}}{\partial \bar{u}}|_(\bar{x}_k, \bar{u}_k)$.

The feedback design goal is to achieve fast and efficient tracking of near-optimal power trajectories $P_{1,[0:N]}$, $P_{2,[0:N]}$ with zero steady state tracking error and ensure that the linearized constraints (5.23), (5.24) are satisfied. To achieve these goals, the feedback has to seek transient corrections to account for errors resulting from approximating the solutions to $\mathcal{P}_N$ on the slow time scale. In addition to achieve zero steady state error under disturbances in HPS, the feedback has to use offset-free control ($\Delta \bar{u}^{SS}$) for gas turbine and fuel where $\Delta \bar{u}^{SS} = [\Delta u_1^{SS},\ \Delta u_2^{SS}]^T$. The cost function that captures the design goals is given by,

$$\begin{aligned} J_3 = \sum_{i=k}^{k+N_p} \lambda((P_{d,i}^{*,S} - P_{1,i} - P_{2,i} - \Delta P_{1,i})^2 + \Delta P_{2,i}^2) \\ +(\Delta u_{1,i} - \Delta u_1^{SS})^2 + (\Delta u_{2,i} - \Delta u_2^{SS})^2 \end{aligned}$$

Then the trajectory tracking problem can be formulated as an offset-free model predictive control problem [84] with a prediction horizon N_p and is given as,

$$[\Delta \bar{u}^*_{[k:k+N_p]}] = arg \left\{ \min_{\Delta \bar{u}_i} J_3 \right\} \tag{5.25}$$

subject to constraints (5.23), (5.24), where $N_p << N$ in order to facilitate online implementation.

Here, we assume that we know the disturbance at the beginning of the prediction horizon k and that it is constant inside the prediction horizon. Then the offset

free control is given as $\Delta\bar{u}^{SS} = -(C(I-A)^{-1}+D)^{-1}\Delta\bar{d}_k$. The trajectory planning optimization problem in (5.17), (5.24) is solved once at $k=0$ for trajectory planning, while (5.25) is solved for each time instant k, with x_1, x_2 being updated by the new state measurement for each new optimization run. We now summarize the control algorithm.

Algorithm 5.1: Given the power demand $P_{d,[0,N]}$, we propose the following algorithm to solve the optimization problem (5.9):

1. At k = 0, determine the battery-source power split, $P^{*,B}_{d,[0:N]}$, $P^{*,S}_{d,[0:N]}$, by solving (5.17) and compute the associated battery current $I^{*,B}_{[0:N]}$ and steady state control input to power sources $\bar{u}^0_{[0,N-1]}$;

2. At k = 0, using $\bar{u}^0_{[0,N-1]}$ as the initial control trajectory, solve the slow time scale optimization problem (5.20) and determine $u_{[0,N-1]}$ using (5.21);

3. At each time instant k, with $\Delta u_{1,[k:k+N_p]}$=0, $\Delta u_{2,[k:k+N_p]} = 0$ as the initial control sequence, compute $\Delta u^*_{1,[k:k+N_p]}$, $\Delta u^*_{2,[k:k+N_p]}$ by solving offset free MPC problem (5.25).

4. At each instant k, compute ($I^{*,B}_k$, $u_{1,k}+\Delta u^*_{1,k}$, $u_{2,k}+\Delta u^*_{2,k}$) as the approximation to the solution of optimization problem (5.9).

Remark 5.1.5 *It must be noted that the feedback is utilized for primarily two purposes:*

- *Dealing with uncertainties: While knowledge of perfect model is assumed in the near optimal trajectory planning, modeling errors and uncertainties can cause imperfect power tracking. In this work, we rely on the inherent robustness of MPC in order to deal with model uncertainties.*

- *Dealing with load fluctuations: The near-optimal trajectory planning assumes exact knowledge of power demand profiles. While the demand for the pulse*

loads associated with critical missions such as weapon launch can be assumed to be known precisely, there are often fluctuations in the load which cannot be predicted and therefore cannot be planned for. While the lower level control at load level can deal with some of these fluctuations, the higher level power management can also deal with these load variations. In this work, the load fluctuations are treated as output disturbances and the offset-free feedback control is used to reduce the steady state power tracking error in order to achieve fast load following. Here the disturbance at any time instant is estimated as the difference between the actual power consumed and the demand power.

5.2 Case Study

We apply the proposed control algorithm on the optimization oriented HPS model developed in Chapter 2. The mission considered in this case study is a weapon launch which is represented by a hypothetical power profile (Fig. 5.2 black dotted line), that was chosen based on [3] and consists of pulse power loads. The goal is to utilize the battery power as much as possible to support the pulse power loads and the power sources to achieve perfect load following. Based on the ship-service critical demand requirements [3], we consider 23 battery modules that can provide a maximum of 2185 KW of battery power during pulse power loads. The battery specifications along with other case study parameters are summarized in Table 5.2. The main purpose of the case study is to illustrate the benefits of the controller in Algorithm 5.1 for two cases with and without disturbance. In particular there are two aspects that are highlighted:

S1 Real-time computational efficiency of the proposed three-level controller, that solves optimal power split planning as well as trajectory tracking by leveraging the HPS multi-time scale property, as compared to the full scale optimization

Table 5.2: HPS state and optimization parameters used in the case study.

Name	Value
Gas turbine states ($x_{1,0}$)	[8613 rpm, 2.76 Kg, 1180 K]^T
Fuel cell states ($x_{2,0}$)	[0.23 moles/sec, 9017.5 Pa, 963.2 K]^T
Battery SOC states (SOC_0)	0.95
Battery Type	VL-39P Li-Ion (23 modules)
Critical Demand	$P_{cr,k} \geq$ 1000KW
Base Power Demand	3000 KW
Surge Constraint	$0.00385 m_{b,k} T_{b,k} - 0.98(\omega_{tc,k} - 19.483) \leq 0$
Starvation Constraint	$0.04 - \frac{p_{H_2,an,k}}{p_{an,k}} \leq 0$
Maximum Battery Power (P_B^{Max})	95 KW per module
Maximum Battery Capacity (Q_B^{Max})	22Amp Hr per module
Sample Times	$T_f = 0.05s$, $T_s = 0.2s$
Planning Horizon	$N_s = 200$, $N = 800$

when the system properties are not explored. We make the comparison using the no disturbance case and show how the proposed controller achieves better power tracking performance and fuel economy.

S2 Steady state offset-free power tracking using the proposed feedback controller as compared to the case when we only solve the optimal trajectory planning problem when disturbance in HPS are present.

We discuss these aspects mainly to show that even with the specific shipboard problem characteristics (See C1-C5), the proposed controller can still solve both long term optimal trajectory planning and short term disturbance rejection in real-time without any computational delay unlike the other existing methods.

The implementation of the three level hierarchical controller was done both off-line and real-time where we used a Pentium® processor for the off-line and a dual core OpalRT® realtime target for online optimization. First, we present the results of the level 1 controller. Fig. 5.2 shows the battery-source power split determined using (5.17) for the given pulse power demand over $[0 : 40]s$. It can be seen that the battery is utilized to support pulse loads while the power sources are utilized to support base loads and to recharge the battery.

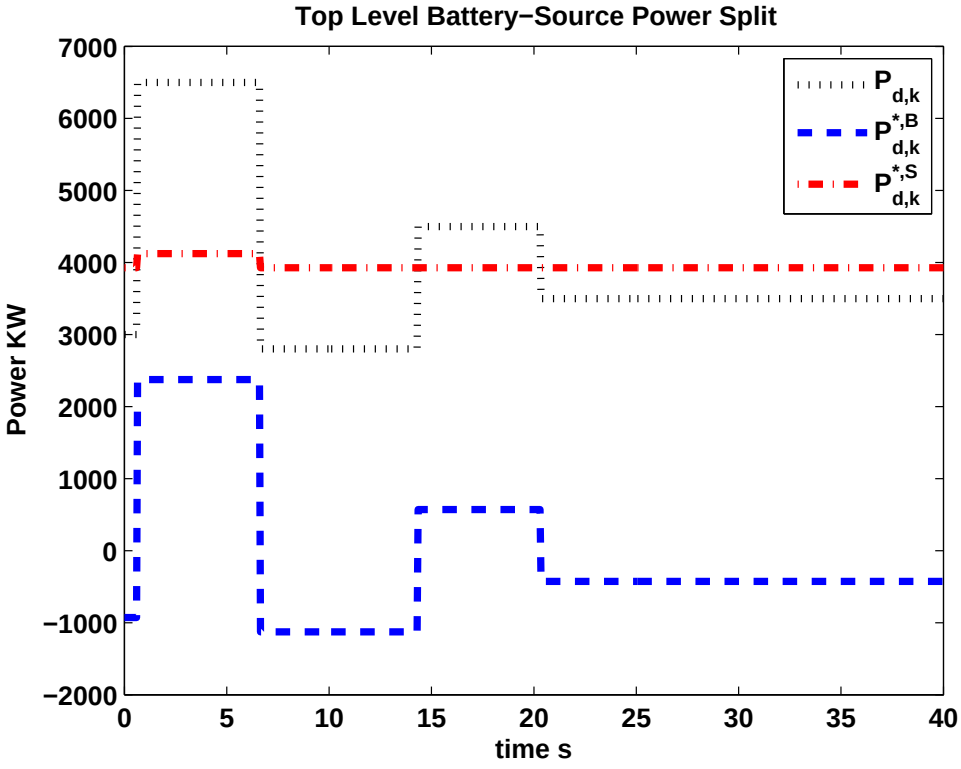

Figure 5.2: Optimal Battery-Source Power Split

We consider the case when no disturbances are present (See S1) and solve the level 2 optimization using SFM with and without leveraging TSS. The real-time computational effort along with the off-line and real-time performance is shown in Table 5.3

Table 5.3: Real-time Effort and Performance Comparison.

Level 2 Method	RT Comp. (s)	Off-line Total Cost	RT Cost	RT $RMSD$ [2] (KW)	RT Mean Fuel Usage(kg)
Full Scale Optimization	1.1	19.77	19.92	1.92	0.025
Leveraging Multi-time Property	0.024	19.98	19.772	0.1342	0.025

It can be seen that because of the complementary time response characteristics between gas turbine and fuel cell, the slow time scale solutions approximate the true optimal solution well, with the loss in optimality being about (Column 3) 2%. In real-time, it takes $0.024s$ ($< T_f$) for the slow time scale approximations to be available as compared to the $1.1s$ ($= 22T_f$) to compute the optimal solutions. Hence till the optimal solutions become available, we use the steady state values as the control associated with trajectory planning. We then rely on the feedback to reduce the performance loss (See *Remark 5.1.2*) due to the computational delay when the multi time scale property is not leveraged. As expected the real-time closed loop performance leveraging time scale separation (19.772) is better than the cost associated with full scale optimization (19.92). It must be noted that using Algorithm 5.1, we achieve better root mean square deviation (RMSD) performance (14 fold improvement) with similar fuel usage as shown in the last two columns of Table 5.3.

Fig 5.3 shows the power tracking and the fueling trajectories with (P^{rt}_{act}) and without (P^{rt}_{slow}) feedback corrections for the case when disturbances in HPS are present (See S2). We consider the following disturbance profile: A 20KW output disturbance on the gas turbine for the first half of the planning horizon and a 10KW disturbance on both the power sources during the remaining period. It can be seen that the feedback uses the offset free control to achieve zero steady state error which is not

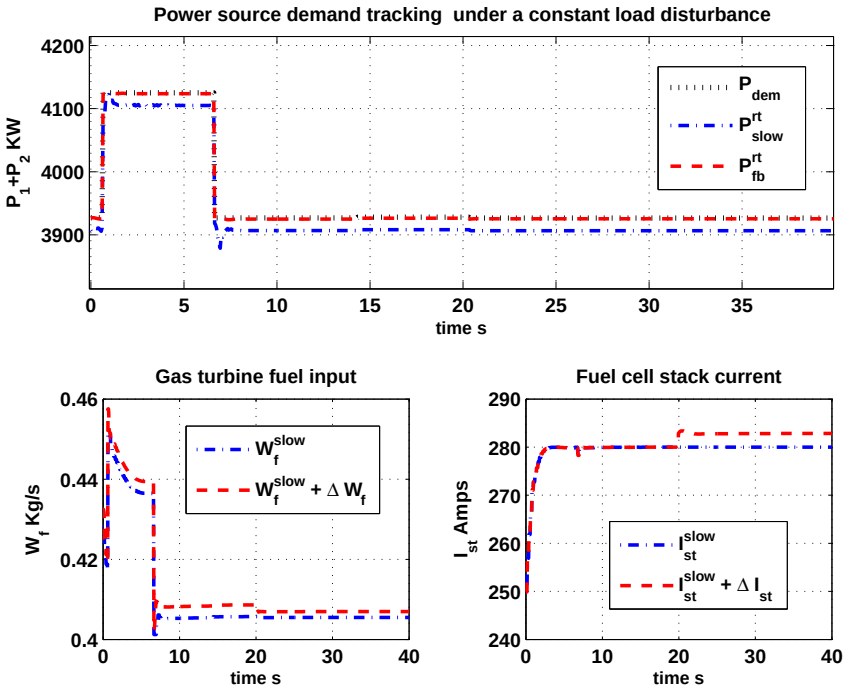

Figure 5.3: Real-time optimal power and fuel trajectories: 20KW load disturbance

possible if we only solve the trajectory planning problem. The proposed controller satisfies all the constraints for both the case S1 and S2 where the maximum values of the surge and starvation constraints are -0.2 and -0.005 respectively.

5.3 Summary

A hierarchical controller is proposed in this chapter to solve the power management problem for normal operating scenarios. The proposed approach is beneficial in ensuring mission effectiveness due to the realtime computational efficiency which has been illustrated through a case study of the real-time simulator. While the design has focussed on performance considerations, those of survivability during failure needs to be addressed. The next chapter will precisely focus on the improving survivability through power management.

Chapter 6

Failure Mode Power Management of HPS in All-Electric Ship Applications

This chapter deals with the design of a power management scheme during a shipboard power source failure, which is an important scenario that the all-electric ships used for military applications have to deal with. A special treatment for the PM is required as the design considerations to deal with these failures are quite different from the normal mode requirements. While achieving performance in terms of efficiency and fast load-following is of prime importance during the normal operating conditions, sustaining this may not even be possible when the HPS is damaged. For that reason, recovering normal functions without causing further damage to the HPS is of primary importance. Hence the goals of failure mode power management is to ensure survivability, namely, the capability of power management system to sustain critical shipboard operations and recover normal functions quickly while ensuring the safety of the HPS components.

One approach to deal with failures that has been proposed in the shipboard power system literature [24–31] is determining the power flow paths in order to keep the high priority loads energized while shedding the non-essential loads. This mechanism is known as network reconfiguration. However, in order to improve the survivability, al-

ternate approaches for maximizing the load support needs to be investigated, thereby motivating the power management strategy developed in this chapter. Traditionally, backup power sources have been utilized to deal with the failures, but these sources may take longer times to warm up. During this time, the ability of the power system to meet the onboard demand is greatly compromised. Heuristic methods of increasing the demand on the working power sources may not be possible due to the risk of violating the component's physical constraints, thereby necessitating rigorous PM schemes.

For the HPS considered in this work (Fig. 1.2), the control objectives right after a power source failure are,

- Enforcing the battery and working power source physical constraints throughout the backup power source warming up period.
- Meeting the critical load demand all through the warmup period and support the non-critical loads as much as possible.

While the problem characteristics are very similar to those of normal mode operations, the underlying assumptions for the failure mode are different (namely, existence of multi time scale property). In addition, in this mode of operation, the safety enforcement is of primary importance as compared to the performance which is in contrast with the normal mode considerations. Therefore a separate controller for the failure mode power management is developed. Given the unpredictable nature of failures, the optimal control has to be executed in real-time and enforce component safety all through the extended horizon till the back-up source is warmed up. The two requirements make the optimal control development challenging.

Even though the failure mode power management can be treated as a trajectory optimization problem, all the open issues associated with both the grid based (DP, IDP, SDP, Shortest path-SDP) and gradient based (SQP) approaches still ex-

ist. In addition, given the unpredictable nature of failures, we cannot assume that the un-failed HPS components exhibit time scale separation, making the methodology proposed in Chapter 4 also unsuitable. While MPC is another possible method, the main issue here is the difficulty in achieving a good tradeoff between real-time computational efficiency and guaranteeing safety throughout the warmup period.

We propose a hierarchical optimal control strategy that utilizes the power demand profile information to enforce component safety during the warm-up period and resume the support for the non-critical loads as quickly as possible. The key merits of the proposed approach are the real-time efficiency as well as the long term constraint enforcement which have been experimentally validated on the scaled test-bed developed in Chapter 3. To achieve real-time efficiency, we explored the nature of the failure mode problem where constraint enforcement (to ensure component safety) is the key consideration and hence recast the optimal control problem to treat safety and performance separately.

The proposed method is a two level approach, where at the top level we ignore the component dynamics and determine the sub-optimal power split between the battery and the working source to meet the HPS load demand. At the second level, we formulate the constraint enforcement problem using reference governor (RG) [85, 86], where the demand to the working source and energy storage is governed to ensure safety. The RG approach is a natural formalism for constraint enforcement. This approach is much simpler (1-D search space) as compared to other MPC methods and allows long horizon look ahead without compromising real-time performance. In order to account for the performance deterioration due to ignoring power source dynamics at the top level, we utilize the battery to improve the power tracking performance based on coordination between the working source and energy storage. The problem formulation along with the controller development as well as validation is delineated in the remainder of this chapter.

6.1 Problem Formulation and Proposed Hierarchical Controller

We consider the scenario of a power source failure with unpredictable failure time, even though the ideas used in the controller development can be extended to failure of other HPS components. We assume that a back-up source is added to the HPS at the failure instant and define the warmup period as the time from the instant of failure to the time when the back-up source is fully functional. During this time, we assume that the back-source cannot be used to support any loads. For the HPS considered in this work, the working power source can be either gas turbine or fuel cell. We first describe the power plants and the safety constraints before formulating the optimal control problem. The nomenclature adopted in the power management controller development is given in Table 6.1.

Table 6.1: Nomenclature used in PM controller design

Variable	***Description***
x_S, u_S, P_S	Working source states, control inputs and power output
SOC, Q_B	Battery state of charge and capacity (Amp-Hr)
I_B	Current drawn from the battery (Amps)
V_B, P_B	Battery voltage and power output
x_1, u_1, P_1	Gas turbine states, control inputs and power output
x_2, u_2, P_2	Fuel cell states, control inputs and power output
Script	***Description***
cr	Vital/critical load
d	Demand/ reference variable
rg	Reference governor output
SS, $*$	Steady state and optimal variables

We denote $T_F = 0$ [1] as the instant when one of the power source fails, at which an additional power source is brought on with a warm-up time represented by T_w discrete time steps, where $[0,\ T_w]$ is the warmup horizon. Let $f_S(x_S, u_S)$, $h_S(x_S, u_S)$

[1] We assume $T_F = 0$ in this chapter to simplify the exposition without losing generality.

denote the working source (gas turbine or fuel cell) dynamics and output function respectively. Then, the nonlinear HPS dynamics are described by

$$x_{S,k+1} = f_S(x_{S,k}, u_{S,k}) \tag{6.1}$$

$$SOC_{k+1} = f_B(SOC_k, I_{B,k}) \tag{6.2}$$

$$P_{S,k} = h_S(x_{S,k}, u_{S,k})$$

$$P_{B,k} = h_B(SOC_k, I_{B,k})$$

where $u_{S,k}$ is the fuel input to the working power source.

We consider two constraints that the control algorithm has to enforce inside the warmup horizon:

1. Component Physical Constraints:

   - To prevent gas turbine compressor surge or fuel cell hydrogen starvation, depending on which power source fails (Φ_S). To ensure that the battery power and capacity are less than their corresponding maximum limits (P_B^{Max}, Q_B^{Max}). These constraints are given by,

$$\Phi_S(x_{S,k}, u_{S,k}) \leq 0, \tag{6.3}$$

$$\Phi_B(SOC_k, I_{B,k}) \leq 0. \tag{6.4}$$

   where $\Phi_B = \begin{bmatrix} P_{B,k} - P_B^{Max} \\ Q_{B,k} - Q_B^{Max} \end{bmatrix}$

   - To ensure that the control inputs are within the saturation limits given by,

$$u_{S,k} \in [u^{Min},\ u^{Max}] \tag{6.5}$$

2. Critical demand constraint given by,

$$-P_{S,k} - P_{B,k} \leq -P_{cr,k}. \tag{6.6}$$

The cost function J captures the performance in terms of minimizing the power tracking error and working source fuel consumption over the warmup horizon and is given by

$$J = \sum_{k=0}^{T_w} u_{s,k} + \lambda(P_{d,k} - P_{S,k} - P_{B,k})^2$$

where $\lambda >> 1$ is a penalty factor to achieve accurate demand tracking. Then the optimal control problem formulation is given by

$$[I^*_{B,[0:T_w]}, u^*_{S,[0:T_w]}] = arg \min_{I_{B,k}, u_{S,k}} J \tag{6.7}$$

subject to constraints (6.1)-(6.6) that need be enforced over $[0,\ T_w]$

Given the extended warmup horizon, we have to consider a shorter prediction horizon of length N ($N << T_w$) in order to use the MPC approach for real-time control. The optimal control inputs at every time instant ($u^*_{S,k}$, $I^*_{B,k}$) are then determined by solving the following problem ,

$$[I^*_{B,[k:k+N-1]}, u^*_{S,[k:k+N-1]}] = arg \min_{I_{B,k}, u_{S,k}} \sum_{i=k}^{k+N-1} u_{S,i} + (P_{d,i} - P_{1,i} - P_{Batt,i})^2 \tag{6.8}$$

subject to constraints in (6.1)-(6.6). Note that for the MPC formulation, the constraints are enforced over the prediction horizon, namely $[k,\ k+N-1]$, where k is any given time instant. To determine the optimal control inputs over the entire warmup period, the problem in (6.7) is solved repeatedly for every time instant $k \in [0,\ T_w]$ adopting receding horizon approach.

Remark 6.1.1 *The MPC problem in (6.8) is a nonlinear optimization problem whose computational effort depends on the dimension of the problem, namely the number of states (n), control inputs (m) and length of the optimization horizon (N). For most of the existing algorithms, the computational effort required to determine the optimal solution does not scale linearly with the addition of more HPS components. In addition the choice of N plays a very important role as there exists a trade-off between reducing the computational effort and enforcing safety constraints. A short-sighted approach (small N) may significantly reduce the computational effort, but cannot guarantee successive feasibility* [2] *during the warmup period.*

The issue raised in *Remark* 6.1.1, motivates the need for alternate control approaches to solve the failure mode PM in (6.7), given the real-time control requirement.

6.1.1 Hierarchical RG based control

Given the large scale nature of the problem, our goal is to simplify the problem in (6.7) by leveraging the nature of the control required for failure mode operations. Here the primary function of the PM is mainly to achieve safety enforcement over the warmup period and performance is on secondary importance. The key idea used in the proposed controller is to decouple the performance from constraint enforcement considerations and recast the optimization problem in (6.7) to treat the two considerations separately. This approach allows using simpler mechanisms targeting constraint enforcement (e.g reference governor). The following assumptions that are made for controller development.

A1 For the battery used in military applications, we can draw power instantaneously subject to the capacity limits.

[2] This is defined as the existence of a feasible solution for the optimization problem at every iteration.

A2 For the HPS considered in this work, the fuel consumption for the power sources at steady state (W_f) is a quadratic function of the power demand (P), with $W_f = \Lambda(P)$ (See Remark 5.1.1).

A3 The power demand profile, namely the load demand on the HPS during the warmup period, is piecewise constant with κ step changes in load, where the constant value and the time associated with each step is denoted by P_d^j and K^j for $j \in [1, \kappa]$.

Under these assumptions, we propose a two level hierarchical controller (Fig 6.1) to approximate the optimal solutions to the problem in (6.7). At the top level, the working source dynamics are ignored and, an approximation to the optimal power split between the battery and power source is computed by solving a steady state optimization problem. Here we treat the battery storage mechanism and capacity as constraints. At the next level, we deal with the constraint enforcement over the warmup period using reference governor based approach.

Remark 6.1.2 *Even though the RG can strictly enforce safety constraints, this being an add-on mechanism requires the reference inputs, namely the power demand to the working source and battery to be pre-computed. Hence we need to solve the top level optimization problem in order to determine the sub-optimal battery, source power demand trajectories.*

We delineate the proposed two level controller (Fig.6.1) in the remainder of this section.

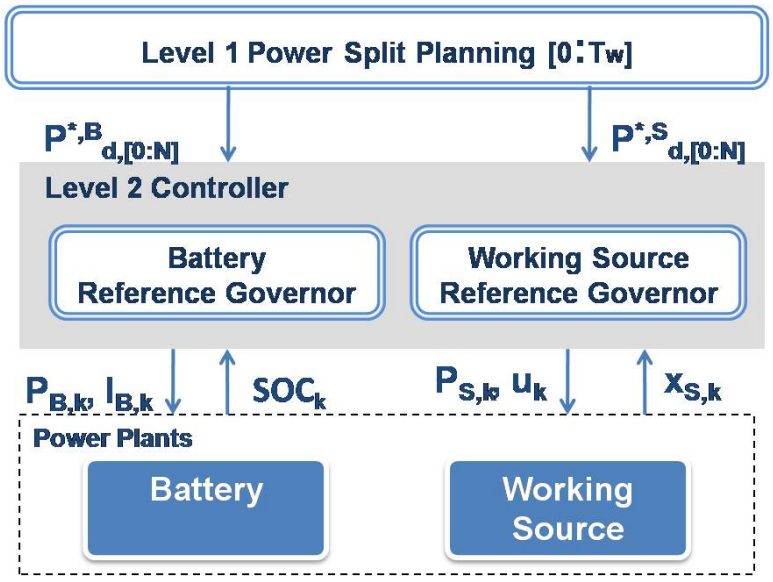

Figure 6.1: Structure of the proposed hierarchical controller.

6.1.2 Level 1: Quadratic Programming for Battery Source Power Split Planning

In this level, an approximate power split between the battery and the working source over the warmup period $[0 : T_w]$ is determined using similar ideas from Section 5.1.2 where a steady state optimization problem was solved. Note that unlike section 5.1.2 which had both the power sources working, here we consider only one working power source. Therefore, α_B^j, α_S^j denotes the power split parameters for the battery and the working power source respectively, associated with each piecewise constant power level P_d^j and $P_{d,k}^S$, $P_{d,k}^B$ denote the power demand on the battery and the working source as defined in (5.10), (5.11).

The cost function to maximize the non-vital support during the warmup period is given by,

$$J_1 = \sum_{k=0}^{T_w} \lambda((P_{d,k} - P_{d,k}^S - P_{d,k}^B)^2 + W_{f,k},$$

where $W_{f,k} = \Lambda(P^S_{d,k})$ is the fuel consumption.

For the working power source, the input saturation constraints in (6.5) are specified in terms of the steady state minimum (P^{Min}) and maximum (P^{Max}) power corresponding to the working source fuel limits and is given by,

$$P^{Min} \leq P^S_{d,k} \leq P^{Max}, \tag{6.9}$$

The battery is primarily used in the discharge mode, unlike the problem in Section 5.1.2, and the constraints namely the power and capacity limits are hence given as,

$$P^B_{d,k} \leq P^{Max}_B, \ \forall k \in [0 : T_w] \tag{6.10}$$

$$\frac{1}{V_{dis}} \sum_{i=0}^{k} P^B_{d,i} \leq Q^{Max}_B \tag{6.11}$$

where V_{dis} denote the battery voltage discharge limit.

The critical demand constraint in (6.6) is enforced using (5.16) using the working source. If $\alpha_S = [\alpha^1_S, ..., \alpha^\kappa_S]$ and $\alpha_B = [\alpha^1_B, ..., \alpha^\kappa_B]$, the top level static optimization problem is then given by

$$[\alpha^*_S, \alpha^*_B] = \arg \min_{\alpha_S, \alpha_B} J_1 \tag{6.12}$$

subject to constraints (6.9) - (6.11) and

$$-P^S_{d,k} - P^B_{d,k} \leq -P_{cr,k} \tag{6.13}$$

The top level battery, source power demand trajectories denoted as $P^{*,B}_{d,[0:T_w]}$, $P^{*,S}_{d,[0:T_w]}$ is then computed using (5.10), (5.11).

Remark 6.1.3 *Under assumption A3, the optimization problem in (6.12) is a quadratic programming (QP) problem. The computational effort does not depend on the length*

of the planning horizon (N) or the number of states (n) and control inputs (m) and hence suitable for real-time implementation.

Remark 6.1.4 *We consider the discharge voltage limit in (6.11) instead of the actual battery voltage (2.1) to compute the current drawn from the battery. This is done for two reasons: First, to formulate the capacity constraint linear so that the top-level problem is a QP problem. Second, to ensure the nonlinear capacity constraint satisfaction (6.4), whenever the linear capacity constraint in (6.11) is enforced, where the nonlinear capacity constraint is given by*

$$\frac{1}{V_{batt}} \sum_{i=0}^{k} P_{d,i}^{B} \leq Q_{B}^{Max}$$

To see this, note that since $V_{dis} \leq V_{batt}$*, if* $\frac{1}{V_{dis}} \sum_{i=0}^{k} P_{d,i}^{B} \leq Q_{B}^{Max} \Rightarrow \frac{1}{V_{batt}} \sum_{i=0}^{k} P_{d,i}^{B} \leq Q_{B}^{Max}$*. Even though this approach will result in a lower battery utilization as compared to the optimal solutions by solving (6.7), the benefits of the computational efficiency makes it attractive.*

6.1.3 Level 2: Reference Governor For Constraint Enforcement

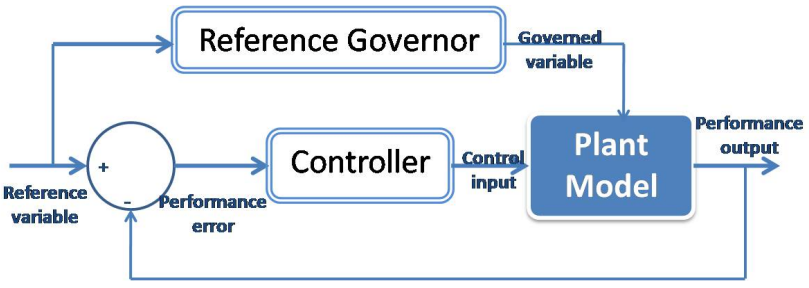

Figure 6.2: Schematic of Reference Governor

At this level, the reference governor is designed to track the power demand trajectories passed on from level 1 ($P_d^{*,S}$ and $P_d^{*,B}$) under component dynamic constraints

(6.3)-(6.6). This is an add-on mechanism (Fig 6.2), where there is a designed nominal controller in the loop to regulate the performance variables. In this work, it is assumed that the nominal controllers are available and only focus on the reference governor design. Based on [86], the reference input, which is the power demand in this case, is modified at every time instant till the constraints are satisfied and is determined as follows:

$$P^S_{rg,k} = P^S_{rg,k-1} + \beta^{*,S}_k (P^{*,S}_{d,k} - P^S_{rg,k-1}), \tag{6.14}$$

$$P^B_{rg,k} = P^B_{rg,k-1} + \beta^{*,B}_k (P^{*,B}_{d,k} - P^B_{rg,k-1}). \tag{6.15}$$

where β^S_k, $\beta^B_k \in [0, 1]$ can be viewed as nonlinear, time-varying filter parameters for the working source and battery respectively.

In order to have the governed value, namely $P^S_{rg,k}$, $P^B_{rg,k}$, track the power demand, the RG maximizes the filter parameters (β^S_k, β^B_k) at every instant. The optimal filter parameters for the working source and battery are then determined as,

$$\beta^{*,S}_k = \arg\max \beta^S_k \tag{6.16}$$

subject to constraints

$$\Phi_S(x_{S,i}, u_{S,i}) \leq 0, \, \forall i \in [k : k + N_s] \tag{6.17}$$

$$-P_{S,i} \leq P_{B,i} - P_{cr,i}, \tag{6.18}$$

$$\beta^{*,B}_k = \arg\max \beta^B_k$$

subject to constraints

$$\Phi_B(SOC_i, I_{B,i}) \leq 0, \forall i \in [k : k + N_s] \tag{6.19}$$

$$-P_{B,i} \leq P_{S,i} - P_{cr,i}, \tag{6.20}$$

where N_s is the simulation horizon inside which the constraints need to be enforced. This is done by simulating the model multiple times at each sampling instant in order to check the constraint feasibility given in (6.17), (6.18), (6.20), (6.21).

Remark 6.1.5 *The optimization problem in (6.8) is an 1-D search problem as compared to the RHC approach where the dimension of the search space is mN. At each instant the optimization parameter (β_k) is determined using bisectional search, where the HPS model is simulated for the simulation horizon ($[k : k + N_s]$). If constraint violation occurs then β is reduced and the simulation is re-initiated. If all the constraints are satisfied, then the value of β is increased to achieve better power tracking and the search is repeated till β converges.*

Remark 6.1.6 *The simulation horizon is chosen such that if the reference input is held constant throughout the simulation horizon $[k : k + N_s]$, then all the constraints are satisfied, which is typically the settling time of the system dynamics. To guarantee feasibility throughout the reconfiguration process, we choose a relatively large simulation horizon which is 3-5 times the speed of the system dynamics. Even though a larger simulation horizon N_s implies increased model simulation time, since the search is over the optimization parameter space, this does not increase the optimization problem dimension and hence the computational effort. However, in the model predictive control approach, an increase in optimization horizon N will increase the computational effort.*

Remark 6.1.7 *In standard reference governor implementation, the input is held con-*

stant over the simulation horizon $[k : k + N_s]$. *However, since the time-varying reference input is known during the entire warmup period for both the battery and the working power source, we utilize this information and hence consider the time varying reference input* ($P^S_{d,[k:k+N_s]}$, $P^B_{d,[k:k+N_s]}$) *in the implementation which is given as,*

$$P^S_{d,i} = min(P^{S,*}_{d,i}, P^{S,*}_{d,k}) \ \forall i \in [k, k + N_s] \tag{6.21}$$

$$P^B_{d,i} = min(P^{B,*}_{d,i}, P^{B,*}_{d,k}) \tag{6.22}$$

The schematic of the reference governor implementation is given in Fig. 6.3.

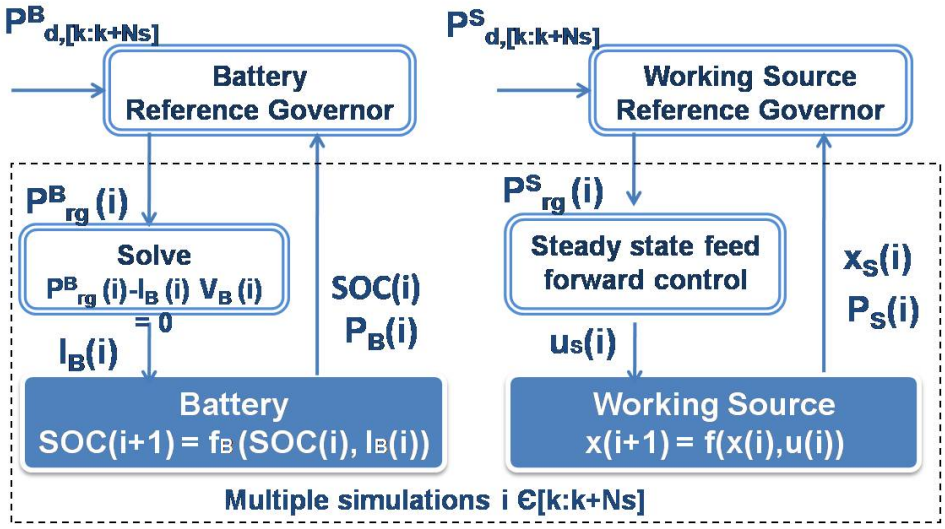

Figure 6.3: Schematic of Reference Governor Implementation

Modifying Reference Input Using Coordination Under assumption 1, the battery power output (P_B) will track the reference input ($P^{*,B}_d$) perfectly when $\beta^{*,B}_k$=1. However for the working source, even if the $\beta^{*,S}_k$=1, there will be imperfect transient power tracking due to ignoring the source dynamics in the top-level optimization. Note that, since the battery can be used to support pulse loads (Assumption A1), we can utilize the battery in order to improve the transient power tracking. To do so, we use ideas from distributed model predictive control [87], where coordination between the battery and working power source is required. Here, the

implementation requires communication of the steady state control associated with the optimally governed reference trajectories at every instant from the working source to the battery. Then, at the next time instant, the reference input to the battery is modified based on the predicted working source power tracking performance.

The optimal power split planning problem (6.12) is solved once at $k = 0$, while (6.16) and (6.19) are solved at each instant k, with $x_{S,k}$, SOC_k being updated by the new state measurement for each new optimization run.

Algorithm 6.1: Given $x_S(T_f)$, $SOC(T_f)$ and the power demand $P_{d,[T_f:T_f+T_w]}$, we propose the following algorithm to solve (6.7)

1. At $k = 0$, determine optimal power split $P^{*,S}_{d,[T_f:T_f+T_w]}$ and $P^{*,B}_{d,[T_f:T_f+T_w]}$ by solving (6.15).

2. At each time instant k, using $P^{*,S}_{d,[k:k+N_s]}$, $P^{*,B}_{d,[k:k+N_s]}$,

   (a) Modify the reference input to the battery as $P^{*,B}_{d,[k:k+N_s-1]} + e^S$, where

$$e^S = \begin{cases} \mathbf{0}_{1,N_s}, & k = T_f \\ P^{*,S}_{d,[k:k+N_s-1]} - P^{C}_{[k:k+N_s-1]}, & k > T_f. \end{cases}$$

   where $P^{C}_{[k:k+N_s-1]}$ is the output trajectory associated with $u^{C}_{[k:k+N_s-1]}$ given by (6.25).

   (b) Compute the time varying $P^{S}_{d,[k:k+N_s]}$ and $P^{B}_{d,[k:k+N_s]}$ using (6.22) and (6.23). bisectional search algorithm, solve (6.16) and (6.19) and determine $\beta^{*,S}_k$ and $\beta^{*,B}_k$.

   (c) Determine $P^{S}_{rg,[k:k+N_s]}$, $P^{B}_{rg,[k:k+N_s]}$using (6.14), (6.15).

   (d) Determine the feed-forward steady state control input $u_{S,[k:k+N_s]}$ associated

with $P^{S}_{rg,[k:k+N_s]}$ and battery current $I_{B,[k:k+N_s]}$, given as

$$P^{B}_{rg,[k:k+N_s]} - I_{B,[k:k+N_s]} V_{B,[k:k+N_s]} = 0, \tag{6.23}$$

where the battery voltage $V_{B,k}$ is defined in (2.1).

(e) Apply the first value of the feed-forward control and battery current sequence computed in step 2.d($u_{S,k}$ and $I_{B,k}$) as the approximation to the optimal solutions of (6.7).

(f) Construct and transmit the coordination control sequence, to the battery which is given as

$$u^{C}_{[k+1:k+N_s+1]} = [u_{S,[k+1:k+N_s]},\ u^{SS}_{[k+N_s+1]}], \tag{6.24}$$

where $u^{SS}_{[k+N_s+1]}$ is the steady state control associated with the power demand to the working source $P^{*,S}_{d,[k+N_s+1]}$.

Remark 6.1.8 *It should be noted that we denote the controller implementation as uncoordinated (UC) if the step 2(a) of Algorithm 6.1 is not implemented and with coordination (WC) if Algorithm 6.1 is exactly implemented.*

6.2 Case Study

We consider a gas turbine failure for the case study and apply the proposed controller on the HPS model developed in the previous section. The demand on the HPS is represented as a hypothetical power profile (Fig. 6.4) that was chosen based on the ship-service power requirements given in a previous work [3]. The case study parameters are shown in Table 6.2. Since we are emulating a gas turbine failure, the T_w is chosen to be of the order of a few minutes ($T_w = 5min$), which corresponds to

the warm-up times for ship-service gas turbines [3]. The main purpose of the case

Table 6.2: HPS state and optimization parameters used in the case study.

Variable	Value
Fuel cell states ($x_{S,0}$)	$[0.23$ moles/sec, 9017.5 Pa, 963.2 $K]^T$
Battery SOC states (SOC_0)	1
Battery Type	VL-39P Li-Ion (23 modules)
Critical Demand	$P_{cr,k} \geq 1000$KW
Starvation Constraint	$0.04 - \frac{p_{H_2,an,k}}{p_{an,k}} \leq 0$
Maximum Battery Power (P_B^{Max})	95 KW per module
Maximum Battery Capacity (Q_B^{Max})	22Amp Hr per module
Sample Time	$T_s = 0.05s$,
Failure Instant	$T_f = 0$
Warmup Period	$T_w = 5$min

study is to illustrate the benefits of the controller in Algorithm 6.1. In particular two aspects are highlighted:

- Real-time computational efficiency of the proposed controller as compared to the MPC. We make the comparison using short and long constraint horizons in order to show that the proposed controller can have a longer simulation horizon without incurring polynomial increase in the computational effort. Therefore the proposed method can be used to achieve long term constraint enforcement in real-time.

- Real-time performance improvement using the proposed controller as compared to the MPC method in terms of power tracking and fuel consumption.

We discuss these aspects mainly to show that even with the specific shipboard problem characteristics (described at the beginning of this chapter), the proposed controller

can still enforce the safety constraint all through the warmup period and support non-critical loads quickly in real-time. Even though safe backup strategies always exist, without the real-time efficiency, the survivability of the HPS will be compromised, either in terms of non-vital load support or the component safety.

The implementation of the two level hierarchical controller was done both off-line and in real-time where we used a Pentium® processor for the off-line optimization. The OpalRT® realtime target and the scaled test-bed developed in Chapter 3 is used for online optimization. We consider two different lengths for the prediction (N) and simulation horizon (N_s) and solve the optimal control problem in (6.8) using the proposed controller and the RHC approach. We do so to understand the tradeoff between computational effort and constraint enforcement, where a larger prediction horizon is required to ensure long term system safety.

Table 6.3 shows the comparison of the offline computational effort of the RHC and RG methods as the optimization and simulation horizon is increased respectively. We denote the computation effort associated with the shorter horizon for RHC ($N = 40$) and RG ($N_s = 40$) methods as T_{40}^{RHC}, T_{40}^{RG}. For this case study, we have $T_{40}^{RHC} = 1783s$ and $T_{40}^{RG} = 6s$ for a single optimization run at each sample instant. It can be seen that for the RHC based approach the increase is $\mathcal{O}(N^2)$ (24.1 times) as compared to RG (1.2 times) which is in accordance with Remark 6.1.6.

Table 6.3: Comparison of RHC and RG Methods for Computational Effort Vs Length of Horizon

Method	Horizon length	Off-line computation effort
RHC	$N = 40$	T_{40}^{RHC}=1783s
RHC	$N = 200$	24.1 T_{40}^{RHC}
RG	$N_s = 40$	T_{40}^{RG}=6s
RG	$N_s = 200$	1.2T_{40}^{RG}

The performance benefits of the proposed controller, due to its real-time computational efficiency, is illustrated in the sequel. Here, the performance is specified in terms of working source fuel consumption and power tracking error over the warmup period given as $\sum_{k=0}^{T_w} \lambda(P_{d,k} - P_{S,k} - P_{B,k})^2 + u_{S,k}$. The real-time computational effort along with the off-line and real-time performance is shown in Table 6.4. The off-line cost using the proposed control approach is suboptimal as compared to the model predictive control approach (Column 3), which is due to ignoring the working source dynamics at the top level controller. In real-time it takes $0.3ms$ ($< T_s$) for the sub-optimal solutions to be available using the reference governor approach as compared to the 0.642s ($> T_s$) when RHC method is implemented. Hence till the optimal solutions become available, we apply the control input at the previous instant to ensure constraint satisfaction which results in a performance loss in real-time using the MPC approach (Column 4).

Table 6.4: Real-Time Computational Effort

Method	Real-time Computation effort	Off-line Cost	Real-time Cost
RHC $N = 40$	0.642 sec	16.1	647
RG $N_s = 150$	0.0003 sec	34.4	34.4

Fig. 6.4 shows the real-time power tracking trajectories with (WC) and without (UC) using coordination (*Remark 6.1.8*). It can be seen that the demand tracking can be improved using coordination, where the battery can be utilized in order to compensate for the performance loss due to ignoring the fuel cell dynamics in the top-level optimization as shown in Fig. 6.5. The proposed controller enforces the fuel cell starvation constraint and the battery capacity constraint as shown Fig. 6.6. It can be seen that the battery state of charge constraint at the end of the warmup period is not active, which means that we are under utilizing the battery. Even though this may

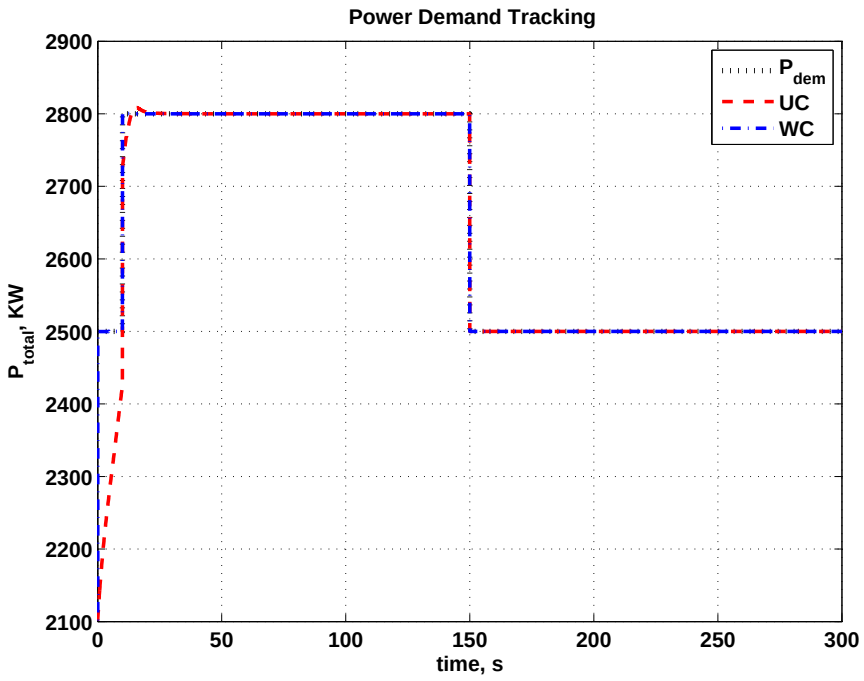

Figure 6.4: Real-time power tracking with (WC) and w/o (UC) coordination

seem counter-intuitive at the onset, this is very much in accordance to *Remark 6.1.5*. Note that the capacity constraint will be active only when the discharge voltage V_{dis} is used instead of the battery terminal voltage V_B to compute the battery current.

6.3 Summary

In this chapter, we have proposed a hierarchical optimal controller for failure mode power management of HPS for shipboard applications to sustain critical functions and recover normal operations during failures. The use of this approach is beneficial in ensuring HPS survivability due to the real-time computational efficiency. We have demonstrated using a case study that the proposed controller enforces the safety constraints in the long-term and also achieves better performance as compared to model predictive control based approach.

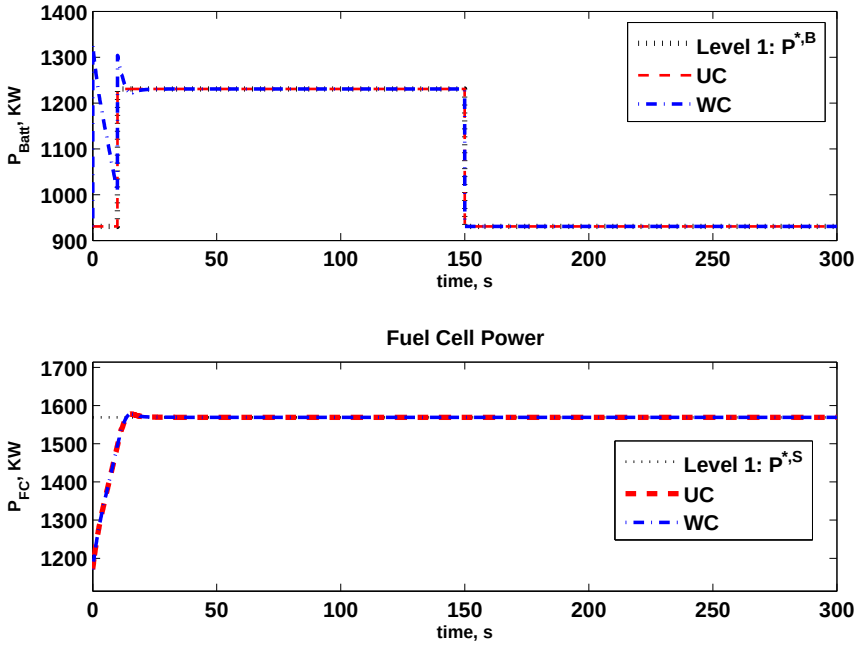

Figure 6.5: FC and Battery Power Split with (WC) and w/o (UC) Coordination

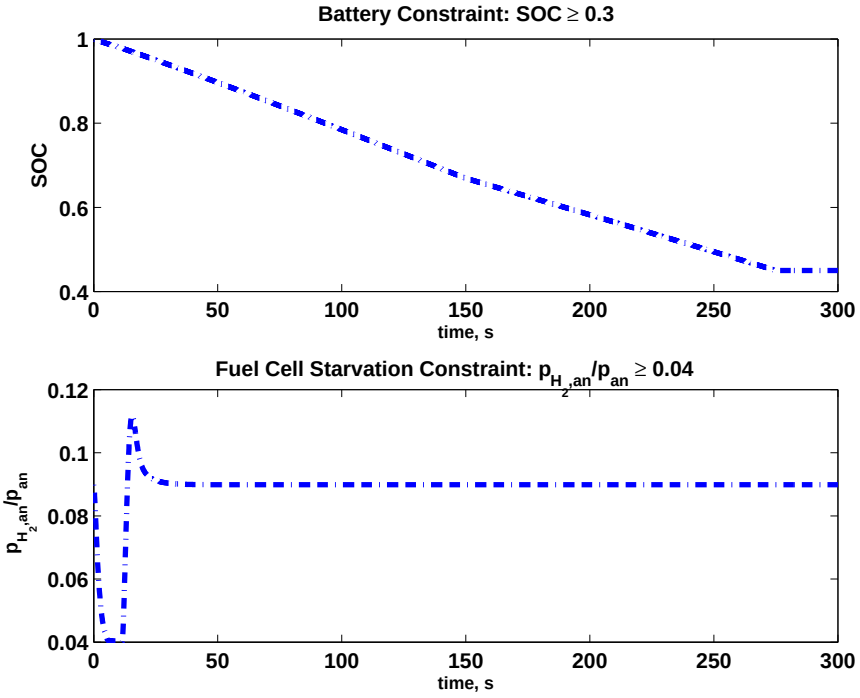

Figure 6.6: Battery and Fuel cell Constraints for the case with coordination

Chapter 7

Conclusions and Future Work

This dissertation has addressed the real-time power management of hybrid power systems for all-electric ships targeting military applications. While the HPS enables ship-electrification which ushers in many opportunities in terms of clean and efficient power generation, the unique nature of the military applications makes the real-time control quite challenging. Therefore, the central theme of this dissertation has focused on power management schemes that can be executed in real-time. To this effect, the research effort has focused on tools for both modeling and analysis as well as control design and validation. The tool development included both optimization and simulation oriented models as well as a scaled test bed which will be used for all-electric research and development purposes. On the methodology aspect, by exploiting the dynamic characteristics of the HPS, real-time power management schemes that can deal with both normal and failure mode of operations were developed and validated on the scaled test-bed.

7.1 Conclusions

The main work and results of this dissertation are summarized as follows:

- *Developed a modularized model for shipboard HPS:*

  The dynamic model has been developed in Chapter 2, where two versions, namely optimization oriented and simulation oriented models, were considered. A six state optimization oriented HPS model comprising of power sources and energy storage was developed, where the power sources were gas turbine and fuel cell/reformer and the energy storage was Lithium-ion battery packs. The simulation results of the lower order model verify that the components exhibit complementary dynamic and efficiency characteristics and capture the component nonlinearities. This model was integrated with distribution and load networks to get a detailed simulation oriented IPS model.

- *Developed a scaled test-bed of HPS as rapid prototyping platform for control algorithm:* In chapter 3, a PC cluster based real-time OpalRT® system was developed to serve as a real-time computation platform. A shipboard power system real-time simulator was developed using the simulation oriented IPS model which was used to perform failure emulation and power flow path reconfiguration and provides an effective tool for AES system level analysis. In addition, a scaled test-bed for the DC hybrid power system was presented in Chapter 3. This consists of power plant emulators to represent the electric characteristics of gas turbine/ generator sets and fuel cells. The emulators were integrated with DC power converters and provide the rapid prototyping platform for control strategy validation for multi-load, multi-source power management.

- *Developed a novel trajectory optimization methodology for time scale separated systems:*

  The proposed methodology (Chapter 4) achieved real-time computational efficiency for long time horizon, nonlinear constrained optimization problem by leveraging the multi time scale property of hybrid power systems. This method

approximates the true optimal solutions on slow and fast time scales, where the approximations can be made available much more quickly than the optimal solutions. It was illustrated through a case study that the timeliness of this method resulted in better real-time performance, compared to the conventional optimization methods, thereby making it more suitable for safety and performance critical hybrid power system application.

- *Developed and implemented a real-time power management strategy for normal mode operation:*

  While Chapter 4 presented a real-time methodology for open loop trajectory optimization, considerations such as disturbance rejection and active energy storage utilization are required in the design of normal mode power management schemes, which are the focus of Chapter 5. In this chapter, a hierarchical controller with feedback is developed that addresses the power management problem for shipboard HPS used in military applications to support critical missions in a fast and efficient manner. The proposed method solves both long term demand planning and short term disturbance rejection in real-time by using a three-level controller. In addition, the energy storage device is actively utilized to meet the pulse power requirements associated with critical missions. The proposed approach achieves better mission effectiveness as compared to a holistic optimal control approach, due to the realtime computational efficiency which has been illustrated through a case study on the real-time simulator.

- *Developed and implemented real-time power management strategy for failure mode scenario:*

  A reference governor based hierarchical controller is developed in Chapter 6 to address the power management for shipboard HPS used in military applications to recover from component failures and damage. Both the proposed and

the holistic MPC based methods were applied to solve the failure mode power management problem. By treating the performance and constraints separately, the proposed method achieved long term safety enforcement throughout the warmup period as well as maximum load support, both in real-time. The advantage of this approach, as compared to the conventional MPC approach, is improved survivability due to the real-time computational efficiency which was demonstrated through a case study.

7.2 Future Work

This dissertation is one of the early works reported for optimization-based real-time power management of shipboard power systems focusing on military applications. In the process of pursuing this research, the author identified many new opportunities in the control of all-electric ships. Although substantial progress has been made on the modeling, analysis and optimization, of the AES hybrid power system, the results of this dissertation point to several interesting directions for future work:

- *Integrating optimal power management with optimal network reconfiguration schemes:* Since the dynamics of power sources are much slower than those of power converters and distribution networks, the problem of optimal power management and network reconfiguration have been decoupled. However there are many factors such as line losses, current ratings etc., that would influence the overall system efficiency. Hence, optimal power management has to be integrated with optimal network restoration strategies to improve the performance of HPS in terms of system efficiency to minimize losses due to conversion and distribution. Such an effort would also benefit the control of HPS for stationary power generation.

- *Improvements to the HPS control-oriented model:* The dissertation specifically focused on disturbance rejection and relied on the inherent robustness of the feedback mechanism in both the normal and failure mode PM to deal with modeling errors. However, impact of environmental and aging factors of the components can potentially induce large modeling errors. Therefore, extending the control oriented model to include these factors is essential to prevent performance deterioration and/or constraint violation due to modeling errors.

- *Experimental validation of optimal power management:*

  The power management schemes developed in this work have achieved real-time computational efficiency and performance on the scaled test-bed and have demonstrated their potential for the real-time control of shipboard HPS. Nonetheless, further validation on a real-world experimental platform is needed to quantify the actual improvements in fuel savings. Only with successful experimental validation could the feasibility of the optimal power management controller for real-world military applications be claimed.

- *Develop an optimization-based methodology for power management of hybrid power systems using renewable energy:*

  Recently the control of HPS using wind and solar energy have attracted a lot of research interest as utilizing renewable energy for power generation has become quite appealing. For example, the applications that consider such hybridization include wind-diesel, solar panel-fuel cell systems as well micro-grids. All these HPS share some common features with AES hybrid power systems, namely complementary efficiency and time response characteristics, where the most efficient power source has a slower dynamic response. Hence ideas from this dissertation can be extended to develop a framework for the power management of hybrid systems that utilize renewable energy.

Appendix

Appendix A

Gas Turbine Model

The turbine model is based on [50]. For a self contained presentation, we include the key equations in this appendix.

The compressor mass flow is given by

$$W_c = \frac{\sqrt{T_{amb}}}{p_{amb}}\phi_c$$

The mass flow parameter ϕ_c is a function of the corrected speed parameter $\hat{\omega}_{tc}$ ($= \frac{\omega_{tc}}{\sqrt{T_{c,in}}}$) and pressure ratio across the compressor $\Gamma_{PR,c}$. This is determined using zero slope line method ([63]) and is given by

$$\frac{\phi_c}{\phi_{ZS,c}} = \begin{cases} 1 + k_{c2}\left(1 - e^{k_{c1}\left(\frac{\Gamma_{PR,c}}{\Gamma^{ZS}_{PR,c}} - 1\right)}\right), \ (\Gamma_{PR,c} < \Gamma^{ZS}_{PR,c}) \\ 1 - k_{c2}k_{c1}\left(\frac{\Gamma_{PR,c}}{\Gamma^{ZS}_{PR,c}} - 1\right), \ (\Gamma_{PR,c} \geq \Gamma^{ZS}_{PR,c}) \end{cases}$$

where $\phi_{ZS,c}$, $\Gamma_{ZS,c}$ are zero slope mass flow parameter and pressure ratio respectively and are given by,

$$\phi_{ZS,c} = -1.2388 \times 10^{-5}\hat{\omega}^2_{tc} + 0.0193\hat{\omega}^2_{tc} - 3.9488,$$

$$\Gamma_{ZS,c} = 1.9245 \times 10^{-5}\hat{\omega}^2_{tc} - 0.1053\hat{\omega}^2_{tc} + 16.7922.$$

The constants k_{c1} and k_{c2} are polynomial functions of $\hat{\omega}_{tc}$, whose coefficients are determined by regression on the compressor maps and are given by,

$$\begin{aligned} k_{c1} &= -2.0107 \times 10^{-9}\hat{\omega}_{tc}^5 + 4.797 \times 10^{-6}\hat{\omega}_{tc}^4 - 0.0045\hat{\omega}_{tc}^3 + 2.0608\hat{\omega}_{tc}^2 \\ &\quad -466.3395\hat{\omega}_{tc} + 41656, \\ k_{c2} &= 3.6901 \times 10^{-11}\hat{\omega}_{tc}^5 + -7.9632 \times 10^{-8}\hat{\omega}_{tc}^4 6.8174 \times 10^{-5}\hat{\omega}_{tc}^3 - 0.0289\hat{\omega}_{tc}^2 \\ &\quad +6.0878\hat{\omega}_{tc} - 507.5509. \end{aligned}$$

The compressor isentropic efficiency is given by

$$\eta_{is,c} = k_{c3}\phi_c^2 + k_{c4}\phi_c + k_{c5}$$

where k_{c3}, k_{c4}, k_{c5} are quadratic functions of the speed parameter $\widehat{\omega}_{tc}$ whose coefficients are determined by regression on the compressor efficiency maps and are given by,

$$\begin{aligned} k_{c3} &= -3.8776 \times 10^{-4}\hat{\omega}_{tc}^2 + 0.5629\hat{\omega}_{tc} - 226.3203, \\ k_{c4} &= -0.0017\hat{\omega}_{tc}^2 + 1.6863\hat{\omega}_{tc} - 200.9177, \\ k_{c5} &= -2.2272 \times 10^{-4}\hat{\omega}_{tc}^2 - 0.7914\hat{\omega}_{tc} + 298.4219. \end{aligned}$$

The turbine mass flow (W_t) is given by

$$W_t = \frac{\sqrt{T_b}}{p_b}\phi_t$$

$\Gamma_{PR,t}$ is the pressure ratio across the turbine. The function ϕ_t depends on the turbine

expansion ratio $\Gamma_{PR,t}$, corrected speed parameter $\hat{\omega}_{tc}$ and is given by

$$\phi_t = \begin{cases} A_t\sqrt{\frac{2\gamma}{\gamma-1}\left(\Gamma_{PR,t}^{\frac{2}{\gamma}} - \Gamma_{PR,t}^{\frac{\gamma+1}{\gamma}}\right)}, & (\Gamma_{PR,t} > p_{crit}) \\ A_t\sqrt{\frac{2\gamma}{\gamma-1}\left(p_{crit}^{\frac{2}{\gamma}} - p_{crit}^{\frac{\gamma+1}{\gamma}}\right)}, & (\Gamma_{PR,t} \leq p_{crit}) \end{cases}$$

where A_t is the effective flow area and is given by

$$A_t = \frac{k_{t1}}{\Gamma_{PR,t}} + k_{t2}.$$

The coefficients k_{t1} and k_{t2} are polynomial functions of the corrected speed parameter $\hat{\omega}_{tc}$ and is determined using regression on the turbine maps and are given by,

$$k_{t1} = 1.3817 \times 10^{-8}\hat{\omega}_{tc}^4 - 1.2106 \times 10^{-5}\hat{\omega}_{tc}^3 + 0.0040\hat{\omega}_{tc}^2 - 0.5761\hat{\omega}_{tc} + 31.3954,$$
$$k_{t2} = -4.7512 \times 10^{-8}\hat{\omega}_{tc}^4 + 4.1281 \times 10^{-5}\hat{\omega}_{tc}^3 - 0.0134\hat{\omega}_{tc}^2 + 1.9251\hat{\omega}_{tc} - 103.3194.$$

The turbine isentropic efficiency is given by

$$\eta_{is,t} = k_{t3}\Gamma_{PR,t}^2 + k_{t4}\Gamma_{PR,t} + k_{t5}$$

where k_{t3}, k_{t4}, k_{t5} are cubic functions of the speed parameter $\widehat{\omega}_{tc}$ whose coefficients are determined by regression on the turbine efficiency map and are given by,

$$k_{t3} = -0.0601\hat{\omega}_{tc}^3 + 37.8448\hat{\omega}_{tc}^2 - 7.8561 \times 10^3\hat{\omega}_{tc} + 535080,$$
$$k_{t4} = 0.0159\hat{\omega}_{tc}^3 - 10.0123\hat{\omega}_{tc}^2 + 2.0751 \times 10^3\hat{\omega}_{tc} - 14065,$$
$$k_{t5} = -0.001\hat{\omega}_{tc}^3 + 0.6266\hat{\omega}_{tc}^2 - 128.1918\hat{\omega}_{tc} + 8630.2.$$

Appendix B

Fuel Cell and Reformer Model

The anode outlet flow is given by the orifice equation as,

$$W_{an} = W_{0,an}\sqrt{\frac{p_{an} - p_{amb}}{\Delta p_0}},$$

where Δp_0 is the pressure drop across the orifice with $\Delta p_0 = 600Pa$ as given in [54]. The hydrogen consumed is given by the electrochemistry principle as follows:

$$W_{H_2,react} = M_{H_2}\frac{ncI_{st}}{2F}.$$

where n is the number of cells (1000) and F is Faraday constant.

Appendix C

Chapter 4

C.1 Proof Of Proposition 4.2.1

We list the key ideas used in deriving *Proposition 4.2.1.* To determine the order of the SFM algorithm given in Section 4.2, we first list the key tasks along with their flop count to compute control updates per iteration and the order of the algorithm is given by the dominant term to compute the control updates. For example, it can be shown that

- Performance index calculations: $N(p_1 + p_2)$ flops, where p_1, p_2 is the flop count to compute $g(x_k, u_k)$ and $f(x_k, u_k)$ respectively.
- Sensitivity functions calculations: $Np_4 + \frac{N(N+1)}{2}(p_5 + p_6)$ flops, where p_4, p_5 and p_6 is the flops to compute (A_k, B_k, g_{x_k}, g_{u_k}), $\frac{\partial x_{k+1}}{\partial u_i}$ and the inner product $\langle G_x, Z_i \rangle$ given by $\sum_{k=i}^{N} \frac{\partial g}{\partial x_k}' \frac{\partial x_k}{\partial u_i}$.
- Step size (δ^*) computation: $QN(p_1 + p_2) + (Q-1)p_3$ flops, where p_3 is the flop count for comparing floating point numbers and Q is the number of points in the search space of δ at which we evaluate the cost, where we assume a brute force calculations.

- Updating all the control inputs requires $m(N-1)$ flops.

The total FLOP count is given by $\frac{N(N+1)}{2}(p_5+p_6)+N(p_4+(Q+1)(p_1+p_2)+(Q-1)p_3+m(N-1)$. It can be seen that for $N >> n, m$ the dominant term is the effort for SF generation, given as,

$$C_{SF} = \frac{N(N+1)}{2}(p_5+p_6)$$

which is $\mathcal{O}(N^2)$. $\square$

C.2 Proof Of Remark 4.2.6

In order to show the relation given in *Remark 4.2.6*, we first express the optimal solutions in terms of the level 1 solutions and then consider a Taylor's series expansion around the level 1 solution, where

$$u^*_{[0:N-1]} = u_{[0:N-1]} + \delta u_{[0:N-1]} \tag{C.1}$$

Under the assumption that dynamics of the subsystem 1 are much faster (i.e $\varepsilon << 1$) we will have

$$\delta u_k \begin{cases} \in \Re^m, & \forall k \in [\mathbf{K} : \mathbf{K} + \wp\varepsilon], \\ = \mathbf{0}_{1\times m}, & otherwise. \end{cases} \tag{C.2}$$

where $\mathbf{K}$ is the step instant and $\wp\varepsilon$ is the interval in which transient corrections are needed. Then using (4.2) ($J(x_0, u_{[0:N-1]})$=$h(x_N)$ + $g(x_k, u_k)$), the optimal cost can

be expressed as follows:

$$J(x_0, u^*_{[0:N-1]}) = J(x_0, u_{[0:N-1]} + \delta u_{[0:N-1]}) \tag{C.3}$$

$$\approx J(x_0, u_{[0:N-1]}) + E_N \delta x_N + \sum_{k=0}^{N-1} E_k \delta x_k + F_k \delta u_k. \tag{C.4}$$

where $E_N = \frac{\partial g}{\partial x_N}\Big|_{(x_k,u_k)}$, $E_k = \frac{\partial g}{\partial x_k}\Big|_{(x_k,u_k)}$ and $F_k = \frac{\partial g}{\partial u_k}\Big|_{(x_k,u_k)}$.

If A_k, B_k denote the linearized dynamics of the system defined in (4.1) with $A_k = \frac{\partial f}{\partial x_k}\Big|_{(x_k,u_k)}$ and $B_k = \frac{\partial f}{\partial u_k}\Big|_{(x_k,u_k)}$, then we have

$$J(x_0, u^*_{[0:N-1]}) \approx J(x_0, u_{[0:N-1]}) + \sum_{k=0}^{N} [E_k A_{k-1} ... A_1 B_0,\ E_k B_{k-1},\ F_k, \mathbf{0}] \delta \mathbf{U} \tag{C.5}$$

where $\delta \mathbf{U} = [\delta u_0^T, ..., \delta u_{N-1}^T]^T$.

Since the δu_k is non-zero only around the transients, we consider the linearized matrices around the operating point $(x_\mathbf{K}, u_\mathbf{K})$ for the cost function in (C.5). In addition, we consider the band-diagonal structure (See *Remark 4.2.2*) with N_B band-diagonal elements and after some algebraic manipulation rewrite the cost function as follows:

$$J(x_0, u^*_{[0:N-1]}) \approx J(x_0, u_{[0:N-1]}) + [E_\mathbf{K}(I + A_\mathbf{K} + A_\mathbf{K}^2 + ... + A_\mathbf{K}^{N_B}) B_\mathbf{K} + F_\mathbf{K}] \sum_{k=\mathbf{K}}^{\mathbf{K}+\wp\varepsilon} \delta u_k$$

If we denote $\delta u^{Max} = max(\delta u_k)$, $\forall k \in [\mathbf{K}, \mathbf{K} + \wp\varepsilon]$, it can be noted that,

$$J(x_0, u^*_{[0:N-1]}) \leq J(x_0, u_{[0:N-1]}) + \wp\varepsilon [E_\mathbf{K}(I + A_\mathbf{K} + A_\mathbf{K}^2 + ... + A_\mathbf{K}^{N_B}) B_\mathbf{K} + F_\mathbf{K}] \delta u^{Max}$$

Then, the difference in the cost between the full scale and the level 1 optimization can be expressed as $J(x_0, u^*_{[0:N-1]}) - J(x_0, u_{[0:N-1]}) = \mathcal{O}(\varepsilon)$. $\square$

Bibliography

Bibliography

[1] T. J. McCoy, "Trends in Ship Electric Propulsion," *IEEE Power Engineering Society*, 2002.

[2] N. Doerry and J. C. Davis, "Integrated power system for marine applications," *Naval Engineers Journal*, 1994.

[3] N. Doerry, H. Robey, J. Amy and C. Petry, "Power the future with the integrated power system," *Naval Engineers Journal*, 1996.

[4] C. Petry and J. Rumburg, "Zonal electrical distribution systems: an affordable architecture for the future," *Naval Engineers Journal*, 1993.

[5] Y. Xie, G. Seenumani, and J. Sun, "Real-time simulation and optimization of multi-scale shipboard power systems," in *Proc. Grand Challenges in Modelling and Simulation,* 2008.

[6] Y. Xie, G. Seenumani, J. Sun, Y. Liu, and Z. Li, "A PC-cluster cased real-time simulator for all electric ship integrated power systems analysis and optimization," in *Proc. IEEE Electric Ship Technology Symposium (ESTS),* 2007.

[7] R. C. Bansal, "Automatic reactive power control of isolated wind-diesel hybrid power systems," *IEEE Trans. Industrial Electronics,* vol. 53, pp.1116-1126, Jun. 2006.

[8] T. Senjyu, T. Nakaji, K. Uezato and T. Funabashi,"A hybrid power system using alternative energy facilities in isolated island," *IEEE Trans. Energy Conversion,* vol. 20, pp.406-414, Jun. 2005.

[9] N. Hatziargyriou, H. Asano, R. Iravani, C. Marnay, "Microgrids: an overview of ongoing research, development, anddemonstration project," *IEEE Power and Energy;,* Jul., 2007

[10] Chan-Chiao Lin, Huei Peng, Jezzy Grizzle, "Power management strategy for a parallel hybrid electric truck," *IEEE Transations on Control Systems Technology*, Vol. 2, No. 6, pp. 839- 849, 2003.

[11] S.J. Moura, H.K. Fathy, D.S. Callaway, J.L. Stein, "A Stochastic Optimal Control Approach for Power Management in Plug-In Hybrid Electric Vehicles," *Dynamic Systems and Controls Conference*, 2008

[12] V. Tsourapas, A. Stefanopoulou, and J. Sun, "Model-based control of an integrated fuel cell and fuel processor with exhaust heat recirculation," *IEEE Trans. on Control Systems Technology,* vol. 15, pp.233-245, Mar. 2007.

[13] Vasilis Tsourapas, Jing Sun, Anthony Nickens, "Control oriented modeling and analysis of a hybrid solid oxide fuel cell and gas turbine (SOFC/GT) system," *Proceedings of the 2006 Fuel Cell Seminar.*

[14] A. Emadi, S. S. Williamson and A. Khaligh,"Power electronics intensive solutions for advanced electric, hybrid electric, and fuel cell vehicular power systems," *IEEE Trans. Power Electronics,* vol. 21, pp.567-577, May 2006.

[15] A. T-Raissi and D. L. Block, "Hydrogen: automotive fuel of the future," *IEEE Power and Energy Magazine,* vol. 2, pp.40-45, Nov./Dec. 2004.

[16] W. Gao,"Performance comparison of a fuel cell-battery hybrid powertrain and a fuel cell-ultracapacitor hybrid powertrain," *IEEE Trans. Vehicular Technology,* vol. 54, pp.846-855, May 2005.

[17] M.Kim, H.Peng, "Power management and design optimization of fuel cell/battery hybrid vehicles ," *Journal Of Power Sources*, 2007.

[18] Chan-Chiao Lin, Huei Peng, Jezzy Grizzle, "A stochastic control strategy for hybrid electric vehicles," *Proceedings of American Control Conference*, 2004.

[19] Ed Tate, Jezzy Grizzle, Huei Peng,“ SP-SDP for fuel consumption and tailpipe emissions minimization in an EVT hybrid,” *IEEE Transactions on Control Systems Technology*, Submitted March, 2007

[20] D. F. Opila, X. Wang, R. McGee, J. A. Cook, and J.W. Grizzle, “Performance Comparison of Hybrid Vehicle Energy Management Controllers on Real-World Drive Cycle Data,” *Proceedings of 2009 American Control Conference*.

[21] D. F. Opila, D. Aswani, R. McGee, J. A. Cook, and J.W. Grizzle, “Incorporating Drivability Metrics into Optimal Energy Management Strategies for Hybrid Vehicles,” *Proceedings of 2008 Conference on Decision and Control*.

[22] C. Musardo, G. Rizzoni, B. Staccia,“ A-ECSMS: An adaptive algorithm for hybrid electric vehicle energy management,” *Proceedings of the IEEE Conference On Decision and Control*, 2005

[23] P. Rodatz, G. Paganelli, A. Sciarretta, L. Guzzella, “Optimal power management of an experimental fuel cell/supercapacitor-powered hybrid vehicle ,” *Control Engineering Practice*, 2005.

[24] M.E.Baran, N.Mahajan, “System Reconfiguration on Shipboard DC Zonal Electrical System,” *IEEE Electric Ship Technologies Symposium*, 2005.

[25] K.Davey, R.Longoria, W.Shutt, J.Carroll, K.Nagaraj, J.Park, T. Rosenwinkel, W.Wu, A.Arapostathis,“Reconfiguration in shipboard power systems,”, Proceedings of the American Control Conference, 2007.

[26] S.K.Srivastava, K.L.Butler-Purry, N.D.R. Sarma, “Shipboard power restored for active duty,” *IEEE Computer Applications in Power*, 2002.

[27] Karen L. Butler-Purry, Sarma N.D.R,“ Self-healing reconfiguration for the restoration of naval shipboard power systems ,” *IEEE Trasactions on Power Systems*, Vol. 19, No. 2, pp 754-762, 2004

[28] S.Srivastava, K.L.Butler-Purry,"Expert-system method for automatic reconfiguration for restoration of shipboard power systems," *IEE Proceedings of Generation, Transmission and Distribution"*, 2006.

[29] David Montana, Talib Hussain," Using intelligent multi-agent systems for shipboard power systems reconfiguration," *Proceedings of the 13th International Conference on Intelligent Systems Application to Power Systems*, 2005

[30] J.M.Solanki, N.N.Schulz, W.Gao "Reconfiguration for Restoration of Power Systems using a Multi-Agent System," *Proceedings of the 37th Annual North American Power Symposium*, 2005.

[31] K.Huang, D.A.Cartes, S.K.Srivastava, "A multiagent-based algorithm for ring-structured shipboard power system reconfiguration ," *IEEE Transactions on Systems, Man, and Cybernetics*, 2007.

[32] Luca Benini, Alessandro Bogliolo, Giovanni De Micheli,"A survey of design techniques for system-level dynamic power management," *IEEE Transations on Very Large Scale Integration (VLSI) Systems*, Vol. 8, No. 3, pp 299-315, 2000

[33] Luca Benini, Alessandro Bogliolo, Giuseppe A. Paleologo, Giovanni De Micheli,"Policy optimization of dynamic power management," *IEEE Transations on Computer-aided Design of Integrated Circuits and Systems*, Vol. 18, No. 6, pp 813-833, 1999

[34] Yung-Hsiang Lu, Giovanni De Micheli,"Adaptive Hard Disk power management on personal computers," *Great Lakes Symposium, VLSI*, pp 50-53, 1999

[35] Chung E, Luca Benini, Alessandro Bogliolo, Giovanni De Micheli," Dynamic Power Management for non stationary service requests," *Design and Test in Europe Conference*, pp 77-81, 1999

[36] Srivastava M, Chandrakasan A, Brodersen R," Predictive system shutdown and other architechtural techniques for energy efficient programmable computation," *IEEE Transations on Very Large Scale Integration (VLSI) Systems*, Vol. 4, No. 1, pp 42-55, 1996

[37] Arthur E. Bryson Jr., Yu-Chi Ho, *Applied Optimal Control,* Taylor & Francis, Reprint

[38] J. Betts, "Survey of Numerical Methods for Trajectory Optimization," *Journal Of Guidance, Control, and Dynamics*, Vol. 21, No. 2, 1998.

[39] Dimitri P. Bertsekas, *Dynamic Programming and Optimal Control*, Athena Scientific 1995.

[40] Rein Luus, *Iterative dynamic Programming*, Chapman and /Hall CRC, 2000.

[41] Rein Luus,"Application of dynamic programming to high dimensional non-linear optimal control problems," *International Journal Of Control,* Vol. 52, No. 1, pp. 239-250, 1990.

[42] Rein Luus, "Iterative dynamic programming from curiosity to a practical optimization procedure," *Control and intelligent systems,* Vol. 26, No. 1, pp. 1-8. 1998.

[43] Rein Luus, "Optimal control by dynamic programming using systematic reduction in grid size," *International Journal of Control,* Vol. 51, No. 5, pp. 995-1013, 1990.

[44] Rein Luus, *Iterative dynamic Programming,* Chapman and /Hall CRC, 2000.

[45] D. Q. Mayne, J. B. Rawlings, C. V. Rao, and P. O. M. Scokaert, "Constrained model predictive control: stability and optimality," *Automatica,* vol. 36, pp.789-814, Jun. 2000.

[46] M. Morari and J. Lee, "Model predictive control: past, present and future," *Computers and Chemical Engineering*, vol. 23, pp.667-682, 1999.

[47] R. Fletcher, *Practical Methods Of Optimization*, John Wiley and Sons, 1985.

[48] R. Ghaemi, J. Sun, and I. Kolmanovsky, "An integrated perturbation analysis and sequential quadratic programming approach for model predictive control," *Automatica*, vol. 45, pp. 2412-2418, Sep. 2009.

[49] Philip E. Gill, Walter Murray, Michael A. Saunders, "SNOPT: An SQP Algorithm for Large-Scale Constrained Optimization ," *Society for Industrial and Applied Mathematics Review*, Vol. 47, No .1, 2005

[50] Gennady G.Kulikov, Haydn A. Thompson, *Dynamic Modelling of Gas Turbines*, Springer

[51] F. di Mare, W.P. Jones, K.R. Menzies, "Large eddy simulation of a model gas turbine combustor," *Combustion Systems Engineering*, 2004

[52] J. H. Kim, T. W. Song, T. S. Kim, S. T. Ro, "Model Development and Simulation of Transient Behavior of Heavy Duty Gas Turbines," *Journal of Engineering for Gas Turbines and Power*, 2001

[53] James Larminie, Andrew Dicks, *Fuel Cell Systems Explained,* Wiley, 2003.

[54] Jay T. Pukrushpan, Anna G. Stefanopoulou, Huei Peng,*Control of Fuel Cell Power Systems, Principles, modeling, analysis and feedback design,* Springer, 2004.

[55] H. Xi, J. Sun, V. Tsourapas, "A control oriented low order dynamic model for planar SOFC using minimum Gibbs free energy method, " *Journal of Power Sources*, 2007

[56] Y. Xie, J. Sun, J.S. Freudenberg, "Integrated Voltage Regulation and Current-sensorless Power Tracking Control for A DC Hybrid Power System," *Proceedings of 2008 American Control Conference.*

[57] P. Kuchonthara, S. Bhattacharya, A. Tsutsumi, "Combinations of solid oxide fuel cell and several enhanced gas turbine cycles," *Journal of Power Sources,* 2003.

[58] Y. Yi, A.D. Rao, J. Brouwer, G.S. Samuelsen, "Analysis and optimization of a solid oxide fuel cell and intercooled gas turbine (SOFC−ICGT) hybrid cycle," *Journal of Power Sources,* 2004

[59] V. Tsourapas, J. Sun,, A.Stephanapoulou, "Control Oriented Analysis of a Hybrid Solid Oxide Fuel Cell and Gas Turbine System," *Journal of fuel cell science and technology*, 2009

[60] Y.Xie, R. Ghaemi, J. Sun, and J. S. Freudenberg, "Implicit model predictive control of a full bridge DC/DC converter", to appear, *IEEE Trans. Power Electronics,* 2009.

[61] Y. Xie, R. Ghaemi, J. Sun, and J. S. Freudenberg, "Nonlinear model predictive control for a isolated high power full bridge DC/DC converter," submitted to, *IEEE Trans. Control System Technology,* 2010.

[62] P.M. Gomadama, J.W. WeidnerC, R.A. Dougalb, R.E. Whitea, "Mathematical modeling of lithium-ion and nickel battery systems," *Journal Of Power Sources*, 2002.

[63] Paul Moraal, Ilya Kolmanovsky, "Turbocharger modeling for automotive control applications," *Journal of Engg. For Gas Turbines and Power*, 2003.

[64] Kong C,Ki J, Kang M, "A new scaling method of component maps of Gas Turbines using system identification," *Proceedings of American Control Conference*, 2004.

[65] Joachim Kurzke, Claus Riegler, "A new compressor map scaling procedure for preliminary conceptional design of gas turbines," *Proceedings of ASME IGTI*, 2000.

[66] J. G. Ciezki and R. W. Ashton, "Selection and stability issues associated with a navy shipboard DC zonal electric distribution system," *IEEE Transactions on Power Delivery*, 2000.

[67] E. A. Lewis, "Cyclo convertor drive systems," *Sixth International Conference on Power Electronics and Variable Speed Drives*, 1996.

[68] P. Tenti, L. Malesani and L. Rossetto, "Optimum control of N-input K-output matrix converters," *IEEE Transactions on Power Electronics*, 1992.

[69] S. S. Kalsi, B. B. Gamble, G. Snitchler and S. O. Ige, "The status of HTS ship propulsion motor developments," *IEEE Power Engineering Society General Meeting*, 2006

[70] T. I. Fossen, *Marine Control Systems: Guidance, Navigation and Control of Ships, Rigs and Underwater Vehicles,* Marine Cybernetics AS, 2002.

[71] C. Dufour and J. Belanger, "A PC-based real-time parallel simulator of electric systems and drives," *International Conference on Parallel Computing in Electrical Engineering*, 2004.

[72] Y. Xie, J. Sun, C. Mi, and J. S. Freudenberg, "Analysis and modeling of a DC hybrid power system testbed for power management strategy development," in *Proc. IEEE Vehicle Power and Propulsion Conf. (VPPC'09),* 2009.

[73] Petar V. Kokotovic, Hassan K. Khalil, John O'Reilly, *Singular Perturbation Methods in Control Analysis and Design,* Prentice-Hall, 1996.

[74] Anthony J. Calise, "Singular Perturbation Techniques for On-line optimal flight path control," *Journal of Guidance and control,* 1980.

[75] P.K.A.Menon, M.M. Briggs, "Near-optimal midcourse gidance for air-to-air missiles," *Journal of Guidance and control,* 1987.

[76] Zigang Pan, Tamer Basar, "Model simplification and optimal control of stochastic singularly perturbed systems," *Proceedings of 1994 Conference on Decision and Control.*

[77] M. Bidani, M. Djemai, "A multirate digital control via a discrete-time observer for non-linear singularly perturbed continuous time systems," *International Journal of Control,* 2002.

[78] Peteros A. Ioannou, Jing Sun, *Robust Adaptive Control*, Prentice-Hall, 1996.

[79] Gayathri Seenumani, Jing Sun, Huei Peng "A Numerically Efficient Iterative Procedure for Hybrid Power System Optimization Using Sensitivity Functions," *Proceedings of 2007 American Control Conference.*

[80] M. S. Bazaraa, Hanif D. Sherali, C. M. Shetty, *Nonlinear programming: theory and algorithms*, John Wiley and Sons, 2005

[81] Steven Boyd, Lieven Vandenberghe, *Convex Optimization*, Cambridge University Press, 2004

[82] G. Seenumani, J. Sun, and H. Peng, "Exploiting Time Scale Separation For Efficient Real-Time Optimization Of Integrated Shipboard Power Systems," in *Proc. ASME Dynamic Systems and Control Conference*, 2008.

[83] G. Seenumani, J. Sun, and H. Peng, "Real-time Power Management of Integrated Power Systems in All Electric Ships Using Time Scale Separation," submitted to *IEEE Transactions On Control System Technology*, 2009

[84] F. Borrelli, and M. Morari, "Offset free model predictive control," in *Proc. IEEE Conference on Decision and Control*, 2007, pp.1245-1250.

[85] E.G.Gilbert, I.V.Kolmonovsky, "Nonlinear tracking control in the presence of pointwise state and control constraints: a generalized reference governor approach,", *Automatica*, 2002.

[86] J.Sun, I.V.Kolmonovsky, "Load Governor for fuel cell oxygen starvation protection: A Robust nonlinear reference governor approach,", *IEEE Transactions on Control Systems Technology*,2005.

[87] W.B.Dunbar, R.M.Murray, "Distributed Receding horizon control for multi-vehicle formation stabilization", *Automatica*, 2006.